Copyright Warning & Restrictions

The copyright law of the United States (Title 17, United States Code) governs the making of photocopies or other reproductions of copyrighted material.

Under certain conditions specified in the law, libraries and archives are authorized to furnish a photocopy or other reproduction. One of these specified conditions is that the photocopy or reproduction is not to be "used for any purpose other than private study, scholarship, or research." If a, user makes a request for, or later uses, a photocopy or reproduction for purposes in excess of "fair use" that user may be liable for copyright infringement,

This institution reserves the right to refuse to accept a copying order if, in its judgment, fulfillment of the order would involve violation of copyright law.

Please Note: The author retains the copyright while the New Jersey Institute of Technology reserves the right to distribute this thesis or dissertation

Printing note: If you do not wish to print this page, then select "Pages from: first page # to: last page #" on the print dialog screen

ABSTRACT

SUPERCAPACITORS WITH GATE ELECTRODES

by
Tazima Selim Chowdhury

A new approach to improve the capacitance of supercapacitors (SC) is proposed in this study. A typical SC is composed of an anode and a cathode; a separator in between them assures an unintentional discharge of the capacitor. The study focuses on a family of structured separators, either electronically active or passive which are called gates. An active structured separator layer has been fabricated and analyzed. The structured separator has characteristics of electrical diode and is fabricated out of functionalized carbon nanotubes (CNT). Improvement of the overall capacitance of SC, equipped with either active or passive structured separators demonstrated a large capacitance increase compared to SC which are interfaced with traditional separators.

Cyclic voltammetry (CV), Chrono-potentiometry (charge-discharge, C-D) and Electrochemical Impedance Spectroscopy (EIS) are used to assess the electrochemical characteristics of these novel devices. Raman spectroscopy is used to assess the quality of the structured CNT. Scanning electron microscope determines the surface morphology and porosity of the films. Current-voltage measurement takes place to ensure non-linear characteristics of the fabricated active separator layer. CV demonstrates that aqueous based electrolyte supercapacitors (SC) does not exhibit reaction peaks. Chrono-potentiometry demonstrates an overall 5-10% larger capacitance then traditional counterparts. EIS exhibits an unusual reduction of the cell's equivalent series resistance (ESR). Additional capacitance increase can be achieved when the active structured separator is biased

between -0.1 V to +0.1 V. The electrical energy, invested in a biased gate is fully captured as a stored energy.

A similar study is performed by fabricating active separator interfacing with ionic liquid electrolyte. Active gates exhibit similar capacitance improvement even after many cycles of charge and discharge when they are interfaced with ionic liquid.

SUPERCAPACITORS WITH GATE ELECTRODES

by
Tazima Selim Chowdhury

A Dissertation
Submitted to the Faculty of
New Jersey Institute of Technology
in Partial Fulfillment of the Requirements for the Degree of
Doctor of Philosophy in Electrical Engineering

Helen and John C. Hartmann Department of Electrical and Computer Engineering

May 2019

.

APPROVAL PAGE

SUPERCAPACITORS WITH GATE ELECTRODES

Tazima Selim Chowdhury

Dr. Haim Grebel, Dissertation Advisor — Date
Professor of Electrical and Computer Engineering, NJIT

Dr. Leonid Tsybeskov, Committee Member — Date
Professor of Electrical and Computer Engineering, NJIT

Dr. Robert B. Barat, Committee Member — Date
Professor of Chemical Engineering, NJIT

Dr. Dong-Kyun Ko, Committee Member — Date
Assistant Professor of Electrical and Computer Engineering, NJIT

Dr. Xuan Liu, Committee Member — Date
Assistant Professor of Electrical and Computer Engineering, NJIT

BIOGRAPHICAL SKETCH

Author: Tazima Selim Chowdhury

Degree: Doctor of Philosophy

Date: May 2019

Undergraduate and Graduate Education:

- Doctor of Philosophy in Electrical Engineering,
  New Jersey Institute of Technology, Newark, NJ, 2019

- Master of Science in Electrical Engineering,
  University of Missouri-Columbia, Columbia, MO, 2011

- Bachelor of Science in Electrical, Electronics & Communication Engineering,
  Military Institute of Science & Technology, Dhaka, Bangladesh, 2007

Major: Electrical Engineering

Publications and Presentations:

T. S. Chowdhury and H. Grebel, "Ion-Liquid Based Super-capacitors with Inner Gate Diode-Like Separators", *ChemEngineering*, vol. 3, 2019.

T. S. Chowdhury and H. Grebel, "Super-capacitors with Electrical Gates", *Electrochimica acta*, vol. 307, pp. 459-464, 2019.

R. Rojass-Cessa, H. Grebel, Z. Jiang, C. Fukuda, H. Pita, T. S. Chowdhury, Z. Dong, and Y. Wan, "Integration of Alternative Energy Sources into Digital Micro-grids", *Environmental progress and sustainable energy*, vol. 37, no. 1, pp. 155-164, 2018.

T. S. Chowdhury and H. Grebel, "Supercapacitors", *Materials Research Society Meeting*, Boston, MA, November 2016.

T. S. Chowdhury and H. Grebel, "Supercapacitors", *229th Electrochemical Society Meeting*, San diego, CA, May 2016.

T. S. Chowdhury and H. Grebel, "Gate electrodes in Electrochemical Cell", *227th Electrochemical Society Meeting*, Chicago, IL, May 2015.

T. S. Chowdhury and H. Grebel, "Effect of Gate Electrode in Electrochemical Cells", *227th Electrochemical Society Meeting*, Chicago, IL, May 2015.

T. S. Chowdhury and H. Grebel, "Effect of Permeable Gate Electrode on Electrochemical Cells", *Dana Knox Research Showcase Poster Presentation*, NJIT, Newark, NJ, Spring 2014.

T. S. Chowdhury and H. Grebel, "Electrochemistry with Carbon-Based Gate Electrodes", *24th Annual Sigma Xi Student Research Symposium*, Saint Joseph's University, Philadelphia, April 2013.

To my parents,

Sayeeda Khanam Chowdhury

And

Nasim Ali Chowdhury

ACKNOWLEDGMENT

I am grateful and thankful to my dissertation Advisor, Dr. Haim Grebel, who has been a perfect mentor for me. Without his continuous encouragement, constant guidance and support, this research could not have been completed. He has been very patient and understanding during the long journey towards successful completion of my studies. He has been very empathetic towards my rough times of my entire journey. He ensured time to time that I was in good condition both academically and emotionally to continue towards finishing my research work. He has been always there to listen and help if any situation occurs which obstructs the progress of research work. He provided me with freedom and communicated regularly by asking me if I need anything to finish my writing.

I would also like to express my gratitude to my dissertation committee members, Dr. Leonid Tsybeskov, Dr. Robert Barat, Dr. Dong Ko and Dr. Xiau Liu for their fruitful discussions. I am grateful for their thought provoking advising about my electrochemical method analysis. Their suggestions and constructive reviews really helped me to improve my dissertation a lot.

My journey was a long one and quite a difficult one. It would be impossible to make the journey by myself alone. It is worth mentioning the people behind the scenes who contributed towards my journey of completion. I would like to thank my friends and colleague who have been a great moral support. During the tough time of my stay in NJIT, Dr. Selina Akter Mala has eased me with her constant and positive encouragement. At times when the journey towards the completion seems far-fetched to me, she constantly reminded me of having the tenacity to finish. Her constructive feedback and suggestions

as a friend and colleague helped me to focus on my strengths and amend my weaknesses. I will always be grateful to her for that. I am also thankful to my school friends for making time for me to socialize and help me relieve my stresses from time to time.

I am grateful to my parents, Nasim Ali Chowdhury and Sayeeda Khanam Chowdhury for their affection, enormous patience and countless mental supports during my tumultuous journey. I am also thankful to my eldest sister, Dr. Nasima Selim who has been lifting me by inspiring conversation to complete my study. I am grateful to my sisters: Fahima, Mahima, Razima and brother-in-law's whose encouragement helped me to go forward. Last but not least I am thankful to my nieces Sumehra, Arissa, Fariza and nephews Rudro and Aareez for keeping me happy and feeling alive and making me realize that life is beautiful by their presence.

TABLE OF CONTENTS

TABLE OF CONTENTS
(Continued)

TABLE OF CONTENTS
(Continued)

Chapter **Page**

LIST OF TABLES

LIST OF FIGURES

LIST OF FIGURES
(Continued)

LIST OF FIGURES
(Continued)

LIST OF FIGURES
(Continued)

LIST OF FIGURES
(Continued)

LIST OF FIGURES
(Continued)

LIST OF FIGURES
(Continued)

CHAPTER 1

INTRODUCTION

1.1 Energy Storage Devices and Global Issues

Environmental issues and concerns over the availability of fossil fuels have been the driving force towards renewable and sustainable resource development. The electric power grid and the various means of transportation are major pollutant of the environment. In order to mitigate their effect, sustainable resources such as solar systems and wind turbines have been suggested as viable substitutes and opened up new energy markets. Due to their intermittent power generation, sustainable resources require energy storage units to smooth their operation. Energy storage units, such as batteries and electrochemical capacitors find an increasing role in these new markets. Electrochemical capacitors, also known as supercapacitors, or ultra-capacitors are currently incorporated in portable electronics, hybrid electric vehicles, large industrial equipment and other grid applications. Supercapacitors may be used in applications, which require charge-discharge of large currents in relatively short times. Due to these properties, they play an important role in complementing or sometimes replacing batteries in energy storage arena.

Ragone plot provides an overall comparison between various available energy storage devices in terms of power and energy density. Figure 1.1 illustrates that supercapacitors exhibit larger specific energy than conventional capacitor and larger specific power than batteries.

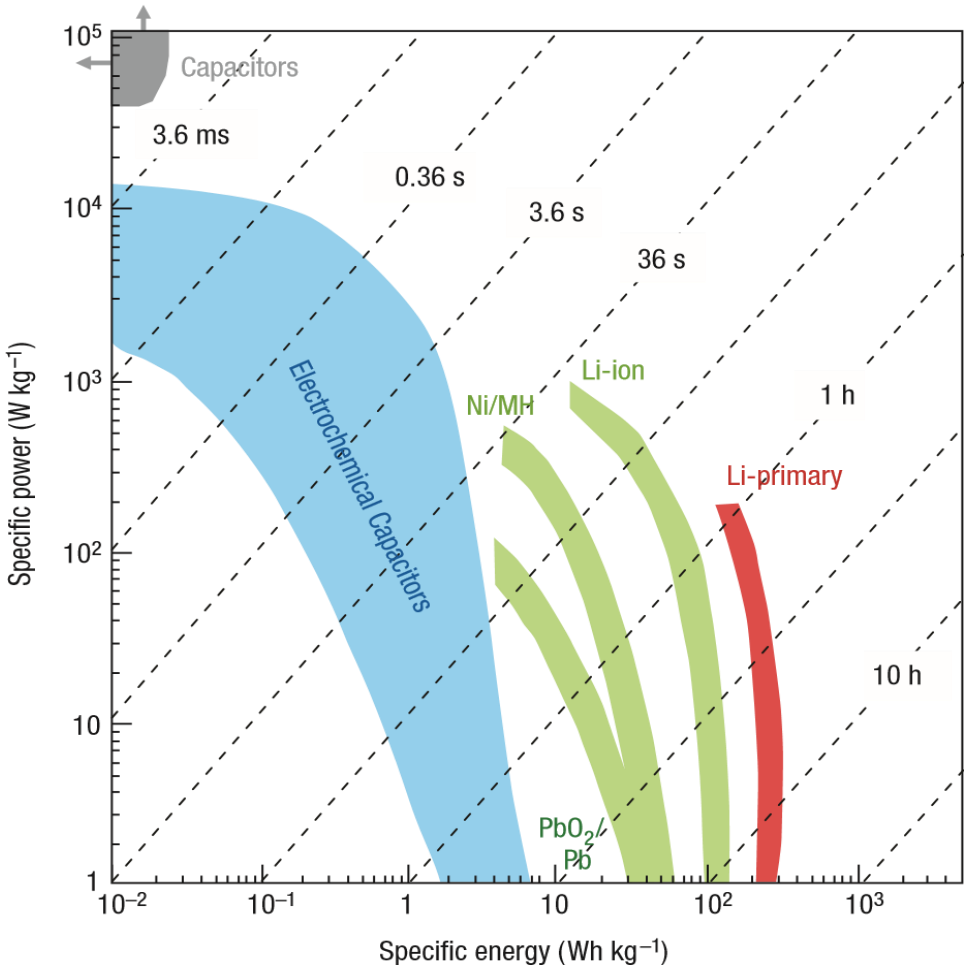

Figure 1.1 Ragone plot of specific power as a function of specific energy for various electrical energy storage units.
Source: [3].

Electrochemical capacitors have specific energy densities of the order of 5 $Whkg^{-1}$ which is much smaller than lithium ion batteries (150 $Whkg^{-1}$) [1]. Research has been going on to increase the performance of supercapacitors. Maxwell and a few suppliers in China claimed to have commercially available supercapacitors that produce 10 $Whkg^{-1}$ which gives researchers hopes for further improvements.

1.2 Concerns in Developing High Energy Density Supercapacitors (SC)

A supercapacitor consists of three major parts: electrodes, separator and electrolyte. Electrical contact between two electrodes is prevented by a separator layer. The porous separator layer and the pores in the electrodes are impregnated with supporting electrolyte. When a voltage is applied between the two electrodes, positive charge which are exposed at pore surface of one electrode attracts the negative ions from the electrolyte and the negative charge at the exposed pore surface of the other electrode attracts the positive ions from the electrolyte existing in the pores [1]. SC can store energy by non-faradaic process (electric double layer capacitor, EDLC) or faradaic process (also called pseudo-capacitor). Both processes rely on the nature of the electrode material, which is under continuous development [2-6].

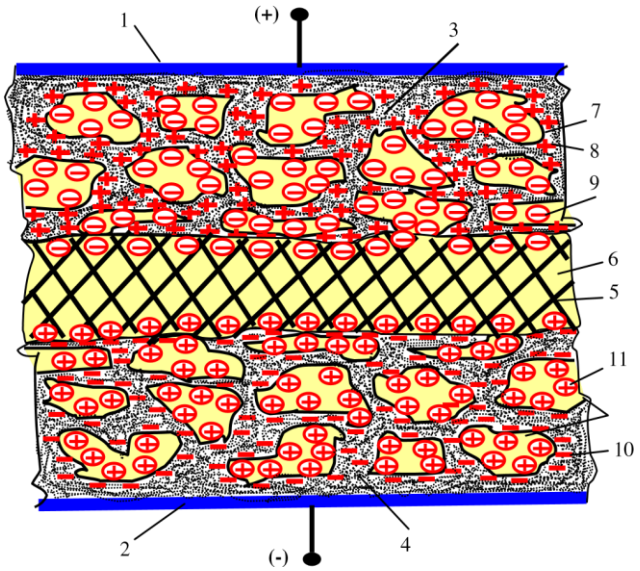

Figure 1.2 Schematics for a charged supercapacitor: current collectors (1,2), positive electrode (3), negative electrode (4), separator (5), electrolyte (6), electrode material pores (7), positive and negative ion (11, 9), positive and negative charge (8, 10).
Source: [1].

In order to improve the performance of supercapacitors, increasing the electrodes' porosity and the electrolytic material were the main focus of research so far [7]. Choice of a proper separator was also found crucial to the capacitance increase of the cell. Still left unexplored is the choice of optimal separator layer [8]. Separators have been constructed of plastic, rubber, aquagel, polyolefin films to prevent any conduction between electrodes. Those membranes exhibit poor ionic conductivity since they have tendency to dry out or to collapse over longer period of time [9-11]. The separator is a major contributor to the resistance of a supercapacitor and a major factor in dictating its power density. There have been a few detailed studies on the contribution of structured separator on the performance of supercapacitor. The research described in this dissertation will focus primarily on how incorporating structured separator can affect the resistance and capacitance of supercapacitors. Nafion membrane, which is commonly used for commercial applications, consists of hydrophobic backbone and hydrophilic side chains [12, 13]. Even though it possesses suitable properties in terms of efficiency and cost [14-16] it became apparent that a new kind of separator structure is needed for large scale applications.

1.3 Scope of the Study

Long lifetime, namely, many of cycles of operation and high rate of charge and discharge make supercapacitors a very propitious alternative to batteries and fuel cells. Yet, more research is needed to improve existing them. In particular, one unexplored area is the separator layer. As mentioned earlier, currently, separators are made of an insulating membrane. This work aims at developing a new structured separator membranes. As will be shown below, incorporation of structured separator membrane increases the overall

cell's capacitance. .

In the past, most research has been focused on new porous electrode material or electrolytes with wider potential windows. While separators play a key role in supercapacitors, only limited effort has been devoted to their study. Here we propose to turn the otherwise passive separator membrane into an electronically one. Such new class of separators may open new venues for supercapacitor modes of operation, in addition to increasing the capacitance of traditional ones. In order to realize an electronically structured membranes, we propose to use functionalized, single wall carbon nanotubes (SWCNT) as well as carbon nano-powder as the separator material. Carbon nanotubes have many possibilities in a wide range of applications, such as lightweight elements for spacecraft, novel electronic devices, as well as electrode material for supercapacitors [17]. Thus, this thesis proposes to use current technology for electrode materials for the newly designed separator structure. This structure is in the form of an electronic diode, placed inside the supercapacitor cell.

1.4 Dissertation Outline

In this dissertation, background information is discussed in Chapter 1. Chapter 2 provides in depth description of the theory behind traditional supercapacitors and a comprehensive review of past results. In Chapter 3, the process of separator fabrication and the various characterization techniques to study them are discussed.

Chapter 4 describes key general methods of supercapacitor analysis. It provides description of two and three electrode configuration and choice of analysis. Three universal electrochemical methods: Cyclic voltammetry (CV), Chronopotentiometry and

Electrochemical Impedance Spectroscopy (EIS) have been used. The results are discussed in Chapter 5. Details of measurement procedures are mentioned in each segment. Conclusion are given in Chapter 6. Finally, Chapter 7 suggests the future work related to this research.

CHAPTER 2

BACKGROUND

2.1 Introduction

A supercapacitor, also known as electrical double layer capacitor, ultra-capacitor, or electrochemical capacitor, is an electrical energy storage device. The first concept of supercapacitor was based on porous structure of carbon material which possesses large surface area. In 1957, the first patent for supercapacitor was granted to Becker at General Electric Corp. The design was based on aqueous electrolyte [18] and is shown in Figure 2.1. The capacitor, consisted of two porous carbon electrodes was partially immersed into an electrolyte. A considerably higher capacitance is measured with capacitors of comparable size. A compact, low voltage, high capacitance electrolytic capacitor which operates with a high efficiency has been reported too [18].

In 1966, while working on experimental fuel cell designs, researchers from Standard Oil of Ohio (SOHIO) accidentally rediscovered the effect of a double-layer capacitor [19]. A researcher from the same company patented disc-shaped supercapacitors in 1970 [20]. The basic approach was to make two carbon paste electrodes. The distinct feature of the electrode was they are made by mixing activated carbon with an electrolyte to form paste. By applying compression, water content is excluded to form a thick slurry paste of electrode. The capacity and resistance were measured with various electrolytes [20]. The company did not commercialize their discovery and licensed it to NEC, who marketed the double layer capacitor as "supercapacitor" for computer memory backup.

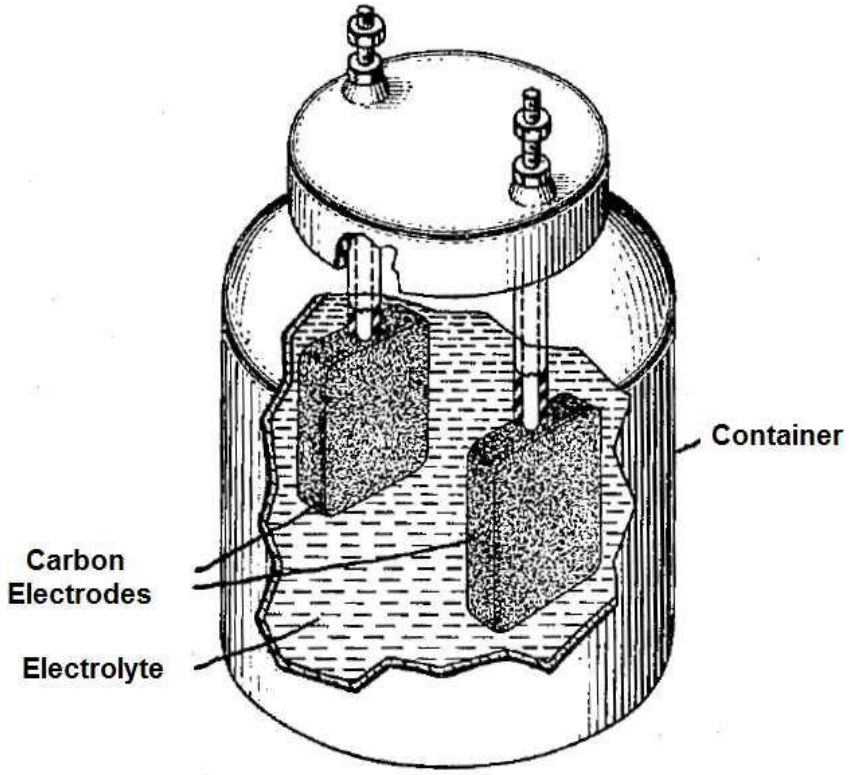

Figure 2.1 The first patent for electrochemical capacitor granted to General Electric. *Source: [18].*

Conway was first to describe the difference between "Supercapacitor" and "Battery" behavior as energy storage elements. In supercapacitors, the electrical charge is partially stored in the Helmholtz double-layer and partially as charge transfer between electrode and electrolyte [21].

Based on transition metal oxide, the first non-carbon electrode material was proposed by S. Trasatti [22]. It led to the understanding of the concept of "pseudocapacitance" by later researchers. High capacitance value is achieved here due to the continuous oxidation or reduction of Ru_2O, coupled with a double layer capacitance [23, 24]. Conway and his colleagues advanced the field by studying the voltage dependent electrochemical reaction of transition metal oxides [25].

In the 90's, supercapacitors received much attention in the context of hybrid electric vehicles. A large number of supercapacitor patents have been granted during that period [26]. U.S. Department of Energy initiated a short-term program and later, after-2003 a long-term supercapacitor development programs to achieve 5 and 15 Wh/kg of specific energy and 500 and 1600 W/kg of specific power, respectively [27, 28].

Currently, most of the commercial productions of electrochemical supercapacitors in the markets are based on the high surface area porous carbon materials as well as on noble metal dioxides [25]. Panasonic, Japan has developed gold capacitors, and Pinnacle Research (USA) made especially high performance supercapacitors for military applications [25]. These commercial supercapacitors are widely used as elements for long time constant circuits, standby power for random access memory devices, and telephone equipment. Maxwell Laboratories in collaboration with research group of Auburn university developed carbon fiber based composite electrodes with high electrical conductivity in 1991. In comparison to traditional capacitors, which have high power but low energy densities, batteries are typically low power devices. Supercapacitors can act as a combination of both elements to achieve high power density, higher energy density, and long life cycles due to the absence of chemical reactions. The detailed description of traditional and supercapacitor type capacitive elements will be discussed in the next sections.

2.2 Traditional Capacitor

Conventional or traditional capacitor consists of two metal plates separated by a non-conducting material or an insulating dielectric material such as, air, glass or even oil. The

field within the capacitor is constant and becomes smaller as the dielectric constant becomes larger. The potential inside the capacitor is, therefore linearly dependent on the distance from one of the electrodes. The electronic charges on either electrodes are kept apart by the dielectric material. The dielectric material is polarized by the charged electrodes and its electric field is in an opposite direction to the field produced by the charged electrodes.

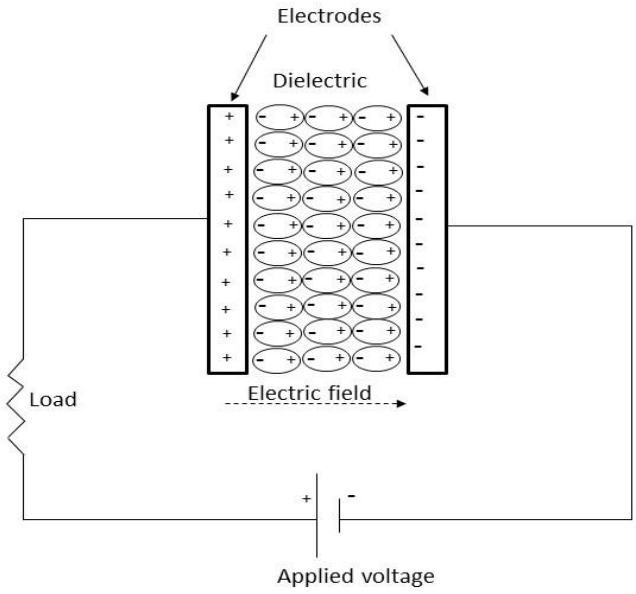

Figure 2.2 Schematic of a traditional capacitor during the charging process.
Source: [25].

Among the traditional capacitors are: electrostatic type capacitor consisting of two parallel plates, which separated by vacuum or a dielectric material; electrolytic capacitor, which employs solid, or liquid electrolytes as dielectric materials [25].

Capacitance is defined as the ratio of accumulated charge, Q and the biasing potential difference, V between electrodes as shown in Equation 2.1:

$$C = \frac{Q}{V} \tag{2.1}$$

The capacitance depends on the area of the charged electrodes (A), the distance between them (d) and the dielectric constant of the material between the two plates. The dielectric constant is the product of dielectric constant ($\in_0$) of free space and the relative dielectric constant ($\in_r$) of the insulating material. The relationship between these parameters is given by Equation (2.2) [25]:

$$C = \in_0 \in_r \frac{A}{d} \tag{2.2}$$

To achieve higher capacitance, larger dielectric constants and large surface area should be used. The dielectric strength of the material is controlled by parameters such as humidity, temperature, and thickness. These parameters determine the breakdown voltage, or the maximum potential bias that the capacitor can sustain. Commonly used dielectric materials are given in Table 2.1.

Table 2.1 Relative Dielectric Constants of Commonly used Capacitor Materials [25]

Materials	Relative Dielectric constant
Tantalum pentoxide	26
Ceramics	20 to 400,000
Aluminum oxide	4.5 to 11.5
Titanium dioxide	14 to 110
Titanates (Ba, Ca, Sr, Mg,Pb)	15 to 12,000

Source: [25]

2.3 Working Principle of Supercapacitor

Supercapacitors are electrochemical energy storage devices. They consist of two porous electrodes which are immersed in an electrolyte. From external circuit point of view, one electrode is called the anode (the negative electrode) and the other is called the cathode (the positive electrode). Each electrode is typically interfaced with a current collector (a metal film) to aid the passage of charge to and from the electrode. A separator layer between electrodes is added to minimize unintentional discharge. When charged, the cathode attracts negative ions from the electrolyte, while the anode attracts positive ions. Unlike ordinary capacitor, the large capacitance is maintained at the interface between the electrolyte and either electrodes. This interface is of the order of nanometers and is called the Helmholtz double layer. Due to its nanometer scale, the effective distance in Eq. 2.2 is very small, giving rise to a very large capacitance.

There are two mechanisms that contribute to the large capacitance in supercapacitors: the electrical double layer (EDL) and the transfer of charges between the ions in the electrolyte and the porous electrode, the so called pseudo-capacitance. The latter is attributed to fast and reversible redox processes. It is more convenient to discuss the two mechanisms separately though they usually lumped together in a typical supercapacitor.

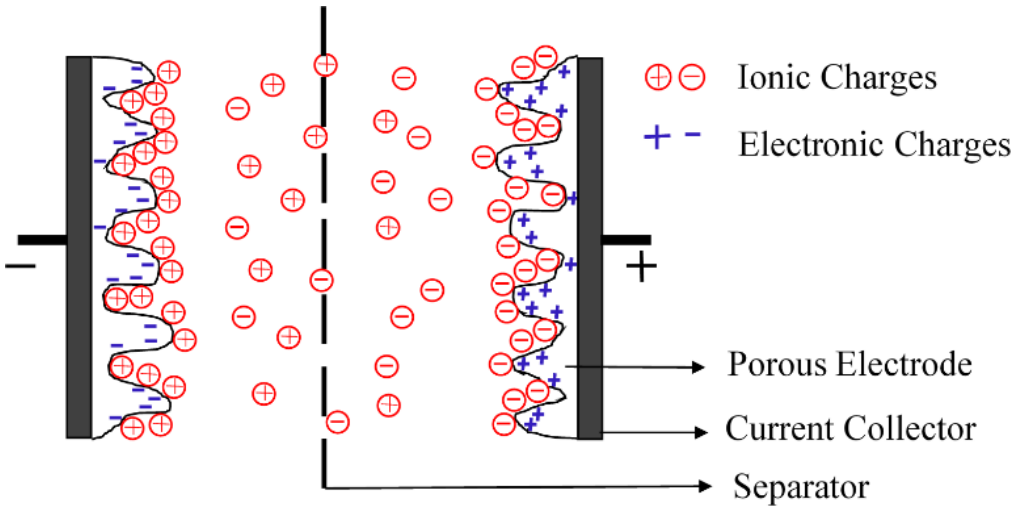

Figure 2.3 Schematic diagram of a supercapacitor device.

2.3.1 Electric Double Layer Theory

Conventional capacitors store relatively little energy. This is due to a small surface area and the minimum distance between the two charged plates before breakdown. On the other hand, supercapacitors, which are based on EDL mechanism can store more energy because of the large interfacial area between electrolyte and the electrodes and the small charge separation at their interface. Schematically illustrated in Figure 2.4a, the concept of the EDL was first described and modeled by von Helmholtz in the 19th century when he investigated the distribution of opposite charge at the interface of colloidal particles (Helmholtz, 1853) [29]. The Helmholtz double layer model describes two layers of opposite charges, which are formed at the electrode-electrolyte interface. The model is similar to a two-plate conventional capacitor [29]; yet, with a much smaller characteristic separation distance. This simple model was further modified by Gouy (1910) and Chapman (1913) [30, 31] to include a continuous distribution of the electrolytic ions (both cations and anions) rather than a step-like Helmholtz profile. The gradual distribution was

accounting for thermal ion motion, and is referred to as the diffuse layer (Figure 2.4b) [30, 31]. However, the Gouy-Chapman model leads to an overestimation of the EDL capacitance; the capacitance of two layers of charges decreases inversely upon increasing the separation distance. Hence, large capacitance would arise from point charges close to the electrode surface [30, 31]. Later, Stern (1924) combined the Helmholtz model with the Gouy-Chapman model to explicitly recognize two regions of ion distribution: the inner region called the compact layer or stern layer and the outer, diffuse layer (Figure 2.4c) [32]. In the compact layer, ions (very often hydrated) are strongly adsorbed by the electrode, thus the name of compact layer [32]. The adsorbed ions, which in most cases are anions irrespective of the charge nature of the electrode, and non-specifically adsorbed counterions. The inner Helmholtz plane (IHP) and outer Helmholtz plane (OHP) are used to distinguish between the two types of adsorbed ions. The diffuse layer region incorporates the Gouy and Chapman model. The IHP refers to the distance of closest specially adsorbed ions and OHP refers to the non-specifically adsorbed ions. The OHP is also the plane where the diffuse layer begins [33]. It defines: d as the double layer distance along with the Helmholtz model. Ψ_0 and Ψ are the potentials at the electrode surface and the electrode/electrolyte interface, respectively shown in Figure 2.4.

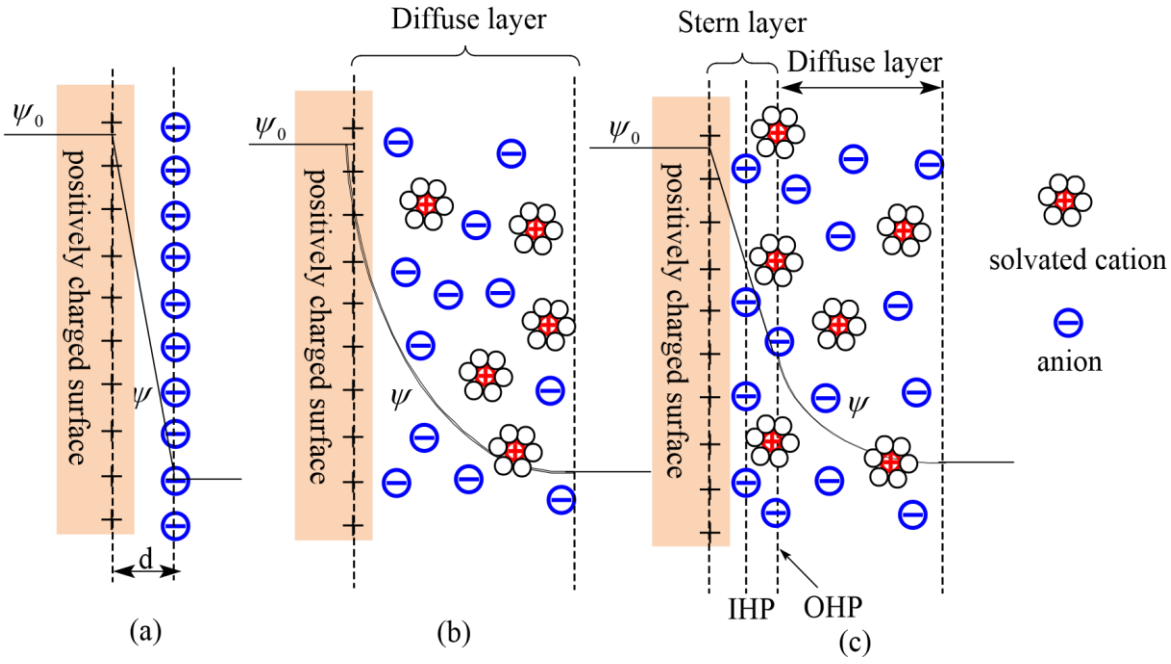

Figure 2.4 Models of electrical double layer at a positively charged surface: (a) the Helmholtz model, (b) the Gouy-Chapman model, and (c) the Stern model showing the Inner Helmholtz Plane and Outer Helmholtz Plane.
Source: [33].

The capacitance of the EDL (C_{dl}) can be measured as the combination of the capacitances of two regions, the Stern type of compact double layer capacitance (C_H) and the diffusion region capacitance (C_{diff}). Therefore, C_{dl} can be expressed by the following equation[33]:

$$\frac{1}{C_{dl}} = \frac{1}{C_H} + \frac{1}{C_{diff}} \tag{2.3}$$

The parameters that determine the EDL behavior at a planar electrode surface include the electrical field across the active electrode, electrolyte type, the solvent in which the electrolyte is dissolved, and the chemical affinity between the electrode surface and the

electrolyte ion with an opposite charge to the electrode charge [33]. Because the electrode is usually made out of a porous material with a high specific surface area, the EDL behavior at the pore surface of the porous electrode is much complex than that at an infinitely planar surface; specifically, the ion transport within a confined system can be drastically affected by the tortuous mass transfer path, the space constrain inside the pores, ohmic resistance associated with electrolyte, and the wetting behavior of the pore surface by the electrolyte [33]. For the EDL type of supercapacitor, the capacitance, C of each electrode is generally tends to follow that of a parallel-plate capacitor [34] of Equation 2.2 where ε_r (a dimensionless constant) is the electrolytic relative dielectric constant, ε_0 (F m^{-1}) is the permittivity of a vacuum, A (m^2) is the surface area of the electrode accessible to the electrolyte ions, and d (m) is called Debye length which is the effective thickness of the electric double layer. It is the quantitative measurement of space charge region from metal electrode to bulk electrolyte. Based on Equation (2.2), a linear relationship between C and A is expected. But, experimental results have shown that this simple linear relationship does not prevail in many cases [46, 55]. It is traditionally assumed that the sub-micropores of an electrode do not participate in the formation of EDL due to their inaccessibility to large solvated ions.

According to the work of Raymundo-Pinero et al. (2006), partial desolvation of hydrated ions can occur and EDL can form in the micropores [35]. Gogotsi and coworkers (2008) observed an anomalous capacitance increase in carbon electrodes with pore sizes less than 1 nm. The authors also reported that the EDL capacitance reached to a maximum when the electrode pore size was very close to the ion size, confirming capacitance contributions from the pores with sizes smaller than solvated ion size. All new

experimental findings, however, cannot be fully interpreted by the EDL theory because in such confined spaces, there would be insufficient room to accommodate both the compact layer and the diffuse layer. Huang and co-workers proposed a trial and error approach to describe the capacitive behaviors of nanoporous-carbon-based supercapacitors [41]. In this approach, the pore curvature is taken into account and different capacitive mechanisms are suggested for electrodes with different pore sizes. An electric double-cylinder capacitor (EDCC) model is used to describe mesoporous carbon electrodes while an electric wire-in-cylinder capacitor (EWCC) model is proposed for modeling microporous carbon electrodes as schematically illustrated in Figure 2.5. When the pores are large enough so that the pore curvature is no longer significant, the EDCC model converges to the traditional planar EDL model given by equation (2.2). The capacitance estimations for the two proposed models are provided by equation (2.4) for the EDCC model and (2.5) for the EWCC model, respectively [41]:

$$C = A\frac{\varepsilon_r\varepsilon_0}{b\ln[b/(b-d)]} \tag{2.4}$$

$$C = A\frac{\varepsilon_r\varepsilon_0}{b\ln(b/a_0)} \tag{2.5}$$

in which b is the pore radius, d is the distance between the approaching ions to the surface of the carbon electrode, and a_0 is the effective size of the counterions.

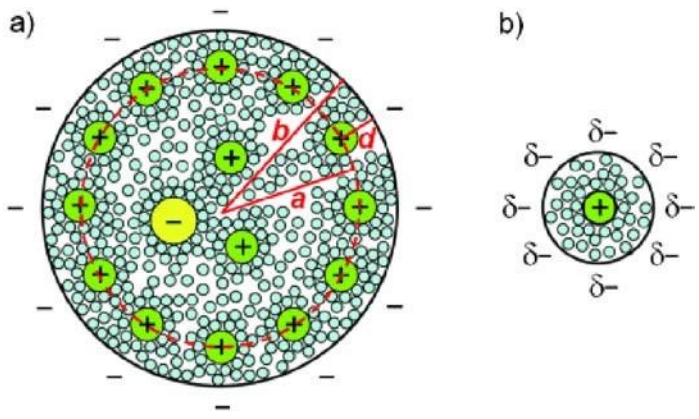

Figure 2.5 Schematic diagrams (top views) of (a) a negatively charged mesopore with solvated cations approaching the pore wall to form an electric double-cylinder capacitor and (b) a negatively charged micropore of radius b with cations lining up along the pore axis to form electric wire-in-cylinder capacitor.
Source: [41].

With these models, the authors were able to fit the experimental data regardless the types of carbon electrode materials and the electrolytes employed. Both the anomalous increase in capacitance for pores below 1 nm and the trend of slightly increasing capacitance with the increase of pore size above 2 nm can be explained by fitting with the proposed EWCC and EDCC models, respectively. In addition, the calculated dielectric constant from the fitting results using Equation (2.5) is close to the vacuum value, which indicates desolvation of hydrated ions before entering the micropores [41].

2.3.2 Pseudo-capacitance Mechanism

Electric double layer capacitor stores charges electrostatically at the interface of electrolyte and electrode which is also called non-Faradaic process. Pseudo-capacitance is a faradaic process, namely, involves chemical reactions. These are fast and reversible redox reactions between electrolyte and some electro-active species on the surface of the electrode. When specifically adsorbed ions out of the electrolyte pervade the double-layer, pseudo-

capacitance can occur. It can also originate due to intercalation and electro-sorption process. The ability of electrodes to accomplish pseudo-capacitance effects depends on the chemical affinity of the electrode materials to the adsorbed ions, as well as on the pore structure and dimension of the electrode.

Due to the functional groups present on the surface, there is approximately 1-5% pseudo-capacitance in a typical double layer carbon capacitor. Oxidation of surface carbons increases the wettability of ionic species due to the increase in polar oxygen molecules. Nitrogen added to carbon nanotubes has been experimentally shown remarkable enhancement to the capacitance of supercapacitors. On the other hand, life cycle and conductivity are typical trade-offs. Several types of materials with significant pseudocapacitance have been investigated: [25] a) electroactive oxide or hydrous oxide films of transition metals, such as MnO_2, IrO_2, RuO_2; b) films of conducting polymers, e.g., polypyrrole, polythiophene, polyaniline, and their derivatives; c) electrosorbed H at Pt metals.

2.4 Electrolytes

The performance of supercapacitors largely depends on the electrolytic material. It is as important as the electrode material. The operating voltage of electrochemical devices is determined by the selection of the electrolyte. Electrolytes exert critical effects on the development of the double layer and accessibility of pores by the electrolyte ions.

Generally, three major types of electrolytes are used: aqueous, organic and ionic liquids (IL). Organic and ionic liquid falls under non aqueous electrolyte category. Organic electrolytes are used in most of the currently available capacitors. The electrochemical and

physical properties of the electrolytes are key factors of determining the internal resistance and the power output, the voltage range of supercapacitor cells. The concentration of free charge carriers and the ionic mobility per dissociation ion in the electrolytes are two factors affecting the conductivity of any electrolyte. There are secondary factors which also helps determine the electrolytes: low flammability, volatility and corrosion potential. Solubility, concentration, temperature, viscosity and permittivity of the solvent are also equally important characteristics when choosing an electrolyte. Since supercapacitor undergo thousands of charge discharge cycles the solvent has to be chemically stable.

2.4.1 Aqueous Electrolytes

Aqueous alkali/acid electrolytes such as potassium hydroxide (KOH) [35] and aqueous sulphuric acid (H_2SO_4) [36] are commonly used in low voltage applications of less than one volt. Both electrolytes are considered hazardous. There are other aqueous electrolytes which are easy to use such as (NaCl, KCl). Due to good kinetics, relatively high conductivity, low viscosity at high concentration and efficient charge-discharge rate, aqueous electrolytes are a good choice. The electrolytic conductivity of aqueous based supercapacitors is relatively high (0.8 S/cm for H_2SO_4). In order to bypass electrolyte depletion during charging, concentrations higher than 0.2M are sufficient while the related electrode pore size is small (~2-5Å). In contrast, the pore size requirements for electrode interfaced with organic electrolytes is larger, ~7-10Å. Table 2.2 shows the range of ion dimension for various electrolytes:

Table 2.2 Size of Ions in Aqueous Electrolytes

Aqueous Electrolyte	Ion Dimension (nm)	
	Cation	Anion
H_2SO_4		0.533
KOH	0.26	
Na_2SO_4	0.36	0.533
NaCl	0.36	

Source: [45]

Aqueous electrolytes are cost effective. They are used at the development stage of

Table 2.3 Conductivity and Voltage Window in Aqueous and Ionic Liquid Electrolytes at Room Temperature

Electrolyte	Conductivity (mS/cm)	Voltage Window (V)
KOH	540	1
KCl	210	1
H_2SO_4	750	1
Na_2SO_4	91.1	1
NaCl	171	1

Source: [25]

new capacitive structures. They can be used in open environment with less safety concerns and do not require water free environment like their organic counterparts. Their only disadvantage is a low stability window, which restricts their related energy and power density. Table 2.3 summarizes their conductivity and operational window.

2.4.2 Non-Aqueous Electrolytes

In comparison, non-aqueous electrolytes provide larger energy than aqueous electrolytes at room temperature. They exhibit larger operating voltage window, due to a lesser decomposition [37-39]. Ionic liquids are room-temperature molten salts, composed mostly of organic ions that may undergo almost unlimited structural variations. The ionic liquid, 1-butyl-3-methylimidazolium tetrafluoroborate ($BMIMBF_4$) has relatively large ionic radius ($BMIM^+$ - 3.39 Å and BF_4 2.29 Å) [40, 41] compared with aqueous KCl (ionic radius – K^+ - 1.38 Å and Cl^- - 1.81 Å) [41]. Due to the large ionic radii, the mobility of ions in ionic liquids are somewhat low and the internal resistance is larger than for aqueous

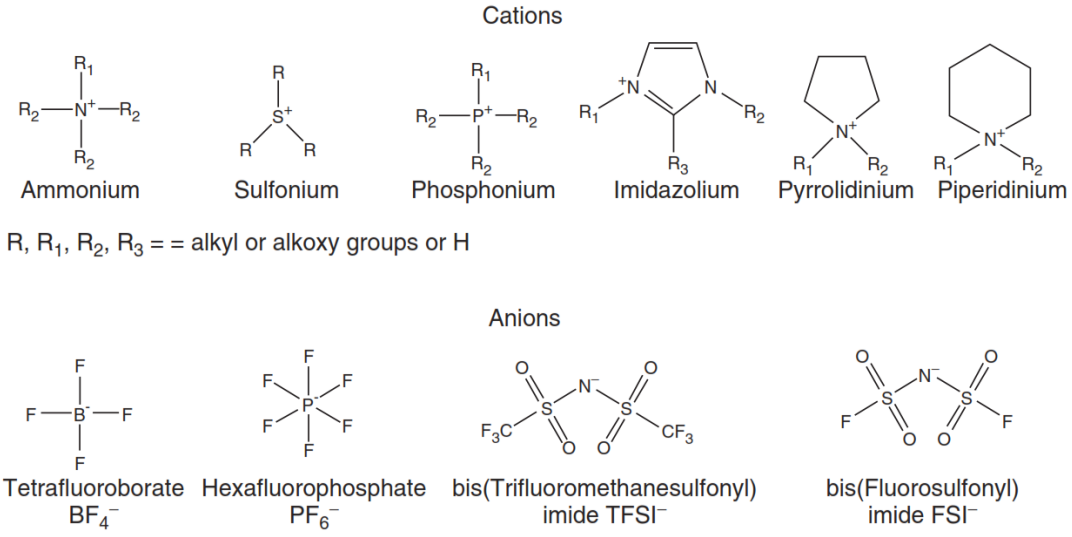

Figure 2.6 Chemical formula and structure of different ionic liquids.

electrolytes. By dissolving ionic liquids in a non-aqueous solvent, their mobility is enhanced. The most commonly used solvents for blended non-aqueous electrolytes are listed in Table 2.4. The most common salt consists of lithium ions as these move fast under an electric field, and their effective ionic radius is small (0.76Å).

Preferred solutes for tetraalkylammonium salts are $(PF_6)^-$ and $(BF_4)^-$, which have suitable decomposing potential limit (up to 4 V). Ionic liquids (IL) have been used as electrolytes in supercapacitors due to a large decomposition voltage (~5V), non-flammability, low toxicity, non-corrosiveness to the electrodes and a wide range of concentration (from as low as mM to M). The major drawback to the use of IL is their low conductivity (2-15 mS/cm at 60°C). Solvents such as acetonitrile have been used to increase their conductivity. IL electrolytes are most suitable for high temperature applications.

Table 2.4 Common Non-aqueous Solvents used in Supercapacitor Electrolytes

Solvent	Bp./ °C	Mp./ °C	Permittivity	Viscosity(25°C)/mPa.s
Propylene carbonate	241	-55	65	2.8
Dimethylsulfoxide	189	18.5	29.8	1.996
Ethylene carbonate	260	37	95	1.92
Acetonitrile	82	-45	38	0.369

Sources: [42. 52].

Gel polymer electrolytes are another type of electrolyte used in supercapacitors. They are composed of two phases: ionic conducting medium and a host polymer matrix. Ionic conductors, such as proton (H^+) and lithium (Li^+) are entrapped in the polymer

matrices, such as poly(propylene), poly(vinylidene difluoride), poly(tetrafluoroethylene), poly(ethylene oxide) (PEO), polyaniline (PANI) and poly(methyl methacrylate) (PMMA).

Table 2.5 Conductivity and Voltage Window of Both Electrolyte (Aqueous and Non-Aqueous) Solutions at Room Temperature

Electrolyte Solution	Density (g/cm^3)	Conductivity (mS/cm)	Potential Window
Aqueous, KOH	1.29	540	1
Aqueous, KCl	1.09	210	1
Aqueous, sodium chloride		171	1
Aqueous, sulfuric acid	1.2	750	1
Aqueous, sodium sulfate	1.13	91.1	1
Aqueous, potassium sulfate	1.08	88.6	1
Propylene carbonate, Et_4NBF_4	1.2	14.5	2.5 to 3
Acetonitrile, Et_4NBF_4	0.78	59.9	2.5 to 3
IL, $Et_2MeIm^+ BF_4$.	1.3 to 1.5	8 (25°C)	4
IL, $Et_2MeIm^+ BF_4$.		14 (100°C)	3.25

Sources: [8, 75, 77]

The advantages of using gel polymer electrolytes are: light weight, flexibility, wider operating window and volatile organic free solvents.

2.5 Separator

The separator is one of the key elements in supercapacitors. It is a porous layer of either a polymer membrane or a non-woven fabric mat. The main function of separator is to prevent physical contact between the electrodes while enabling free ionic transport and isolation of electronic flow (namely, minimizing unintentional electronic discharge). It should be chemical and electrochemical stable. The separator should have sufficient porosity for

large ionic flow. The presence of the separator membrane, though, increases the overall cell's resistance and affects its performance. Therefore, selection of an appropriate separator is critical to the supercapacitors efficiency.

2.5.1 Characteristics of a Separator

As supercapacitors employs aqueous and non-aqueous (organic and ionic liquid) electrolytes, the separator material must be chemically stable against strongly reductive and oxidative environments. It should not exhibit any degradation of stability and a mechanical strength under harsh environment. Small thickness separators are desirable for weight purposes. A suitable porosity is a necessity for ion mobility. According to IUPAC classification, there are three classes of pore sizes: micropores (<2 nm), mesopores (2~50 nm) and macropores (>50 nm) [25]. Too high or too low porosity can adversely impact the cell's performance. The pore size must be smaller than the particle size of the electrode components, including the electrode active materials and its conducting components. In practical cases, separators with proper pore sizes have proven adequate to block the penetration of particles from reaching one electrode directly to the opposite electrode. Wettability of the separator is another important characteristic. The separator should wet easily by the electrolyte and permanently retains it. Wettability eases the process of electrolyte filling in the assembly line and the retaining the electrolyte within the separator pores increases the life-cycle of the supercapacitor. The separator should not shrink over a wide temperature range and should stay flat. There is a typical trade-off between all separator requirements.

2.5.2 Separators in Batteries

In most batteries, separators are either made of nonwoven materials or microporous films. Batteries use separators fabricated from organic materials such as cellulosic papers, polymers, and inorganic materials such as asbestos, glass wool, and SiO_2 when operate near ambient temperatures. In alkaline batteries, the separators are made of either regenerated cellulose or microporous films. Lithium batteries with organic electrolytes mostly use microporous films. A novel microporous separator using polyolefins has been developed and used extensively in lithium ion batteries. The microporous polyolefin membranes in Figure 2.7 are thin (<30 μm) and are made of polyethylene (PE), polypropylene (PP), and laminates of polyethylene. Table 2.6 shows comparative analysis

Table 2.6 Typical Properties of Some Commercial Microporous Membranes

Separator properties	**Celgard 2730**	**Celgard 2400**	**Celgard 2320**	**Celgard 2325**	**Asahi Hipore**	**Tonen Setela**
Structure	single layer	single layer	Tri-layer	Tri-layer	single layer	single layer
Composition	PE	PP	PP/PE/PP	PP/PE/PP	PE	PE
thickness (um)	20	25	20	25	25	25
resistivity (Ω cm^2)	2.23	2.55	1.36	1.85	2.66	2.56
porosity (%)	43	40	42	42	40	41

Source: [43].

of currently used commercial separator in batteries.

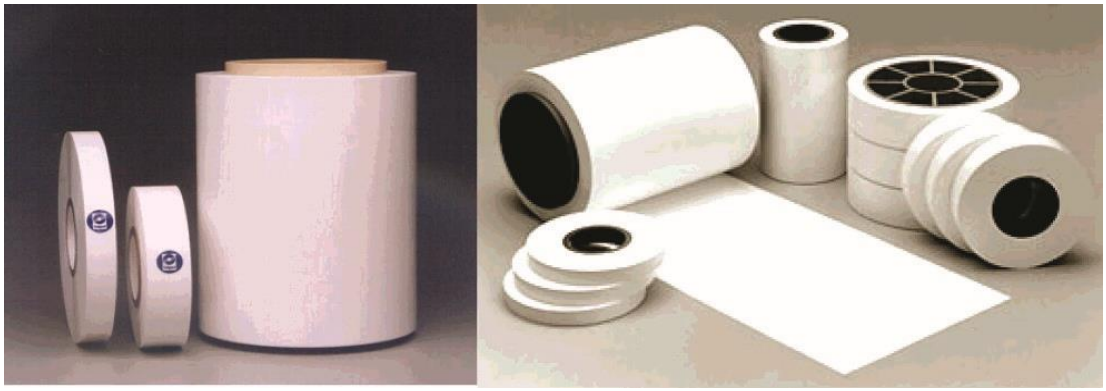

Figure 2.7 Widely used polyolefin separators used in lithium-ion batteries.
Source: [43].

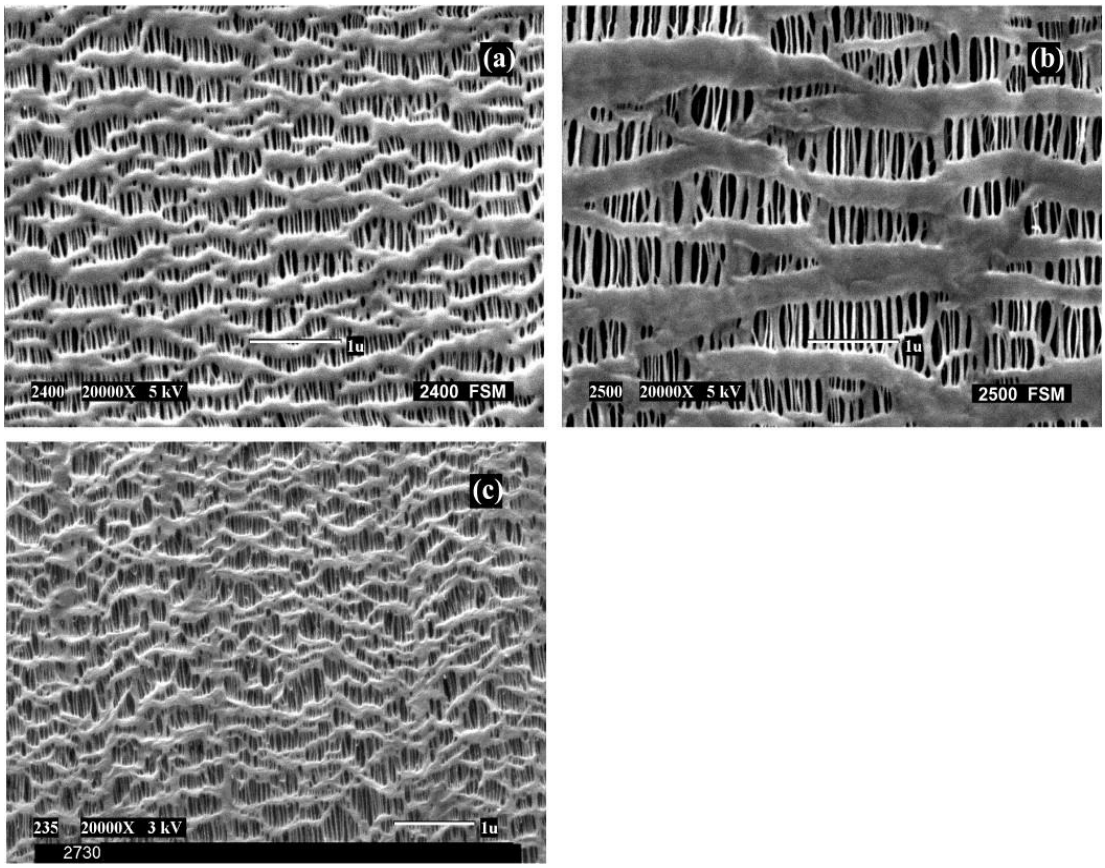

Figure 2.8 Scanning electron micrographs of the surface of single layer Celgard separators used in lithium batteries: (a) 2400 (PP), (b) 2500 (PP), and (c) 2730 (PE).
Source: [43]

2.5.3 Separators in Supercapacitor

Separator materials vary according to electrode materials used, electrolyte choice and temperature of operation. Separators in supercapacitor have been constructed of rubber, plastic, resorcinol formaldehyde polymers, polyolefin films. Such separators have tendency to dry out, to collapse over time, or exhibit poor ionic conductivity [44–46]. Yu et. al used a natural and hierarchically ordered flexible macroporous materials such as egg shell membrane as the separator for supercapacitors. Desirable porous structures for low temperature operation (lower than 100 ◦C) usually have high decomposition temperature (over 200 ◦C), low swelling, and good mechanical strength. Furthermore, it can be concluded that egg shell membrane (ESM) could be also be an excellent material due to its low resistance, fast charge–discharge ability and outstanding cycling stability (92% retention after ten thousand cycles) [47]. SEM of an eggshell membrane, used as a separator is shown in Figure 2.9.

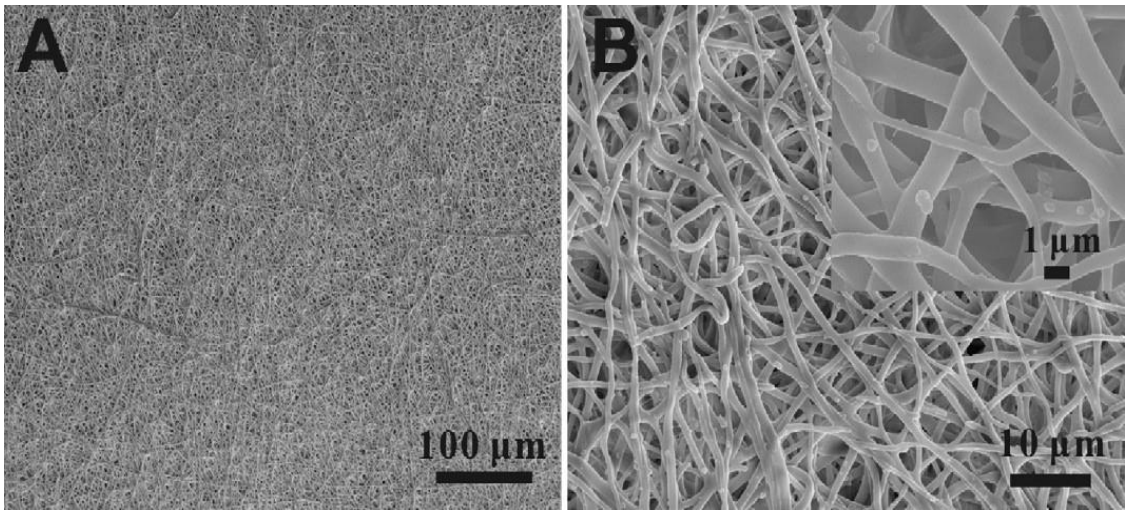

Figure 2.9 SEM image of egg shell membrane used as a separator.
Source: [47].

In another study a supercapacitor with electrodes was fabricated with graphite oxide, reduced by a microwave exfoliation (MEGO) method and a separator, made from a graphite oxide paper (GOP). The separator was formed by a slow evaporation of a graphene oxide solution and by filtration [48]. The study showed that the separator and electrolyte do affect the performance of the supercapacitor. The graphene oxide paper (GOP) does not swell up in octane but significantly swells up in water. The swelling in water caused the membrane width to increase about three times and its porosity and surface became large [48]. Graphene oxide impregnated with water or water based solution tends to show properties similar to Nafion which is widely used for supercapacitor applications.

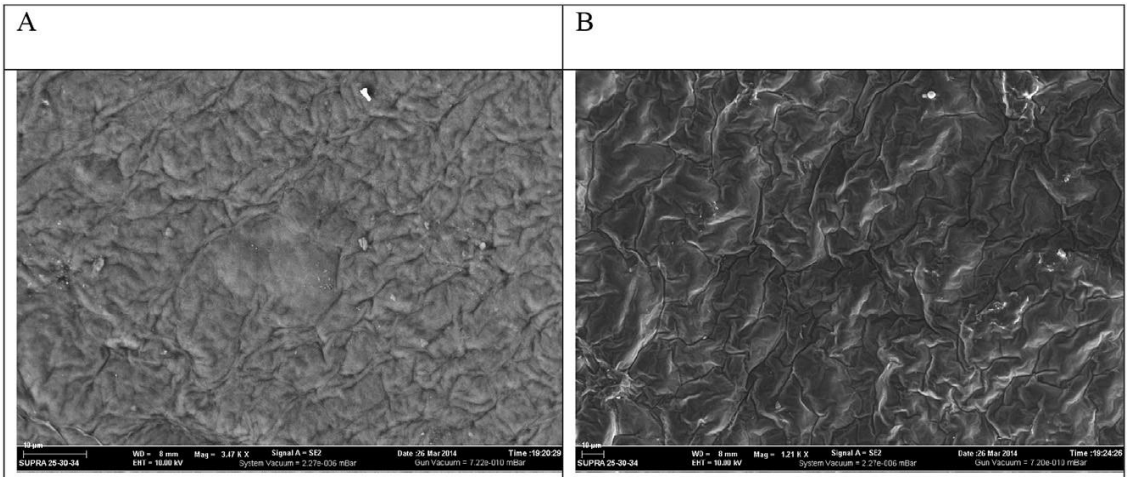

Figure 2.10 SEM image of graphene oxide paper (GOP)(A) bright side, (B) matt side used as a separator in a supercapacitor.
Source: [48].

Macroporous separators based on vinylidene fluoride polymers were prepared successfully using a solvent and non-solvent mixture. The study demonstrated that homopolymer based PVDF is the most appropriate separator for supercapacitor applications. It exhibits higher conductivity than any other commercial separator such as cellulose or Celgard.

Porosity of the separator can be decreased without sacrificing ion conductivity in order to improve the mechanical strength of the separator by pairing it with a liquid electrolyte [49].

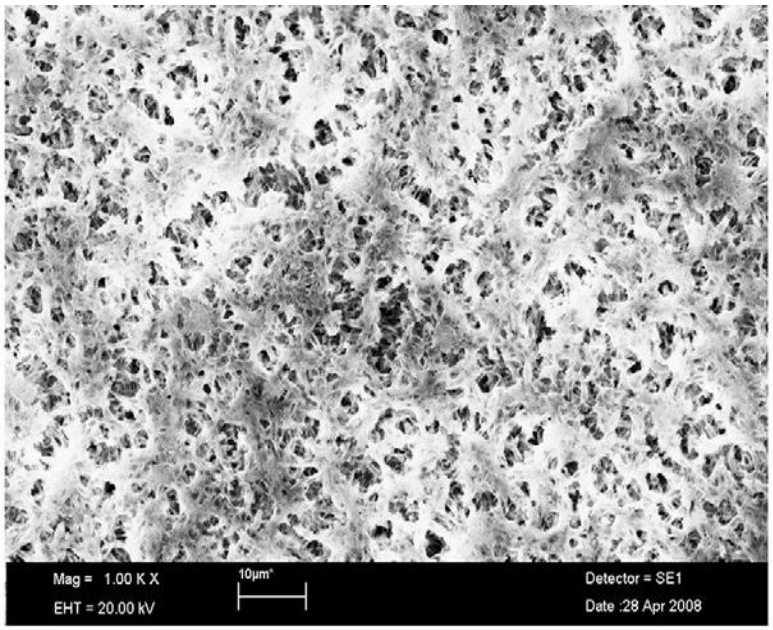

Figure 2.11 SEM image of a Poly(vinylidene fluoride) based macroporous separators for supercapacitors.
Source: [49].

2.6 Electrode Materials used in Supercapacitors

Supercapacitor consists of three key elements: electrode, electrolyte and the separator. In electric double layer capacitor, charge storage mechanism depends on the electrode materials which eventually affect the cell's performance. The principal requirements for the electrode materials include: large surface area, long and stable life-cycle, stability under wide potential window, high electrical conductivity, surface hydrophilicity, minimum reactivity and ability to control morphology and pore size. There are three significant types of electrode materials that have been extensively evaluated. These are: activated carbon, conductive polymer and transition metal based oxides. The problem with activated carbon

is their expense, whereas the oxides have stability issues. However, the requirement for large surface area drives the market towards activated carbon materials.

2.6.1 Carbon-based Material

Carbon is a material which is chemically stable, may be made with large surface area and is a good electrical conductor. It appears in a variety of forms. The most widely used form of high surface area carbon which is cost effective is activated carbon (AC). The process of activating carbon with a precursor such as wood, coconut shell or polymer is called carbonization. It involves heating the precursor in an inert environment at high temperatures (above 800 ˚C) which decomposes the precursor and subsequently leads to its expulsion. Then, the remaining carbon rearrange itself in with irregular bonds thus creating pores. Carbon aromatic rings can have large change in pore size when they undergo through the carbonization process. In order to achieve optimum performance, conditions of the carbonization process must be synchronized for a particular precursor material.

Carbon powders have been also used as a supercapacitor electrodes. These spherical colloidal shape are produced by the combustions of hydrocarbons. It requires a binder for electrode fabrication. Large capacitance was reported for activated carbon/carbon as electrode and sulfuric acid as the electrolyte [50]. The research exhibited the electrode having high surface area and low resistivity with macropore and micropore surface morphology. Another research showed that oxygen content and concentration of acidic surface group on activated carbons have influence on the electrochemical properties [51]. Yoshida et al reported on sheet type electrodes, which are consisted of activated carbon tends to have low resistances. The filling density of activated carbon is affected by

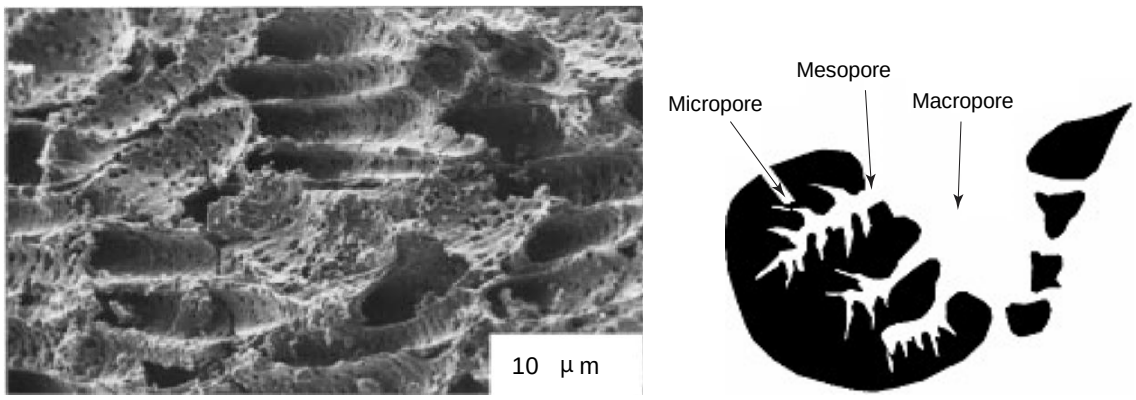

Figure 2.12 (a) Activated carbon produced from coconut shell and (b) relative disposition of the pores in an activated carbon.
Source: [52].

the species and particle size of the activated carbon. Capacitors having sheet type electrode configuration exhibit low internal resistance [53]. The relationship between the ions in the electrolyte and the electrode's pore size substantially influence the capacitance value. Low surface area of activated carbon can exhibit the same capacitance as the high surface area of activated carbon if the pore size and electrolyte ions are synchronized [54, 55]. Electric double layer capacitor performance as a function of pore size distribution were reported in [56]. During the charge discharge process, electrodes with small pores exhibit larger retardation of ion penetration compared with electrodes with larger pores.

There is a substantial interest in the application of carbon nanotubes (CNT) as electrode materials for supercapacitors. The nanoscale tubular morphology can offer properties such as high conductivity and porosity, which are essential for electrode materials. Single walled (SWNT) and multi walled nanotubes (MWNT) have been studied with both non-aqueous and aqueous electrolyte types.

The supercapacitor electrodes prepared from MWNT were first reported by Niu et al. using H_2SO_4 aqueous electrolyte with specific capacitance, power density and energy density of values of 113 F/g, 8 kW/kg and 0.56 Wh/kg, respectively [57]. Though another study reports on a relatively low specific capacitance 15-25 F/g with the same H_2SO_4 concentration with MWNT electrodes [58]. SWNT electrodes provide a specific capacitance of 40 F/g in highly concentrated (6 M KOH) aqueous solution [59], and 20-40 F/g in NaCl aqueous electrolyte [60-62]. Similar results were also reported for 1.0 M $LiClO_4$/propylene carbonate which is a non-aqueous electrolyte by Shiraishi et al.[63] Liu et al. reported that the specific capacitance of SWNTs in acetonitrile electrolyte containing 0.1 M tetra-n-butylammonium hexafluorophosphate which is an ionic liquid is around 280 F/g [64]. The use of carbon nanotube electrode together with ionic liquid is proved to be advantageous because of high conductivity, wider potential window and nonvolatile nature of the supporting electrolyte [65]. Compared with conventional electrolyte, there is a slight capacitance decrease for ionic liquid based supercapacitor but the magnitude is not noteworthy. A research group from Canada reported that redox ionic liquid [66] supercapacitors with activated carbon electrode can increase energy density of the cell. The study used a modified ionic liquids with ferrocene that determines the electroactive ions's polarity thus affecting the energy storage and self-discharge process. There was no previous study on modifying either the cations or anions of ionic liquid that drastically affect the performance of supercapacitor [66].

2.6.2 Conductive Polymer

A large degree of π-orbital conjugations in conductive polymers, such as polyaniline (PANI), polypyrrole(PPy), poly-(3,4)-ethlenedioxythiophene (PEDOT), polyacetylene, [67] can be oxidized or reduced electrochemically by withdrawal or injection of electrons. The charge storage mechanism in conducting polymers involves charge accumulation by doping interaction throughout the backbone of the polymer material and is illustrated in Figure 2.13.

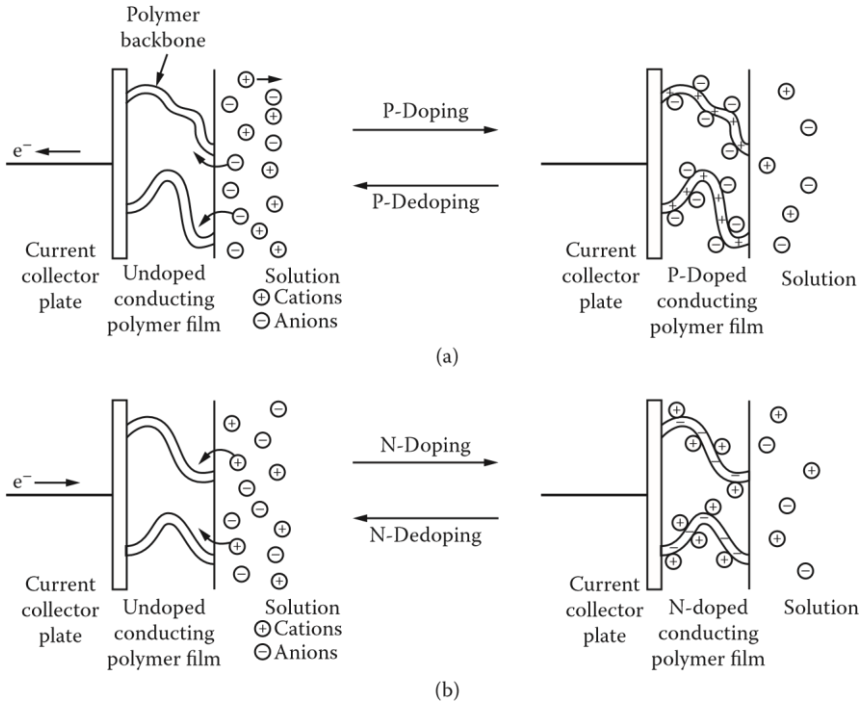

Figure 2.13 Charge storage mechanism in supercapacitors based on conductive polymer materials.
Source: [68].

Conductive polymers are prone to swelling and cracking over time due to the fast charge discharge process. A large amount of irreversible reduction over many cycles can cause the relaxation of the polymer. Slower charging rate is used to avoid the relaxation effect [69].

The potential window for conductive polymer is limited due to the lack of oxidation states. This potential window is restricted leads to polymer breakdown through over-oxidation [70]. The lack of stability during oxidation and the irreversible characteristics outweighs the positive aspects of conductive polymers as electrode materials.

Work by Yan et al. showed that incorporation of additives in CNT can increase percolation and mechanical strength during the doping process, helping the electrode to preserve 94% of the original capacitance after 1000 cycles compared with retention below 50% without the CNT additive [71].

2.6.3 Transition Metal Oxide

Transition metal oxides, especially ruthenium (RuO_2), vanadium (V_2O_5) and manganese (MnO_2) are widely studied in the field of developing pseudocapacitance electrodes [72–74]. Oxide materials exhibits multiple oxidation states within the specific potential window of the electrolytes. Large conductivities is related to the poly-crystalline nature of the oxide. Among the three oxides, Ruthenium dioxide ($RuO_{2)}$ is widely used because it is highly reversible, exhibits very high capacitance, and presents good life cycle. Ruthenium is highly toxic and expensive. This prevents it from becoming material of electrode choice. V_2O_5 (vanadium oxide) exhibits the highest specific capacitance but also poor life cycle. Manganese oxide is a safer material and cheaper than ruthenium. Due to its high capacitance, better cycle stability, and wide potential window manganese is the emerging replacement for RuO_2 [75].

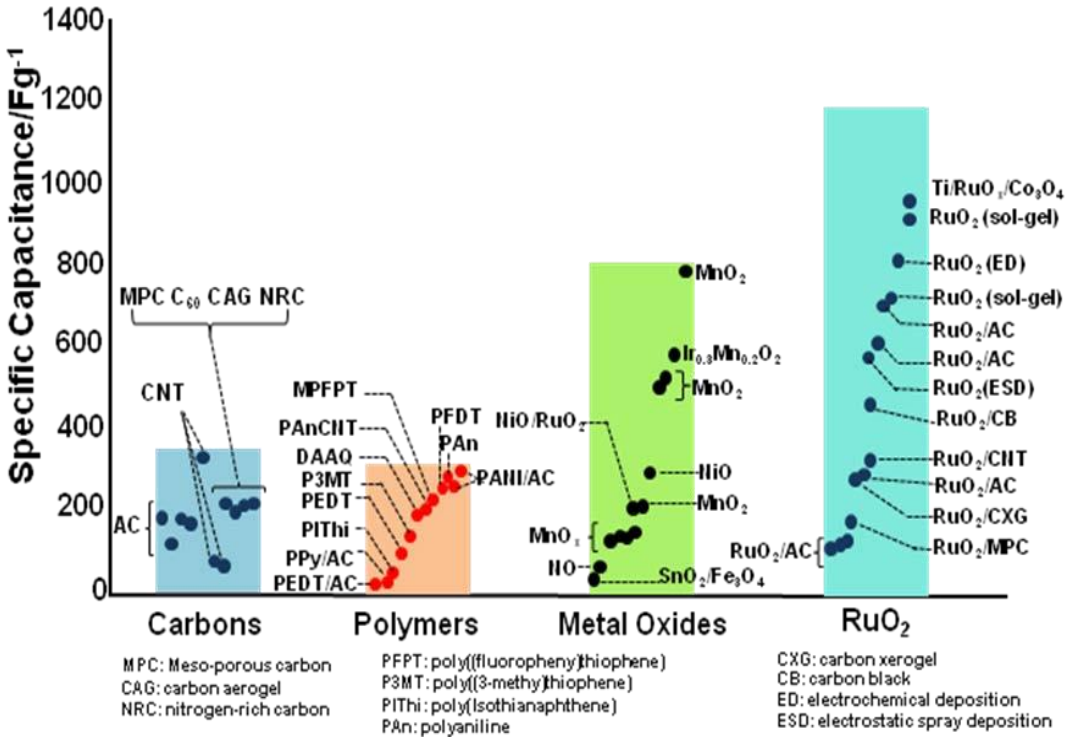

Figure 2.14 The comparative capacitive performance for various carbon and pseudocapacitor electrodes.
Source: [6].

2.7 Supercapacitor Cell Design

A Supercapacitor cell consists of two active layers with a separator between them. The separator is wetted with an electrolyte as indicated in Figure 2.15. The overall performance of a supercapacitor is limited by the internal resistance, which comprises the ionic and electrical resistances. The ionic resistance depends on the ionic conductivity of the electrolyte, the porosity of the electrode, separator and the thickness of the electrode. The contact resistance between the electrode's particles and the contact resistance between the current collector and the electrode are the two major sources of electronic resistance. Surface treatments and conducting coating on the current collector have shown a resistance

decrease for the electrode/current collector interface. The design of nanostructured current collectors with an increased contact area is another way to control the interface between the current collector and electrode. In order to create a good contact, electrode materials are directly deposited or grown on the collector material. Spray coating, drop casting spin coating and application of conductive paste are widely used techniques in this regard [77]. One common technique is the use of silver paste which can adapt to the surface roughness of active materials in order to minimize contact resistance. Gold and thin lead films can significantly enhance interface integration causing better performance [78].

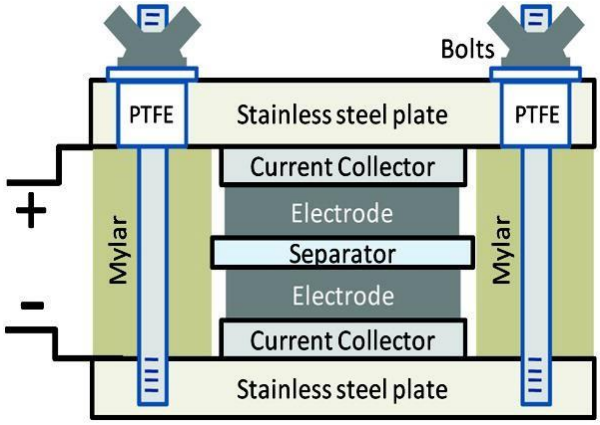

Figure 2.15 Schematic of a supercapacitor cell assembly.
Source: [76].

Test fixture configurations for laboratory experiments closely mimic the unit cell configuration of a packed cell. Two electrode test cells are commercially available or can be designed and fabricated in-house. A cell fabricated from two stainless steel plates is shown in Figure 2.15 [76].

CHAPTER 3

EXPERIMENTAL PROCEDURES

3.1 Functionalization of Carbon-nanotubes

Single wall carbon nanotubes (SWCNT) were obtained from Nano Integris, Canada, with a purity better than 95% (Isonanotube-S). The purchased nanotube were synthesized using arc discharge method. The powder form is comprised of 100% semiconductor nanotubes without binders or fillers used. This forms have been formulated so that they are easy to use and re-suspend. The diameter range of the single walled nanotube is from 1.2 nm to 1.7 nm. The mean length of the single wall carbon nanotube is approximately 1 μm. Catalyst impurities presented in the carbon nanotubes are reported to be less than1% by mass. As the purchased tubes have semiconductor properties and very little catalyst, reflux process is unnecessary. Sodium dodecyl sulfate (SDS) [FW 288.38, Fisher scientific] has been employed as surfactant in the suspension of the tubes in water; the soap eliminates tube agglomeration. Aqueous solutions were prepared using deionized water. Single wall carbon nanotubes were functionalized with polymers. *P*-type and *n*-type tubes were obtained by wrapping the tubes with PVP (Polyvinyl-pyrrolidene) and PEI (Ethylene imine polymer solution, Mr 600000- 1000000, Fluka), respectively [79, 80]. The *p*-type and *n*-type nanotubes were suspended using a horn probe sonicator (Sonics, maximum output 100W, tip diameter approx. 4 mm) for 8 hours. Each layer was drop-casted on a hydrophilic TriSep softening filtration TS80 membrane (Sterlitech) under vacuum condition. TS-80 filter is made of polyamide with pore size approximately 150 Dalton. It

has a wide pH range (pH between 2 and 11). The thickness of each SWCNT film was estimated as a few microns.

3.2 Scanning Electron Microscope (SEM)

SEM, a non-destructive technique utilizes a condensed, accelerated electron beam to focus on the surface of a sample. The electron beam hits the surface of the sample instead of rebounding immediately, it penetrates the sample through some distance before it collides with a surface atom and a region of primary excitation where signals are produced [81]. The most common signals used for imaging are secondary electrons, backscattered electrons, and characteristic X-rays. At normal conditions, the secondary electrons are created through inelastic surface scattering and can reach the detector in large numbers, depending on incidence angle. A topographic information describing the surface morphology is then generated. In order to prevent charging that can blur the image quality at higher resolution, samples must be conductive. For non-conductive samples, a thin conductive coating is sputtered on top of the sample.

Backscattered electrons are higher energy electrons deflected elastically or scattered back to the detector. This backscattering provides specimen composition data because heavier elements produce larger backscattering intensity, resulting in brighter images than those produced by the lighter elements [79, 80]. Characteristic X-rays can reveal the distribution of chemical elements. Drawbacks of an SEM include the requirement for the sample to be in a solid phase and stability inside vacuum conditions. Normally, wet samples, and moisture-containing organic materials and clays are not compatible with SEM [83]. In this dissertation, SEM images were taken with a LEO

1530VP ultra high resolution field emission scanning electron microscope (FE-SEM), which was operated at an acceleration voltage of 10 kV. The samples were put on a double-face conductive adhesive and were mounted on a 1.3 cm diameter aluminum stud.

The samples were coated with a carbon film using a sputter coater (JEOL JFC1300 Auto fine coater). Areas ranging from 5 μm^2 up to 1 cm^2 can be imaged under a scanning mode. Magnification range as large as 30,000X can be achieved resulting in a spatial resolution of 100 nm.

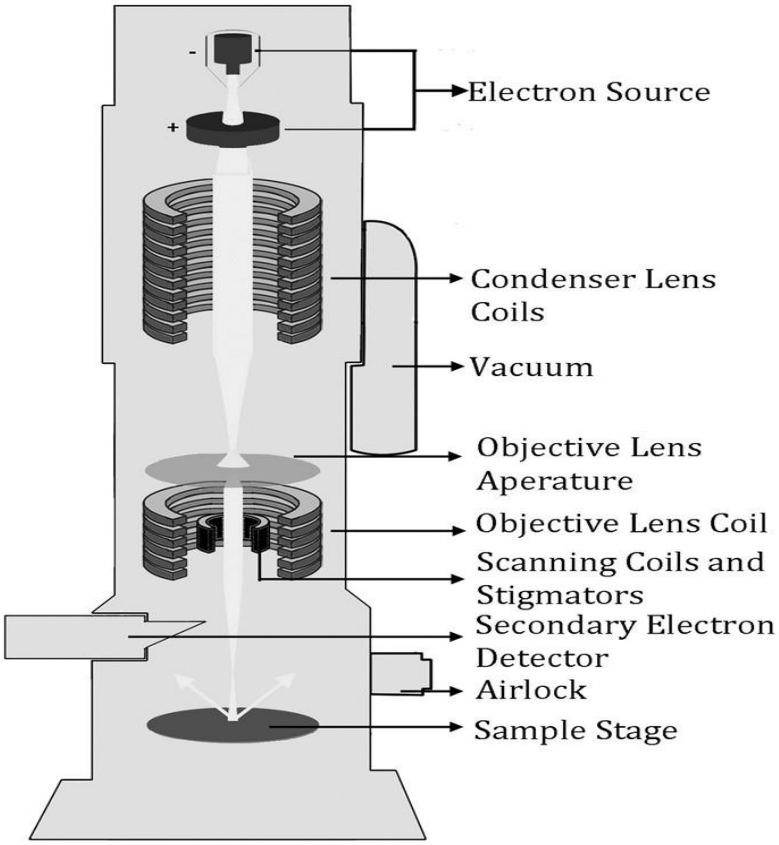

Figure 3.1 Schematic of a Scanning Electron Microscope.
Source: [81].

In the study of supercapacitors, SEM can provide an important information about the surface morphology of the cell components, especially the separator membrane porosity and morphology of the electrodes [84]. Investigation was made of the material surface before and after experimentation.

3.3 Keithley I-V Measurement

Keithley 236 Source-Measure Unit (SMU) is a fully programmable instrument, capable of sourcing and measuring current, or voltage simultaneously. There are four instruments build in one unit: voltage source, current source, measurement systems of voltage and current. The instrument supply voltage from 100 μV to 110 V, and current from 100 fA to 100 mA while acting as voltage and current source, respectively. It is also capable of measuring voltage from 10 μV to 110 V and current from 10 fA to 100 mA. Both source voltages and source currents settle to specified accuracy in less than 500 μs. Programmable delay and fast, integrating measurement capability can provide coordinated source-measurement time delay of the order of 1 ms.

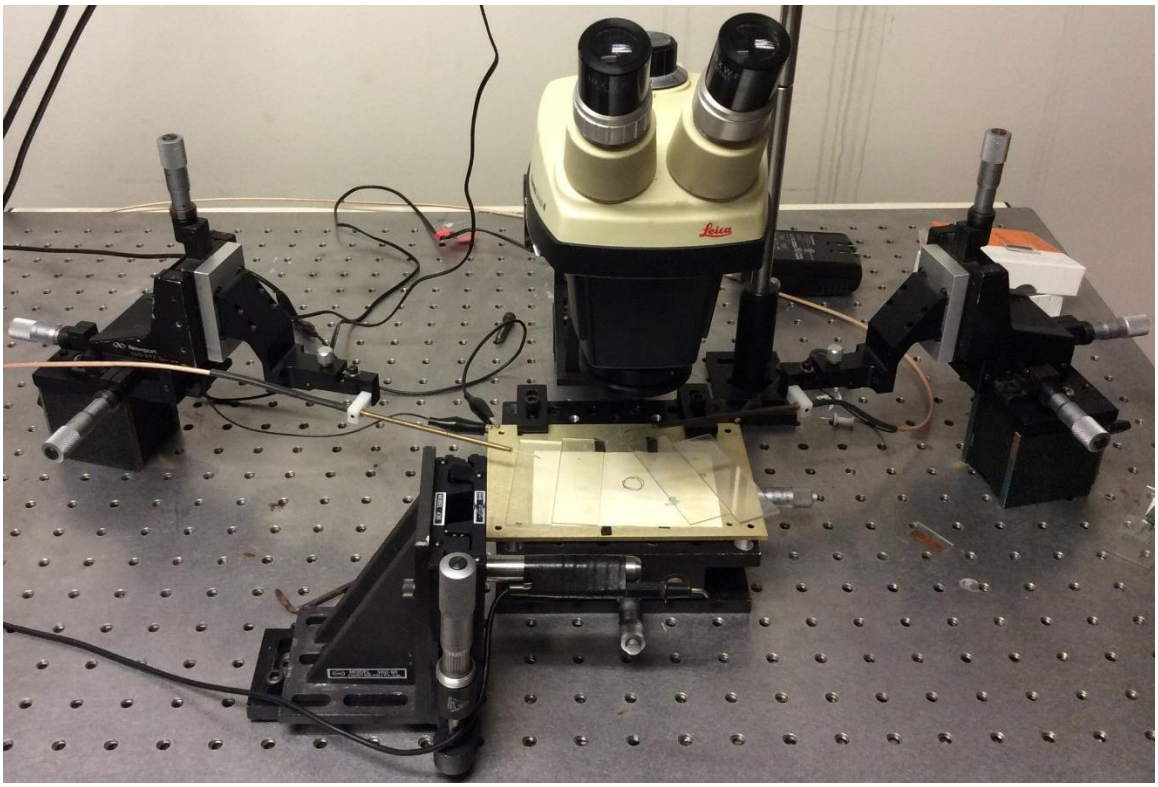

Figure 3.2 I-V characteristics measurement unit using Keithley 236.

3.4 Agilient Gate Current Measurement

The Keysight Technologies, Inc. U2722A USB modular source measurement unit has fast response time, and voltage and current programming/readback with high accuracy measurement capabilities. The U2722A is capable of four-quadrant operation, acting as a current source, as well as a current sink (load) with both polarities of the output voltage. The Keysight Measurement Manager (KMM) is an application data viewer software that comes with the U2722A Series USB modular instruments. This software is designed to help you perform quick device configuration, data logging and data acquisition. The software interfaces a Windows operating system. The unit was used to monitor *in-situ* gate currents when biasing the gate structure during electrochemical measurements.

3.5 Electrochemical Measurement

A three-electrode cell system was used to evaluate the electrochemical performance using cyclic voltammetry (CV). Chrono-potentiometric charge-discharge and Electrochemical Impedance Spectroscopy (EIS) techniques are employed with a two electrode set-up, with and without the structured gate electrode. All these methods have been performed on a compact and modular potentiostat/galvanostat Autolab PGSTAT204 (Metrohm) at room temperature. It can operate in all electrode settings (2-electrode, 3-electrode and 4-electrode). The PGSTAT204 includes a built-in analog integrator. It can be used for most of the standard electrochemical techniques in combination with NOVA software. The Autolab can perform EIS measurements with a built-in FRA32M module. This module allows one to perform both potentiostatic and galvanostatic impedance measurements over a wide frequency range of 10 μHz to 32 MHz. Data may be presented in both Nyquist and Bode plot formats. Graphical equivalent circuit, as well as modified circuit simulation and fitting are also possible. Both aqueous solution and non-aqueous solutions were employed as electrolytes: these include 1 M NaCl, and ionic liquid $C_8H_{15}F_6N_2P$ (1-n-Butyl-3-methyl-imidazolium hexafluro-phosphate). Aqueous electrolyte solution was prepared by mixing the salt in deionized water. Ionic liquid was purchased from Alfa Aesar. A platinum thin wire and a saturated Ag/AgCl electrode were used as the counter and the reference electrodes, respectively for three electrode configuration. All tests were performed at the room temperature (25^{o}C).

The construction of electrodes varied: graphite rod was used as the working electrode for some of the experiments with salt water as electrolyte. Carbon tape on copper interfaced with carbon powder was used with the ionic liquid. Carbon nanotube based structured separator was made as sandwich of a few functionalized layers. All nanotube

based electrodes were drop casted onto a polyamide TS80 membrane and dried before cell assembly.

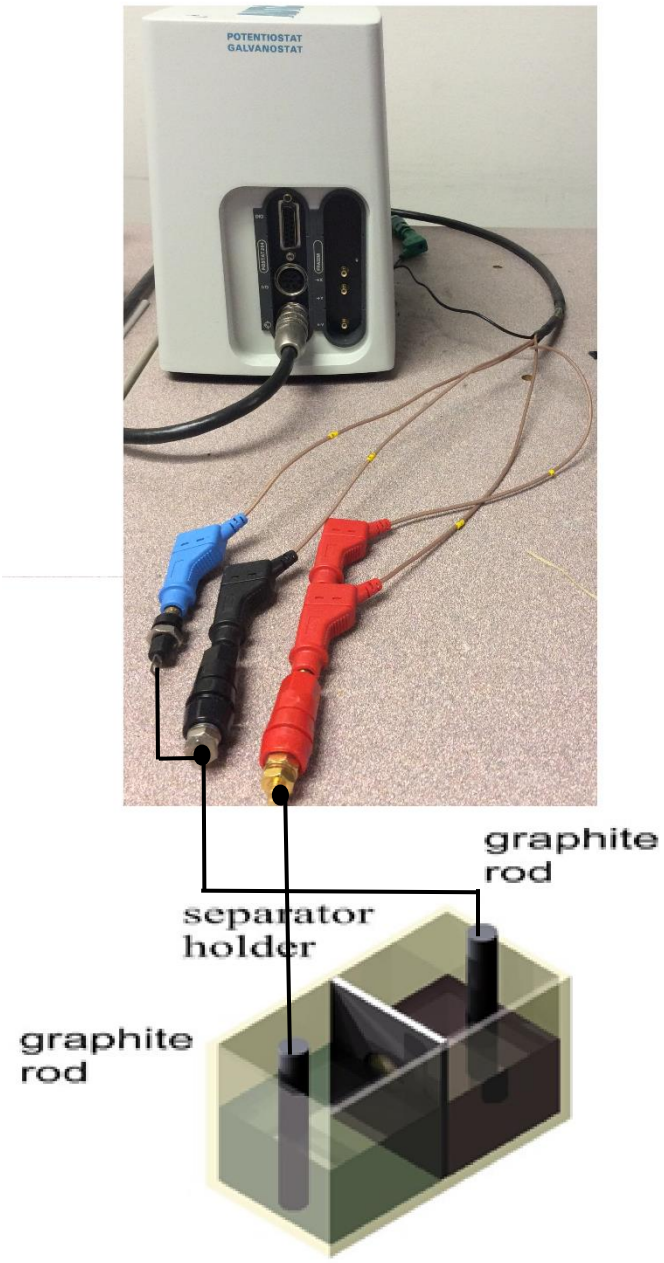

Figure 3.3 The 2-electrode experimental configuration of a compact Autolab PGSTAT204 potentiostat/galvanostat with working electrode (red), reference electrode (blue) and auxiliary electrode (black).

A CV test is carried out by applying a cyclic voltage sweep at a scan rate of dV/dt within a specific voltage range while measuring the current through the cell. A galvanostatic charge-discharge (GCD) test consists of two steps: charging and then discharging of the supercapacitor at a constant current over a specific voltage range. The operating voltage range is determined by the nature of the electrolyte used. The rated voltage includes a safety margin against the electrolyte's breakdown, a point at which the electrolyte decomposes or chemical reactions occur. Standard supercapacitors with an aqueous electrolyte are typically specified with a rated voltage of 1.0 V, and the working voltage for ionic liquids is typically about 2.5 V.

CHAPTER 4

ELECTROCHEMICAL METHODS

Supercapacitor is an energy storage device which consists of multiple components. To ensure proper functioning of each individual component and their synergistic effect electrochemical characterization and diagnosis techniques are performed. Three types of electrochemical methods are used for testing supercapacitor as well as any electrochemical capacitor. Mostly used transient techniques are: cyclic voltammetry (CV), chronopotentiometry (which is also known as charge discharge) and stationary technique which is electrochemical impedance spectroscopy (EIS).

4.1 Electrochemical Cell Set-up

Two main configurations are used for characterizing either a supercapacitor device or a supercapacitor electrode. A three-electrode cell setup is a fast screening process performed to analyze electrode materials, their associated structure and optimization. But in order to validate performance of a supercapacitor in practical operating conditions, two-electrode setup is typically used.

4.1.1 Three Electrode Cell Design

Generally, a three-electrode electrochemical cell consists of three electrodes: working electrode (W), reference electrode (R) and auxiliary or counter electrode (C). A working electrode is the electrode under test. The counter electrode is incorporated so that current can flow from the counter to the working electrode. Pt wire or foil are mostly used as

counter electrodes. A third electrode is the reference electrode and exhibits an ideal non polarizable behavior. The main purpose of this electrode is to maintain a constant voltage over a varying applied current; the working electrode voltage is accurately measured in reference to it. There are several reference electrodes available, such as Reversible Hydrogen Electrode (RHE), Saturated Calomel Electrode (SCE) and Silver/Silver Chloride Electrode (Ag/AgCl). All three electrodes are immersed in the electrolyte solution. Figure 4.1 shows a schematic view of conventional three-electrode setup.

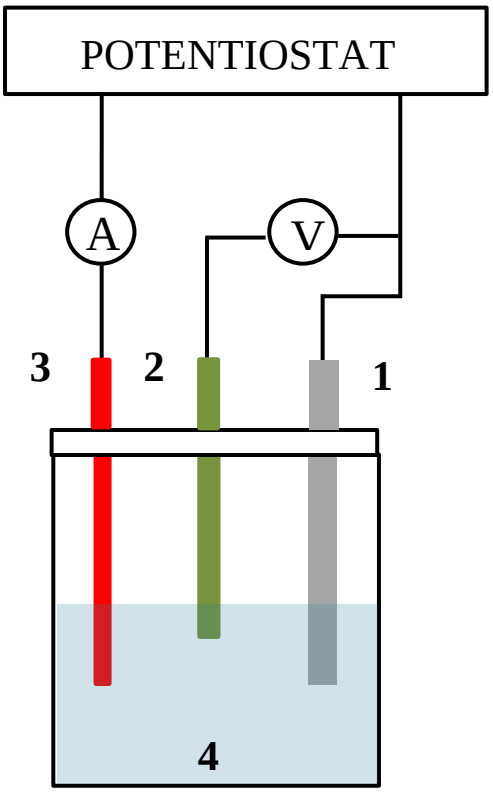

Figure 4.1 A conventional three electrode cell set up where (1) Working electrode (grey), (2) reference electrode (green), (3) Auxiliary or counter electrode (red) and (4) electrolyte (light blue).

4.1.2 Two Electrode Cell Design

The two electrode cell design consists of two active electrode surfaces: one for the positive and one for the negative polarities. Either electrode is connected to a current collector – a metal plate with large conductivity. A separator is placed in between the two electrodes. It is a porous membrane that allows ion flow and is saturated with the electrolyte. For a commercial assemble test cell, proper sealing is also added depending whether a rolled cell or pouch cell. In small scale research, a polybag which is electrically insulating, moisture resistant used as an ideal sealant. The electrolyte solution can be delivered into the test cell externally.

4.1.3 Significance and Differences of Three and Two Electrode Configuration

In several important aspect, two-electrode test and packaged cell and three-electrode cells are different from each other. Three-electrode configuration provides information only for the working electrode which contains the material being analyzed for a particular applied voltage window. The potential across the counter electrode in a three electrode configuration is not controlled and measured. Three-electrode configuration does not require full-cell assembly; only half-cell is needed. Information on individual electrode in 2-electrode setup is possible only if the two electrodes are similar. For asymmetrical supercapacitor, as the electrodes are not identical, it is not easy to extract information from individual electrodes. In these cases, three electrode configuration can distinguish the individual contributions from the two electrodes [87]. Khomenko et al. mentioned the dependence of measured capacitance values based on test cell configuration [86]. Composite electrode made of multi-walled carbon nanotubes and two conducting polymers

were measured in both 2-electrode and 3-electrode configurations shown in Figure 4.2 and the measured capacitance shown in Table 4.1.

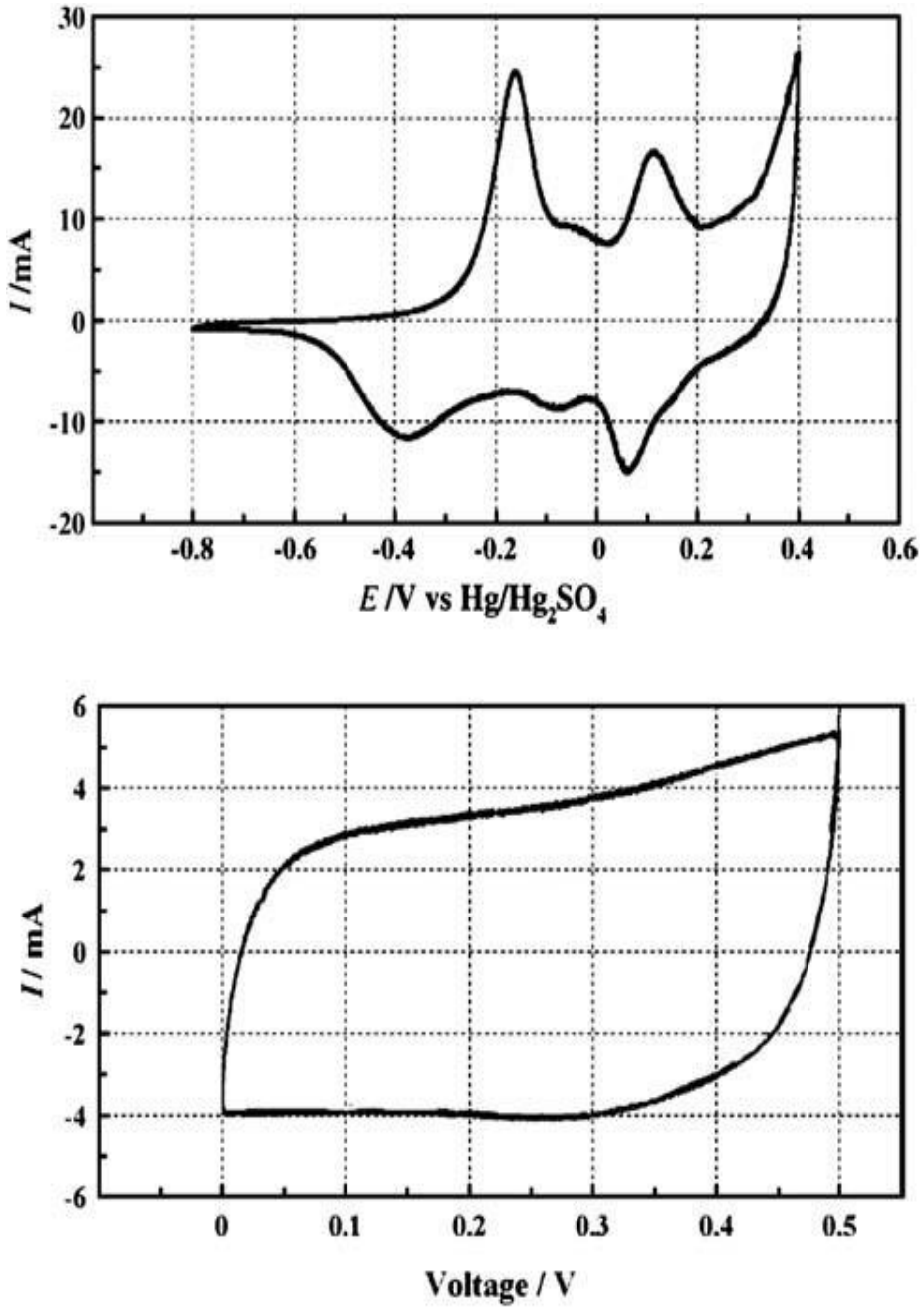

Figure 4.2 (top) CV of three-electrode cell PANI/MWNT electrode in 1M H_2SO_4 at 2 mV/s scan rate, (bottom) CV of symmetric capacitor based on PANI/MWNTs composite electrode in 1M H_2SO_4 at scan rate, 2 mV/s.
Source: [86]

Table 4.1 Dependence of Specific Capacitance of a Composite Electrode on the Measurement Technique used

Composite	Three-electrode cell		Two-electrode	
	CV (F/g)	Galvanostatic discharge (F/g)	CV (F/g)	Galvanostatic discharge (F/g)
PPy/MWNTs	506	495	192	200
PANI/MWNTs	670	650	344	360

Source: [86].

As seen from Table 4.1, three-electrode system gives different capacitance values than the two electrode system. The three-electrode configuration is valuable for the investigation of the material's chemistry, such as diffusion, or Faradaic reactions. However, this method can lead to large errors when projecting the capacitance and energy storage of an electrode used for supercapacitors if the potential window, charging rate and methods of calculation are not chosen properly.

The active material and the thickness of the electrode are also factors that affect the measured capacitance. Supercapacitor electrodes are typically constructed with different thickness for high power density (about 10 μm thick) and for high energy density (several hundred microns thick) [87]. Therefore, laboratory scale test electrodes should be of comparable thickness, to avoid overstatement of the material's performance. The thickness dependence, of capacitance of a SWCNT-based two-electrode cell in an aqueous electrolyte, has been studied [87].

4.2 Cyclic Voltammetry (CV)

Cyclic voltammetry is a versatile and widely used technique in the field of electrochemistry. It has the ability to provide qualitative and quantitative studies about electrochemical kinetics, reaction reversibility and mechanisms and consequences of electrode structures on these parameters. This method also determines the appropriate voltage window for a particular electrode. The main idea is to apply a linearly varying voltage to the working electrode with respect to a reference electrode bounded by low and high values [88, 89]. The linear waveform is cyclic and one measures the resulting current between the working and counter electrodes. The voltage applied can be expressed as [90]:

$$E = E_0 + vt \tag{4.1}$$

$$E = E_0 + 2v\lambda - vt \tag{4.2}$$

Equations (4.1) and (4.2) are valid when $0 \leq t \leq \lambda$ and $\lambda \leq t \leq 2\lambda$, where E_0 is the initial voltage and λ is the time at the maximum potential ($E_0 + v\lambda$), indicating the entire potential scanning from E_0 to $E_0 + v\lambda$ then back to E_0 requires a time of 2λ. Equations (4.1) and (4.2) describe the forward scanning and reverse scanning voltage rate shown in Figure 4.3. The linear slope of the forward and reverse scan process is called the scan rate *v* and is expressed in Volt per second (Vs^{-1}). The values of initial potential and time to reach maximum voltage can be adjusted independently according to the desired potential scan range. Figure 4.3 shows two potential vs time curves at two different scanning rate, high scan rate (black) and low scan rate (red). To complete a CV cycle, more time is needed if the potential scan rate is slower. In order to study electrode kinetics, scan rate is important. If the potential

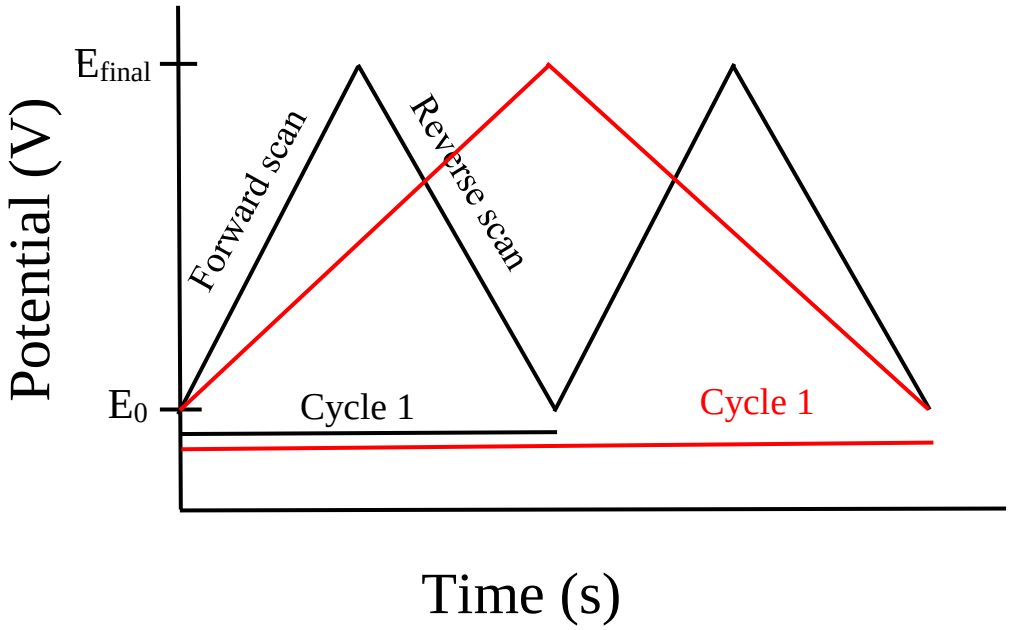

Figure 4.3 Potential vs time curve used for a typical cyclic voltammetry method for a high (black) and low (red) scan rate.

scan rate is too fast, the electrochemical reactions on the electrode might not be able to follow the electrode potential change. It will be reflected on the cyclic voltammetry response which is a current vs potential plot for a specific scan rate for either 2- electrode or 3- electrode configuration shown in Figure 4.2. The reaction kinetics can be extracted qualitatively and quantitatively from the scan rate dependence of a cyclic voltammetry curve. The voltage limit is restricted by the electrolyte degradation or by electrode oxidation. In a typical cyclic voltammetry curve, the current passing between the working and counter electrode is recorded as a function of electrode potential shown in Figure 4.2.

Capacitance can be calculated by the total charge transfer during forward and backward scanning process of CV for the potential range E_1 and E_2 which are lower and upper potential.

Charge Q can be obtained by integrating the area of the enclosed CV curve:

$$Q = \int_{t=0(E_1)}^{t(E_2)} i(E)\, dt \tag{4.3}$$

The capacitance can be calculated using Equation 4.4:

$$C = \frac{1}{v*|E_2-E_1|} \int_{t=0(E_1)}^{t(E_2)} i(E)\, dt \tag{4.4}$$

An ideal double layer capacitance behavior is denoted by the rectangular shape shown in Figure 4.4. The charge storage is purely electrostatic in this case. When an electrochemical capacitors are associated with a resistive component, the measured current exhibits a linear trend. When the electrode undergoes a redox reaction in the operating voltage window, the

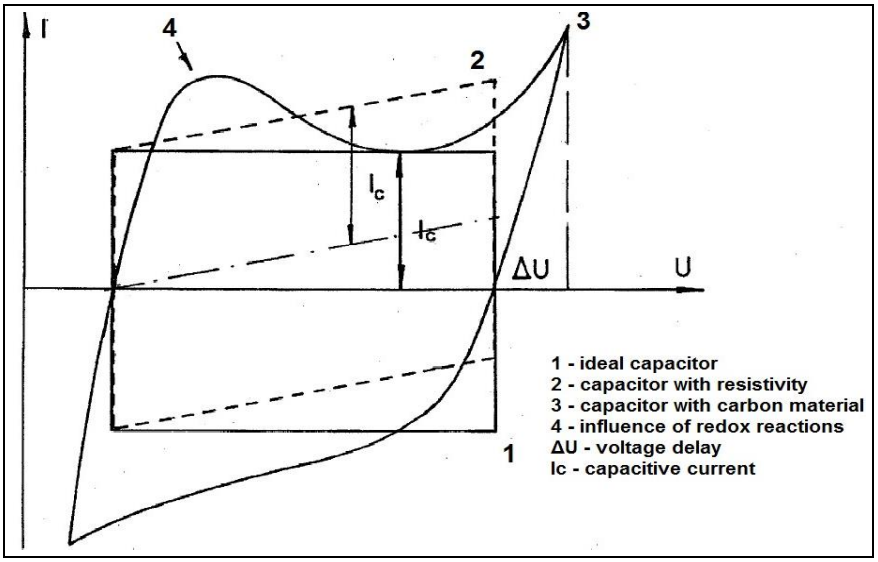

Figure 4.4 Comparison of various types of electrochemical capacitors with ideal capacitors using cyclic voltammetric curve.
Source: [28]

charge is measured as a function of V. The contribution from this capacitance is called a faradaic or pseudo capacitance. The deviation from parallelogram shape and the presence of prominent peaks are evidence for pseudo capacitance behavior. Cyclic voltammetry can also provide information about the degree of reversibility of redox reactions. A mirror image of charging and discharging profiles represents a reversible reaction [89].

4.3 Chronopotentiometry

Chronopotentiometry is an electrochemical method where current is applied to the working electrode and the voltage is measured with respect to a reference electrode as a function of time. The process is also called galvano-static charge discharge and applies a constant current [92]. The charging cycle is performed at a specific current rate from initial voltage to maximum voltage. A discharge cycle is conducted from maximum voltage to zero volt at a specific current rate. The presence of resistance component (equivalent series resistance, (ESR)) in electrochemical capacitor can be detected using an ohmic drop in the charge-discharge curve as seen in Figure (4.5).

This technique is different from cyclic voltammetry since the voltage is measured for a given fixed current value. This method assesses the cell's capacitance, resistance and cyclability (namely, repeatability under charge-discharge cycles). For pseudo-capacitor, the chrono-potentiometric curve is not as linear as it is for a double layer capacitor.

The capacitance of supercapacitor can be calculated from the slope of the discharge portion of the curve using Equation 4.5:

$$C = \frac{I\,\Delta t}{\Delta V} \tag{4.5}$$

where I is the applied discharge current, Δt is the discharge time to go from maximum to minimum voltage and ΔV is the voltage window specified during discharge process [92].

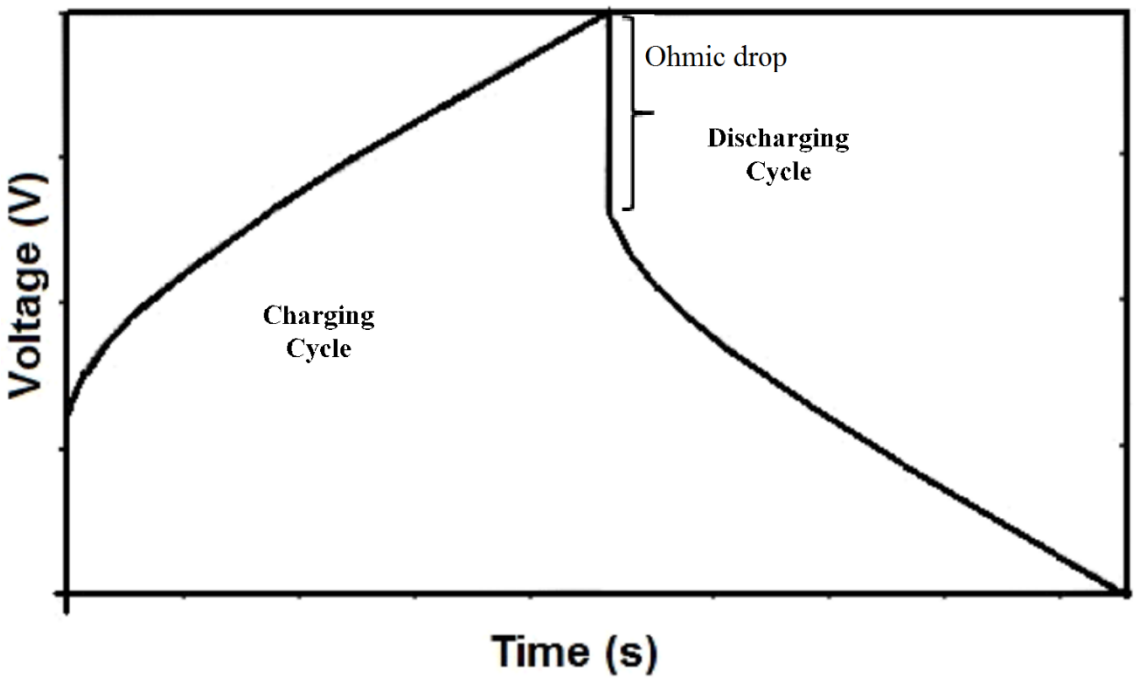

Figure 4.5 Typical charge discharge curve for an electrochemical capacitor electrode.
Source: [90]

Electrolytic solutions have intrinsic resistance (R_{sol}) in the cell. Some potentiostats can compensate for electrolytic solution resistance but a portion of uncompensated resistance will remain between the working and reference electrode. The potential that the potentiostat records may not be the same potential experienced by the analyte in the solution due to the uncompensated resistance during measurements. That phenomenon is called ohmic drop.

The series resistance can also be calculated from the initial voltage drop (V_{drop}) occurs at the discharge cycle using Equation (4.6) [93]:

$$R = \frac{V_{drop}}{\Delta I} \quad (4.6)$$

Ohmic drop should be minimized as much as possible. It can be mitigated by decreasing solution resistance (R_{sol}) thus decreasing the uncompensated resistance [93]. For example, an electrolyte with high conductivity and large concentration can achieve that. One can also decrease the distance between working and reference electrode as much as possible.

4.4 Electrochemical Impedance Spectroscopy

Electrochemical impedance spectroscopy is an important technique for characterizing the properties of electrode-electrolyte interfaces. Capacitance and equivalent circuit model of a supercapacitor can be derived from electrochemical impedance spectroscopy (EIS) data. The technique adds a small perturbation AC signal to the DC component over a wide frequency range while the current is measured. Frequency response analyzer (FRA) module is employed to obtain the EIS data. The EIS measurements have some basic requisites:

i. The system response and the perturbation signal must have a linear relationship.

ii. During the measurement, the system must be stable.

Under steady state condition, if an external perturbation AC voltage is applied to the system, a net current will be observed. If the AC signal amplitude is small then the response observed will be approximately proportional to the applied voltage. The FRA32 analyzer assesses the impedance of the overall cell as a function of certain applied frequency range

from 100 mHz to 50 kHz. Therefore, the applied voltage signal is

$$v(t) = V_0 \cos(2\pi f t) \tag{4.7}$$

The current response of applied voltage will be:

$$i(t) = I_0 \cos(2\pi f t - \phi) \tag{4.8}$$

V_0 is the applied potential amplitude, I_0 is the amplitude of the current response, f is the frequency of the sinusoidal signal (Hz), t is the time, i(t) is the current response over time and φ is the phase difference between applied voltage and current. The impedance is then defined as [28]:

$$Z = \frac{v(t)}{i(t)} = \frac{V_0}{I_0} * \exp(j\phi) \tag{4.9}$$

In general impedance of overall cell is denoted as:

$$Z = Z' - jZ'' \tag{4.10}$$

Z' and Z'' represent the real and imaginary part of the impedance of the overall cell. The impedance responses recorded by the frequency response analyzer is represented normally in two graphical ways: Nyquist plot and Bode plot. Nyquist plot shows the relationship between the real part and imaginary part of the impedance. Bode plot exhibits the

magnitude versus frequency plot as well as phase versus frequency of the impedance measurements. An example of a Nyquist plot is shown in Figure 4.6.

The performance characteristics of electrochemical capacitors differ somewhat from those of conventional capacitors. According to Kotz in Figure. 4.6, the impedance plane represents an ideal capacitor and a simplified electrochemical capacitor, both having the same ESR (equivalent series resistance at 1 kHz). The ideal capacitor exhibits a vertical line; whereas the electrochemical capacitor starts with a 45° impedance line and approaches an almost vertical line for very low frequencies. The non-vertical slope can be easily reproduced by replacing the capacitance expression with a constant phase element

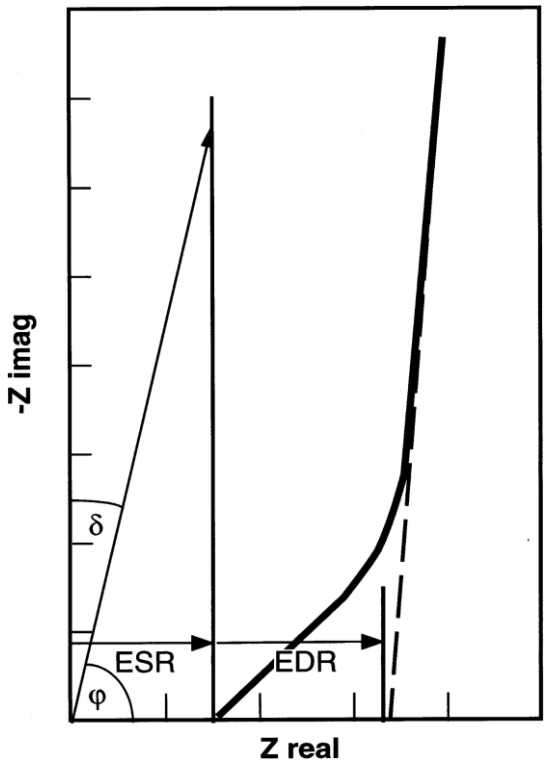

Figure 4.6 Nyquist plot of an ideal capacitor (vertical thin line) and an electrochemical capacitor with porous electrodes (thick line).
Source: [28].

(CPE). The parameter replaces every jω expression with $(j\omega)^p$, where $0<p<1$,. The case for p=1, represents an ideal capacitor with no frequency dependence is mentioned [28]. The 45° region (Warburg region) is a consequence of the distributed resistance/capacitance in a porous electrode was also specified in the analysis. At the high frequency region, the resistance as well as the capacitance of a porous electrode decreases because only part of the active porous layer is accessible to the ions. The electrochemical capacitor may be represented by an ideal capacitor with an ESR increased by the equivalent distributed resistance (EDR) [28]. EIS measurements are also related to physical properties of the cell. The concentration of ion, types of ions and temperature of operation, all affect the solution resistance. ESR depends on the cell geometry and current flow path. Diffusion of ions between the metal contact and the bulk solution results in diffusion impedance. At high frequencies, this impedance is small as the diffusing species do not move in contrast to large distances covered by the ions at low frequencies [28].

CHAPTER 5

RESULTS

5.1 Introduction

A new concept of fabricating structured separator layer is introduced in this dissertation. The otherwise insulating membrane, serving as a separator between the anode and the cathode, is turned into a structured membrane. A structured membrane is fabricated out of functionalized carbon nanotubes (CNT) in a form of an electronically a p-type layer on top of an n-type layers. The structure is call gate. The gate may be left unbiased (passive gate) or may be biased by an additional voltage source (active gate). In any case, the structure exhibits a potential barrier to the ionic flow. The gate is consisted of multiple p-n nano-junctions which are formed at the contact between the p-type and the n-type CNT layers. Current-voltage (I-V) measurements demonstrate diode-like characteristics. Raman spectroscopy and scanning electron microscopy of the gate assessed its interface quality. The ordering of the structure with respect to the direction of ion flow affects the cell's capacitance.

5.2 Experiment

5.2.1 Current-Voltage Characteristics of Single p-type and n-type Layers

A p-type single wall CNT film and n-type single wall CNT film were deposited on a polyamide TS80 filter using drop casting technique. Keithley 236 source meter, interfaced with a computer was used to measure the current-voltage characteristics at a voltage range between -1 V to +1 V at steps of 100 mV.

The current-voltage characteristics were measured on dry samples.

5.2.2 Gate Electrode Preparation

A polyamide TS80 filter of dimension 4 cm × 4 cm was cut from a 1016 × 305 mm long TriSep flat sheet membrane of thickness 0.05 mm. A stripe of 4 cm × 1 cm of CNT was coating one side of the membrane. The boundaries of the stripe was defined with a masking tape. Once the film is dry, the tape is removed from the membrane leaving either a p-type, or an n-type stripe on the TS80 membrane. To create a contact between the film and the copper foil, conductive epoxy (CW2400) is used. CW2400 epoxy contains resin and hardener. Equal amounts of both parts are mixed thoroughly for more than 2 minutes and then applied along 1 cm from the top of the film. Curing time and electrical conductivity depend on temperature. The adhesive is cured inside an oven at 65°C. Maximum adhesion and bond strength between film and copper are achieved after 24 hours. In order to protect the copper current collector from corroding, 5-min epoxy (Loctite) is applied on exposed areas. It reaches handling strength after one hour. It is water resistant and does not shrink or crack over time. As we use water based electrolytes, the characteristics of the epoxy helps to prevent corrosion of the contact. The p-type and n-type films are butt-coupled face to face to create a p-n structured film, which makes the gate electrode. The current-voltage measurement on the p-n structured gate is taken from -1.5 V to +1.5 V at steps of 100 mV.

5.2.3 Electrochemical Tests

The experimental setup for 2-electrode experiments is shown in Figure 5.1a. It involves only two electrodes: the working electrode (one of the graphite rods) and a counter

electrode (the other graphite rod). The two graphite electrodes were immersed in 1 M NaCl. The container body was made of polypropylene. An immovable center plate with a ca 0.3 cm^2 hole was made out of poly(methyl methacrylate) (PMMA). The diode-like separator was held tight by another PMMA plate with a matching hole to ensure ion flow and a proper contact between the p-type and the n-type coated membranes.

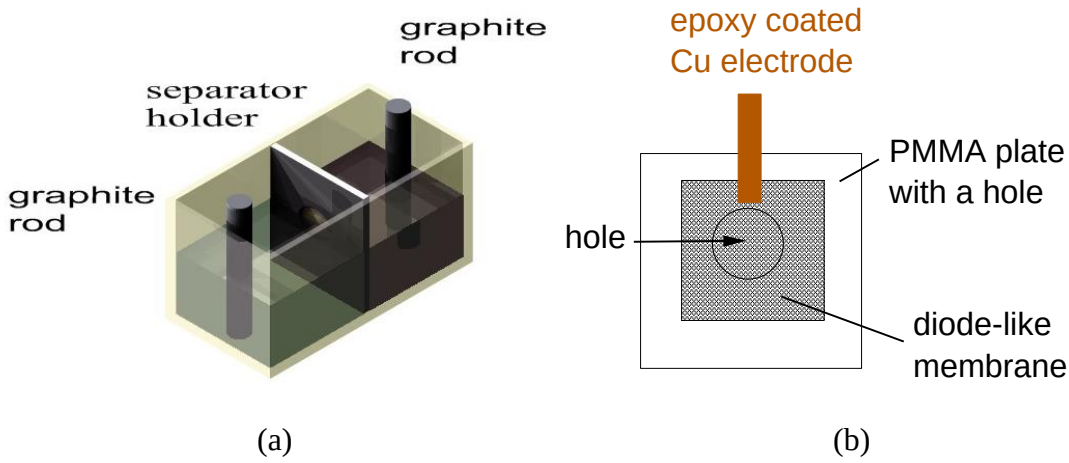

Figure. 5.1 (a) Cell's configuration. (b) The separator holder is composed of two PMMA plates each having a hole. The diode-like separator was held tight between the immovable plate and a removable plate.

Electrochemical measurements were carried out using Metrohm Autolab PGSTAT204 compact model potentiostat/galvanostat system. For CV measurements, the working electrode was scanned from 0 V to 500 mV at rates of 50, 100, 200 300 and 500 mV/sec, respectively. Chronopotentiometry tests were conducted in 2-electrode set up from 0 V to 0.5 V for various discharge currents: 50 µA, 75 µA, 90 µA and 100 µA. Both cyclic voltammetry and chronopotentiometry methods are carried out in two scenarios: (a) the overall cell capacitance with and without the structure on the separator membrane and

(b) by applying an additional a gate voltage across the gate. Electrochemical impedance spectroscopy was performed using FRA32M module of the same electrochemical workstation. Measurements were carried out in the 100 mHz - 50 KHz frequency range with an AC perturbation signal of 10 mV. For 3-electrode set up, a reference electrode, made of Ag/AgCl is added to the configuration.

Current-voltage characteristics of the diode like p-n structured film was measured using Keithely 236 source meter.

5.3 Results

Scanning Electron Microscope picture of CNT coated separator is shown in Figure 5.2. Scanning electron microscope of a p-n structure on TS80 membrane provides surface morphology of the film. The surfaces exhibit highly porous films. A magnified picture of the film's surface is also shown in Figure 5.4. The pore size ranges between 100 to 300 nm. The pores allow ion flow and the large surface area increases the interaction between the electronic charges on the gate with the flowing ions. The current-voltage (I-V) characteristic under dry conditions of either single p-type or n-type film on a polyamide TS80 membrane is shown in Figure 5.3. A single layer of either type behaves as a resistor and therefore, both types exhibit linear characteristics. The junctions were made by pressing two film types, together. A dry diode exhibits a nonlinear I-V curve as shown in Figure 5.4. The interface between the pressed films is consisted of numerous nano-junctions between individual functionalized CNT, and functionalized CNT bundles. The curve exhibits characteristics of a step-junction. It also exhibits a large diode resistance. Thermoelectric measurements of p-type and n-type layer are shown in Table 5.1 for two

different temperatures; 135 °F and 155 °F respectively. The data demonstrate that, indeed the n- and p-type layers behave as semiconductors. Raman spectra of the gate's p-side, n-side and the p-n junction(s) is shown in Figure 5.5. The G^+ peak did not shift, exhibits a small down-shift for the more negatively charged n-type tubes. For n-type and p-type, the down-shift was about 10 cm^{-1}.

Table 5.1 Thermo-electric Measurement of p-type and n-type Layer

	Temperature 135°F	Temperature 155°F
n-type CNT	+0.8mV	+1.2mV
p-type CNT	-1.8mV	-2.5mV

Note: The positive lead was placed on the hot side

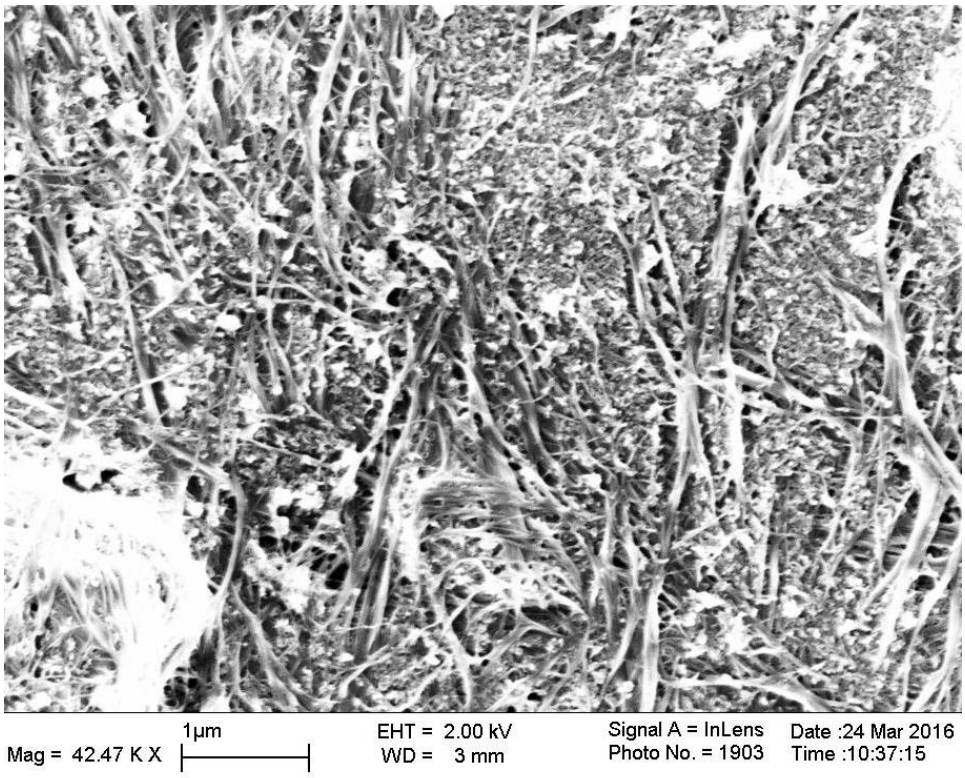

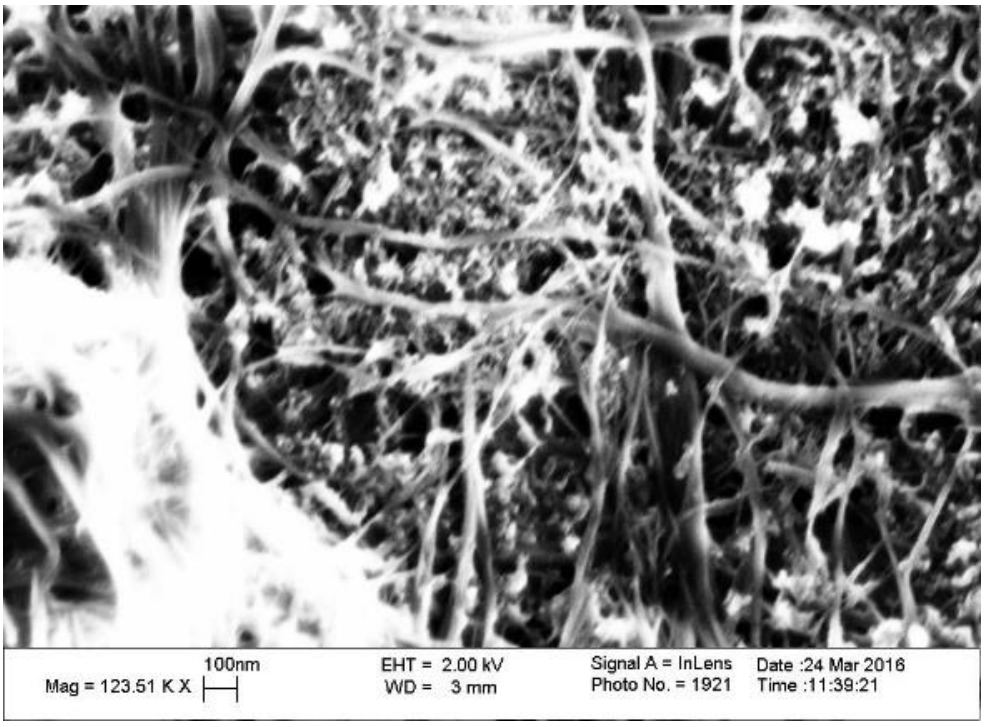

Figure 5.2 SEM picture of the diode-like film on top of the TS80 membrane on 1 µm scale and 100 nm scale. The film was made of two layers pressed together: a *p*-type layer and an *n*-type layer each made of functionalized SWCNT.

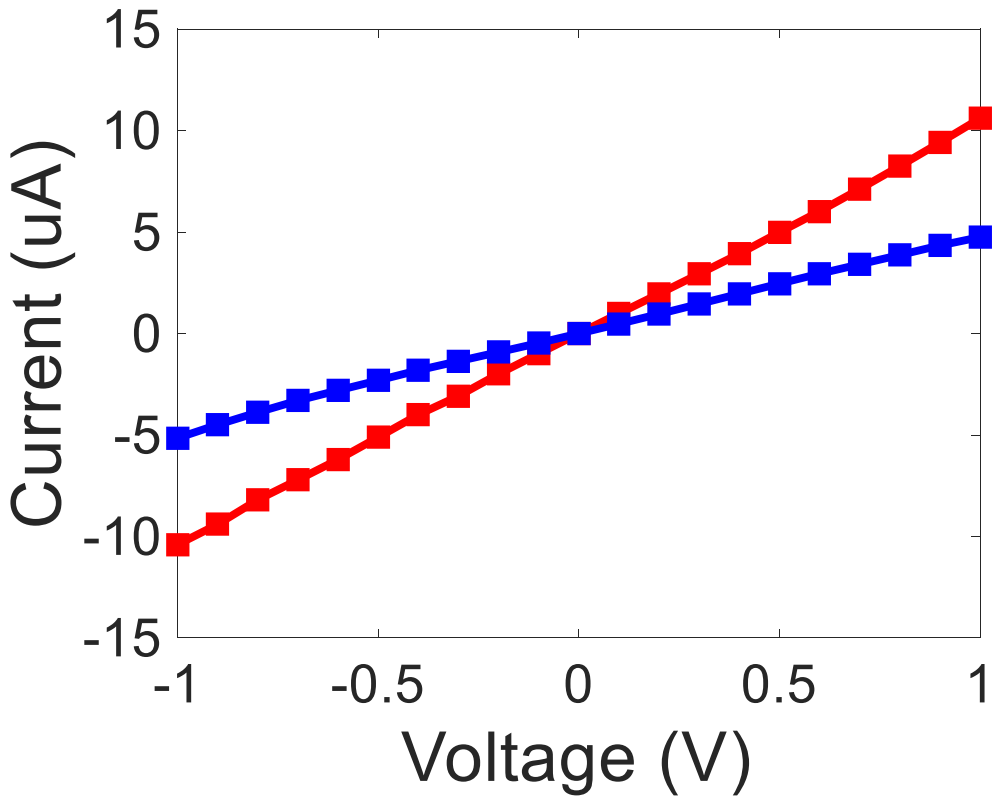

Figure 5.3 I-V characteristics of single p-type (red) and n-type (blue) carbon nanotube layer each imbedded in a PMMA matrix.

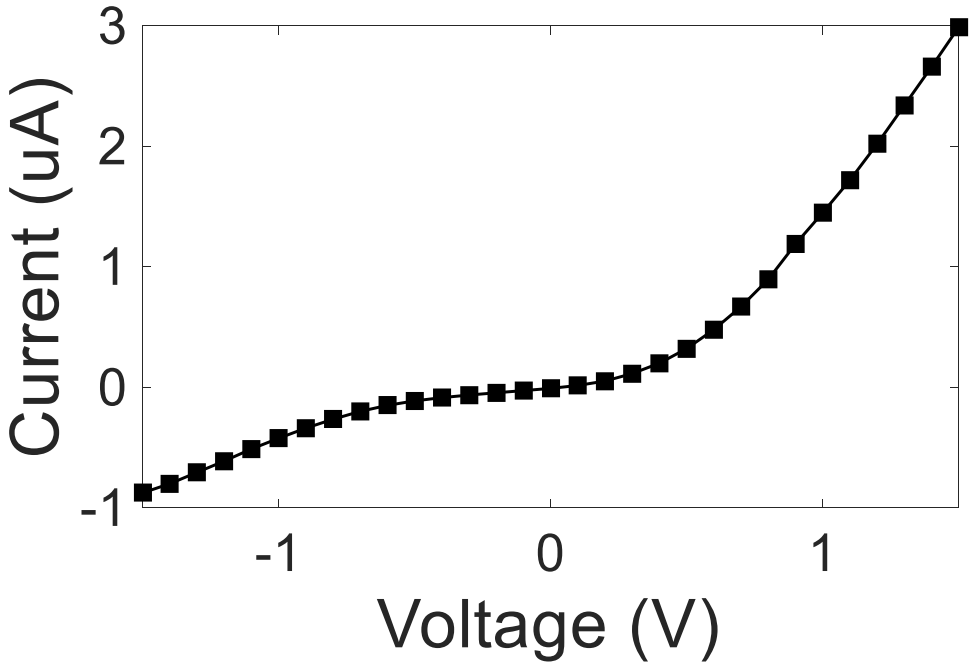

Figure 5.4 I-V characteristics of pressed together p- and n-type CNT films to form a p-n diode-like structure.

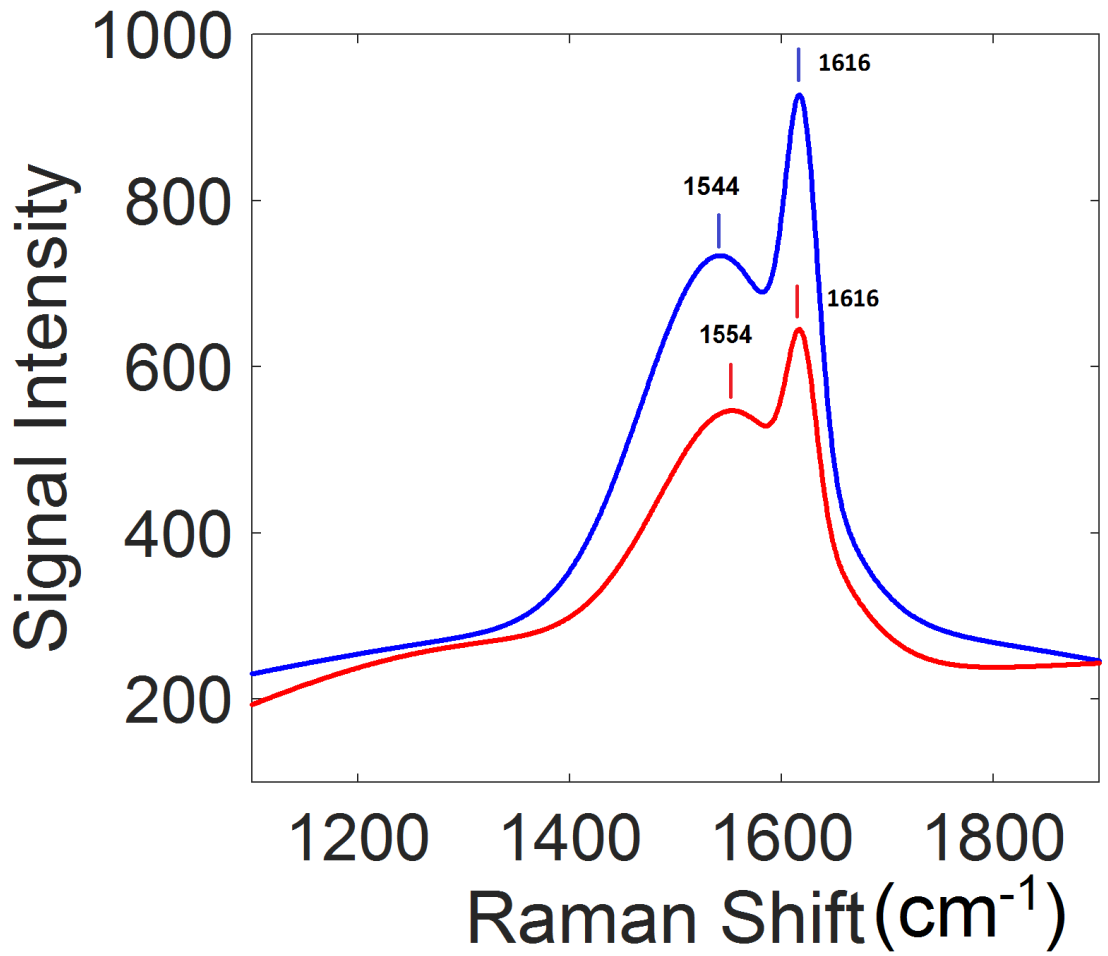

Figure 5.5 Raman signal for n-type (blue) and p-type (red) single walled carbon nanotube layer.

5.3.1 Aqueous Cells with Gate Electrodes

A comparison was made between a bare and p-n structured gate at various scan rates without applying a bias to the gate. 2-electrode cyclic voltammetry (CV) was used. The potential range was 0 to 0.5 V. The potential range is chosen such that the cell remains stable throughout the experiment (namely, does not undergoes hydrolysis or any other chemical reaction). The cell was assembled and the wait time before taking the data was about one hour. The area under the CV plot has increased when the separator was interfaced with a p-n gate. This is indicative of a higher cell capacitance for structured gate. The CV

curve also exhibits no peak; this implies to a lack of reaction in this voltage range. This is important because the capacitor seems to operate at a non-Faradaic mode (namely, there is no charge transfer between electrolyte and electrodes, or put it differently, no chemical reaction is taking place). The CV curve shows quasi-rectangular features indicative of small equivalent series resistance in the low scan rates. High scan rates exhibit larger

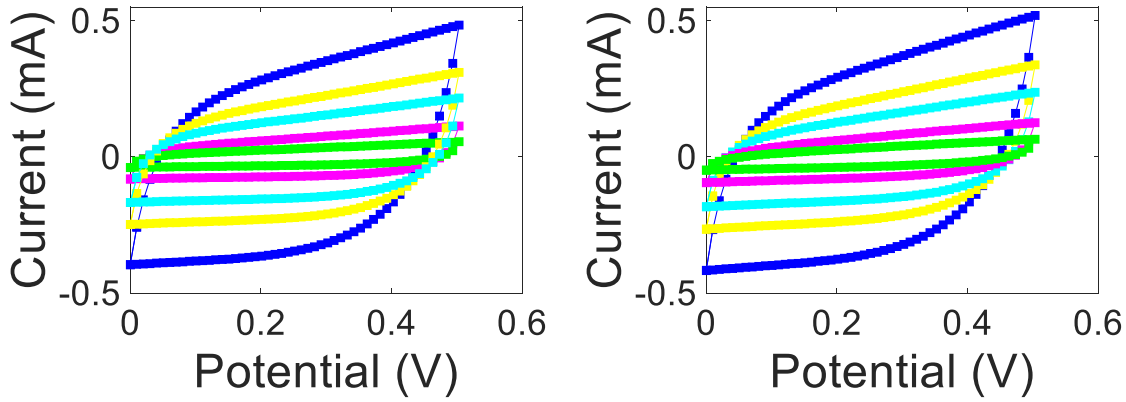

(a) (b)

Figure 5.6 CV curve for various scan rates: 0.05 V/s (green), 0.1 V/s (magenta), 0.2 V/s (light blue), 0.3 V/s (yellow), 0.5 V/s (blue) for both bare (a) and p-n structured separators (b). The larger area in (b) for the corresponding scan rate is indicative of the larger cell's capacitor in the case of the p-n structured separator.

equivalent resistance (the overall curve is more slanted). The effect may be due to ion diffusion from the electrolyte to the electrode: at low scan rate, the ion have more time to reach the electrode than for high scan rates. As a result, the adsorption of ions in the electrode surface is incomplete.

Two-electrode chronopotentiometry for bare and p-n structured gate at various current discharge rates were performed without a bias to the gate. The curves are shown in Figure 5.7. The voltage range was set from 0 to +0.5V. The triangular curve of chronopotentiometry indicates the capacitive behavior of the cell. All the

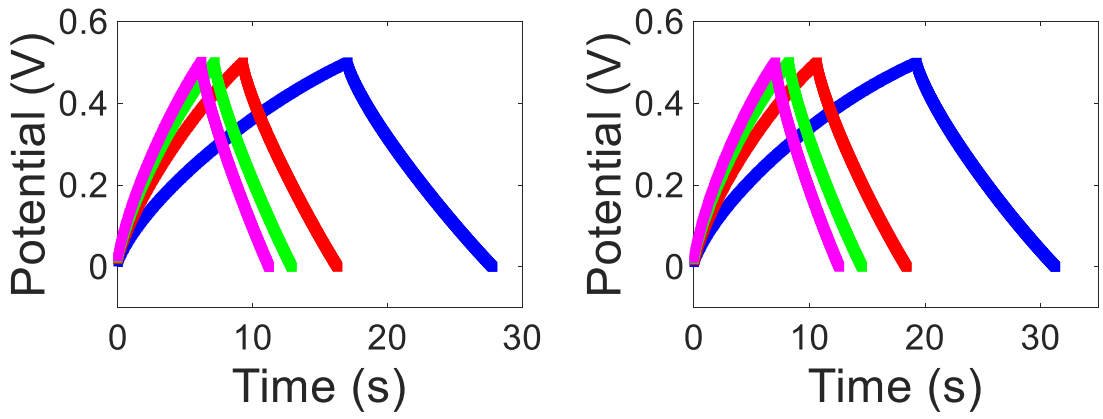

(a) (b)

Figure 5.7 2-electrode C-D at various current levels for both bare (a) and p-n structured separators (b): 50 μA (blue); 75 μA (red); 90 μA (green); and 100 μA (magenta). The voltage ranged between 0 and +0.5V.

chrono-potentiometry curves are well-defined and symmetric. It can be seen that charge and discharge time are decreased as the charge current increased (Figure 5.7a and b). For each discharge current, note the slightly longer cycle for the p-n structured separator when compared to the bare separator; this is attributed to an overall cell capacitance increase when the structured gate is introduced. Note that the ohmic drop for each case is negligible. An Ohmic drop is indicated by a potential drop from the end of the charge stage to the beginning of the discharge stage.

5.3.2. Cell Capacitance Measurement with No Gate Bias

The incorporation of SWCNT based, *p-n* junction(s) on a separator clearly increases the overall cell's capacitance (Figure. 5.8a-b). CV is sensitive to the capacitance of the entire cell as indicated by the optimal scan rate of 0.2 V/sec. But in lowest scan rate 0.05 V/s, the increase of overall cell capacitance is more prominent with the inclusion of structured

separator compared to a bare one. Similarly, using charge-discharge (also known as chronopotentiometry), the overall cell capacitance has increased when the gate was structured. Thus, both methods exhibit capacitance increase between 4-10% for the structure gate with no voltage bias. Chronopotentiometry experiments consistently exhibit larger capacitance values.

Equations (5.1) and (5.2) are used to calculate the capacitance of the cell for CV and chronopotentiometry, respectively.

$$C = \frac{1}{v * |E_2 - E_1|} \int_{t=0(E_1)}^{t(E_2)} i(E)\, dt \tag{5.1}$$

$$C = \frac{I}{\frac{\Delta V}{\Delta t}} \tag{5.2}$$

For CV, the value for E_1 and E_2 are 0 and 0.5 V and *v* is the scan rate. The scan rate varies from 0.05 V/s to 0.5 V/s. The integration part of Equation (5.1) is obtained by calculating the area under the enclosed CV curve of Figure 5.6. For chronopotentiometry, I is the applied discharge current and the denominator is assessed from the slope of the discharge profile. The decreasing of the cell's capacitance with the increasing charge/discharge current is due to slower diffusion at high charge/discharge current levels.

Tables 5.2 and 5.3 compare the capacitance improvement when the structured separator was included in the cell.

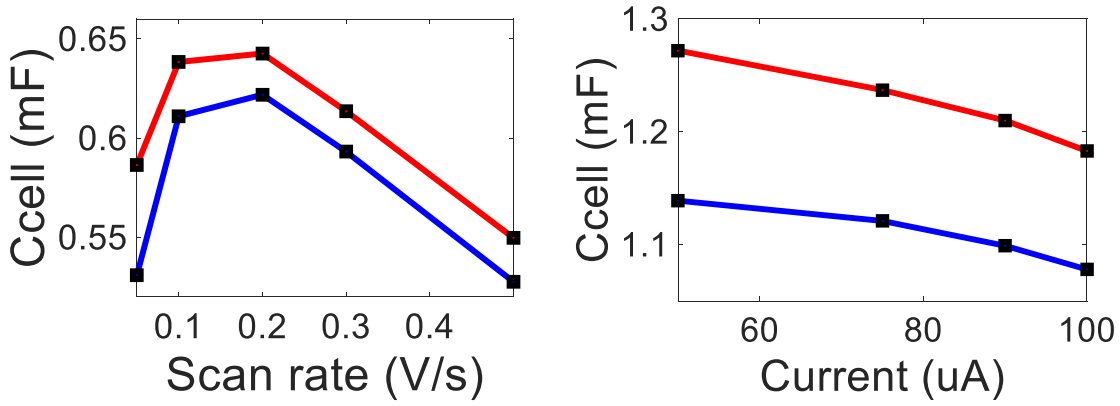

(a) (b)

Figure 5.8 The effect of a p-n gate membrane on the cell's capacitance using: (a) 2-electrode CV and (b) 2-electrode C-D. Experiments were conducted with no gate bias. The red curve was obtained with p-n gate diode while the blue curve was obtained without it.

Table 5.2 Cell Capacitance Increase Structured upon Introducing a Structured Separator and using CV Data from Figure 5.6 a,b

Scan rate	Ccell_with bare separator (mF)	Ccell_with structured separator (mF)	% Increase
0.5	0.527	0.549	4%
0.3	0.593	0.614	3.5%
0.2	0.62	0.643	3.8%
0.1	0.611	0.638	4.4%
0.05	0.53	0.586	10.6%

Table 5.3 Measuring Cell Capacitance Increase upon Introducing Structure Separator and using Chronopotentiometry Data from Figure 5.7 a,b

Discharge Current in mA	Ccell_with bare separator (mF)	Ccell_with structured separator (mF)	% Increase
0.05	1.139	1.272	11.6%
0.075	1.121	1.237	10.3%
0.09	1.099	1.21	10.1%
0.10	1.078	1.183	9.7%

5.3.3. Cell Capacitance under Gate Bias

In Figure 5.9(a), we show CV results for cell capacitance while the gate is under voltage bias. The cyclic voltammetry curve was performed for multiple cycles back and forth. The

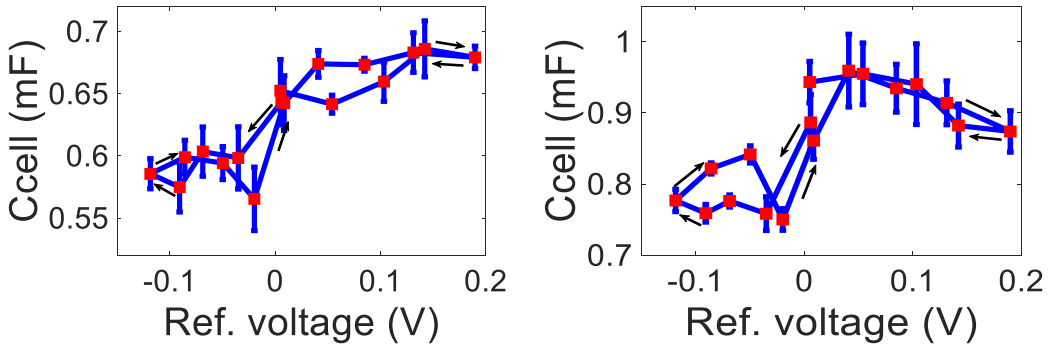

Figure 5.9 Capacitance as a function of reference voltage, Vref: (a) using 2-electrode CV. (b) Using 2-electrode C-D at current level of 50 micro-Amps. The gate voltage, Vg varied from -0.4 to +0.4 Volts. Vg=0 is the starting point.

scans were averaged over four cycles. Similar curves for charge-discharge is shown in Figure 5.9(b). Both curves clearly exhibit additional cell's capacitance of ca 15% as a function of gate bias near a gate bias of Vg~0 V. This additional capacitance comes at some energy costs.

The DC current-voltage curve for only the gate, Ig-Vg is shown in Figure 5.10 while either the CV or the C-D experiments were running. In Figure 5.10, a full cycle of the gate current as a function of the gate bias, Vg is shown. The Ig-Vg curves were taken at various experimental times and the fact that they overlap on top of each other is proof to the stability of the experiment. The gate current vs gate bias curve was performed using

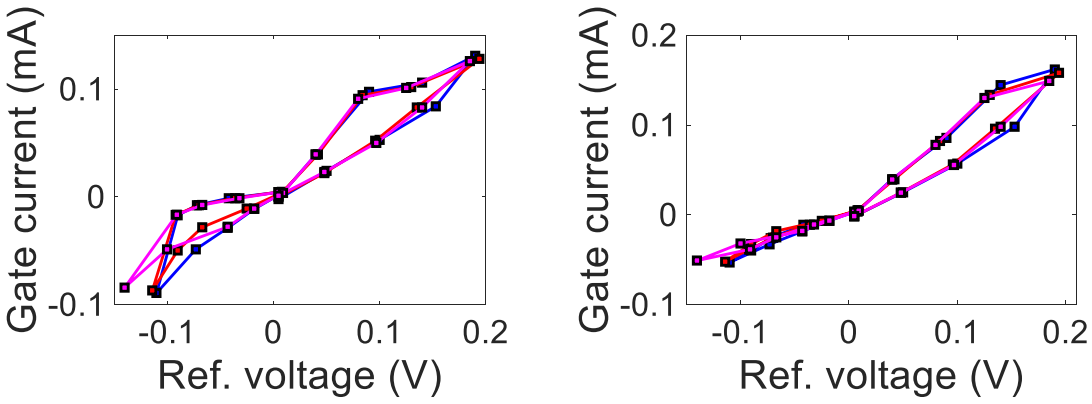

(a) (b)

Figure 5.10 Gate current, Ig as a function of reference voltage, Vref. Data were taken at 30 sec (blue), 40 sec (red) and 50 sec (magenta) while either (a) CV or (b) C-D measurements were running.

Agilient U2722A USB modular source measure unit. It measures the gate current while the source voltage is applied across the gate. The measurements were also taken for four cycles during either the CV or chronopotentiometry.

5.3.4. Energy Considerations for a Biased Gate

Biasing the gate creates additional polarizing effect, yet, costs energy. From Figure 5.10 and assuming a linear change at Vg~0 V, the largest change in the cell's capacitance under bias occurs for Vg between ±0.1 V, for which $\Delta Ig \sim 60\ \mu A$. The energy invested in charge separation at the biased gate is the area under the Ig-Vg curve, or, $\Delta U_{gate} = \frac{1}{2}\Delta Ig \Delta Vg = 6\ \mu J$. Under gate bias, the additional stored energy in our cell may be estimated as follows:

$$U_{cell} = [C_{cell}(V_g)][V_{cell}]^2 \sim \{C_0 + [(\delta C_{cell})/(\delta Vg)](\Delta Vg)\}[V_{cell}]^2 \quad (5.3)$$

$$\Delta U_{cell} = [(\delta C_{cell}/\delta Vg)\Delta Vg](V_{cell})^2 \quad (5.4)$$

$(\delta C_{cell}/\delta Vg) = (0.2mF/0.2\ V) = 1x10^{-3}$ F/V; $\Delta Vg = 0.1$ V; V_{cell} is linearly varying between 0 and 0.5 V so, $\langle V_{cell} \rangle = 0.25$ V. Plugging it into Equation (5.4) we get, $\Delta U_{cell} = 6.25\ \mu J \sim \Delta U_{gate}$. Thus, upon biasing the gate, the invested energy is completely utilized in additional energy storage through the increase in the cell's capacitance.

5.3.5. Cell Model and Impedance Spectroscopy

Charge separation at the gate is the reason for the observed capacitance change. The p-type and n-type SWCNT have different chemical potentials. They equate to one another when pressed together. This results in electronic charge redistribution across the gate's layers. In terms of doping by the polymeric coatings, the functionalized SWCT are considered lightly doped, which means that the junction is extended across the entire two gate layers and not just at the interface alone. The ions respond by creating a double layer

throughout the porous gate and this may be viewed as placing a gate capacitor in parallel to a (large) resistor and the (rather small) capacitor that represents the insulating separator. Our cell model is presented in Figure. 11e. The diode is replaced by a capacitor for fitting purposes (Figure. 11e). Nyquist plot and Bode plots are provided in Figure. 11c-d, for a p-n gate membrane at Vg=0 V. Electrochemical impedance spectroscopy was performed at the overall cell from 50 kHz to 100 mHz at 10 mV of applied signal with a 2 electrode setup. In general, adding a p-n gate structure reduces the cell's resistance, which may be attributed to the larger ion concentration at the gate. EIS characteristics of overall cell with and without the structured separator layer shows two distinct frequency zones, high frequency depressed semicircle and non-vertical line for low frequency values. Due to the non-vertical slope the capacitors can be modelled with a constant phase element (CPE) expression. EIS approaches to the low frequency region at 45^0 due to the distributed resistance and capacitance of the porous electrode. The equivalent circuit with a permeable structured separator is replaced by combination of a permeable gate capacitor and diffusion capacitance. C_1 and C_2 are the double layer interfaces at the cell's electrodes, R_s is the solution resistance of the electrolyte, C_d is the diffusion capacitance and C_g is the gate capacitance.

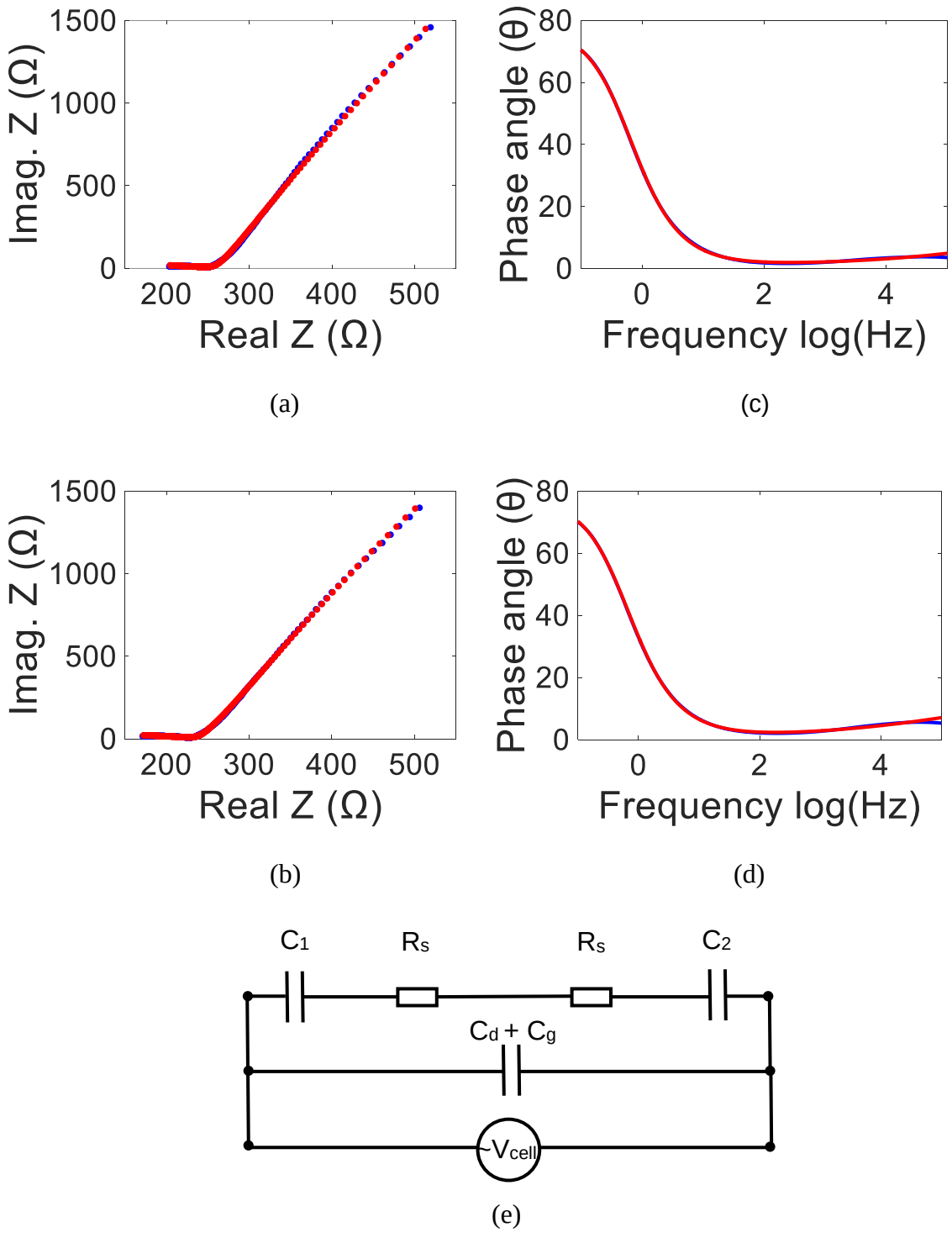

Figure 5.11 Electrochemical impedance spectroscopy for bare and structured separators. Blue: experimental; Red: fitted model.2-electrode cell is using (a, b) Nyquist and (c, d) Bode plots and (e) the equivalent circuit model.

In Figure 5.12 EIS measurements with and without structured separator exhibit low equivalent series resistance (ESR). Incorporating the gate results in a reduction in the overall cell resistance. This is correlated with a higher power cell's capacity according to Equation (5.5).

$$P = \frac{V^2}{4*ESR} \tag{5.5}$$

For both EIS curve, the knee frequency is at 1 kHz. At knee frequency the overall cell resistance with and without a structured separator is measured 220 Ω and 243 Ω, respectively shown in Figure 5.12a. The structured separator enhances the overall power capability of the cell by decreasing overall cell series resistance.

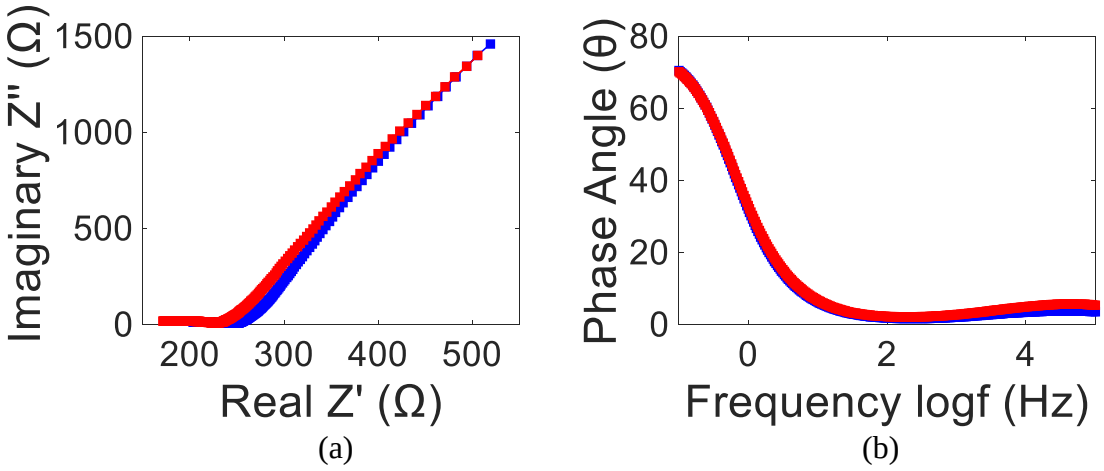

Figure. 5.12 Experiment: Electrochemical impedance spectroscopy of cells using bare (blue) and p-n structured gate (red) in a 2-electrode cell: (a) Nyquist and (b) Bode plots.

After 3 months, we re-assembled the gate (Figure 5.13) and examined the effect of interchanging the order of the p-layer and n-layer with respect to the working electrode.

This was done simply by interchanging the positions of counter and working graphite rods in the cell, keeping the membrane in place. Bare gate membrane experiments were used

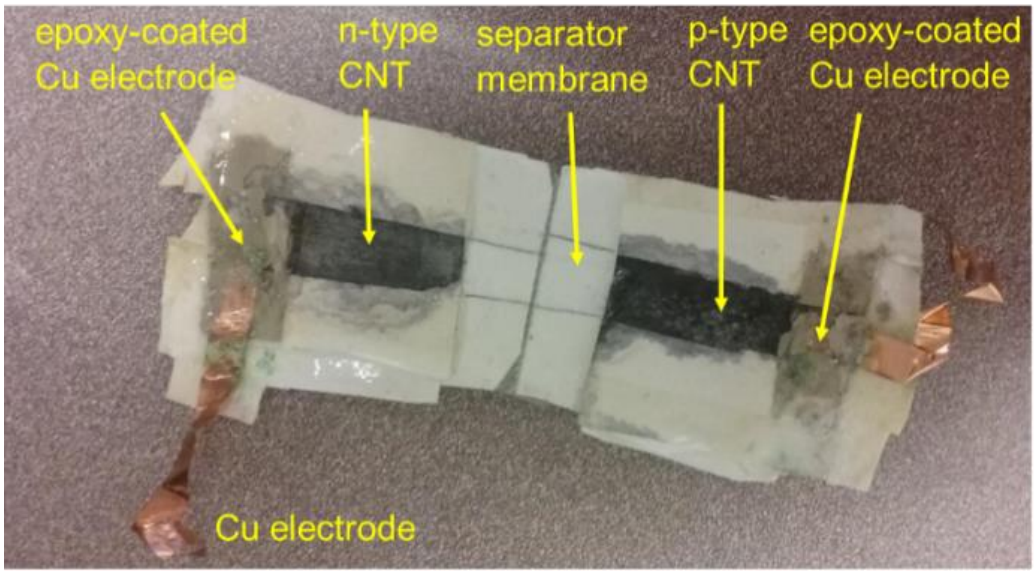

Figure 5.13 A gate structure after the conclusion of a set of experiments.

as reference. We did not re-polish the graphite rods between measurements and note that their surface quality determines the overall cell's capacitance. Also, the p-n junction(s) are formed by contact and are sensitive to local stress inserted on them by the two plastic plates. This means that re-assembling the cell may somewhat change the overall cell's capacitance but not the trend. Figure 5.15 shows a larger cell capacitance when the n-layer faces the working electrode and alludes to the importance of gate's layers order with respect to the cell's electrodes (a capacitance increase of >5%). The overall cell capacitance has reduced somewhat after reassembly. Cyclic voltammetry was performed for both cases for various scan rates and there was no reaction takes place in the cell which exhibits in Figure 5.14.

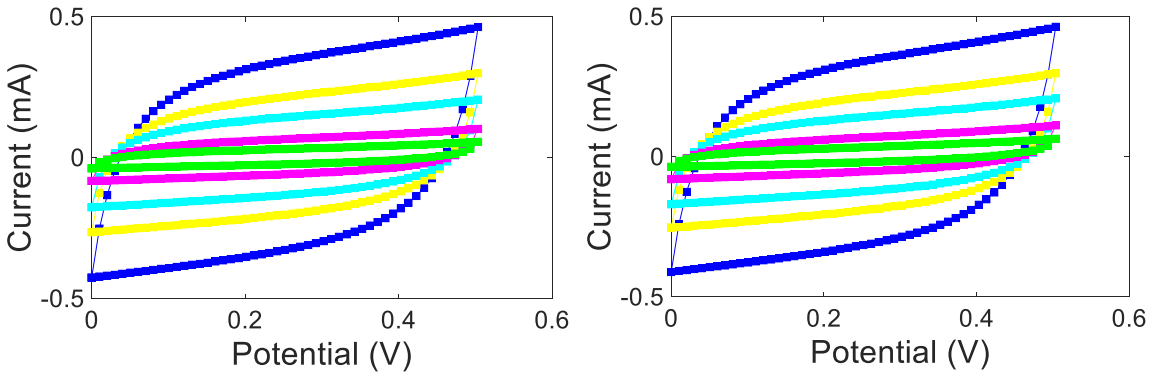

(a) (b)

Figure 5.14 2- electrode cyclic voltammetry using p-n structured separator with interchanging the position, a) n-layer facing towards working electrode b) p-layer facing towards working electrode.

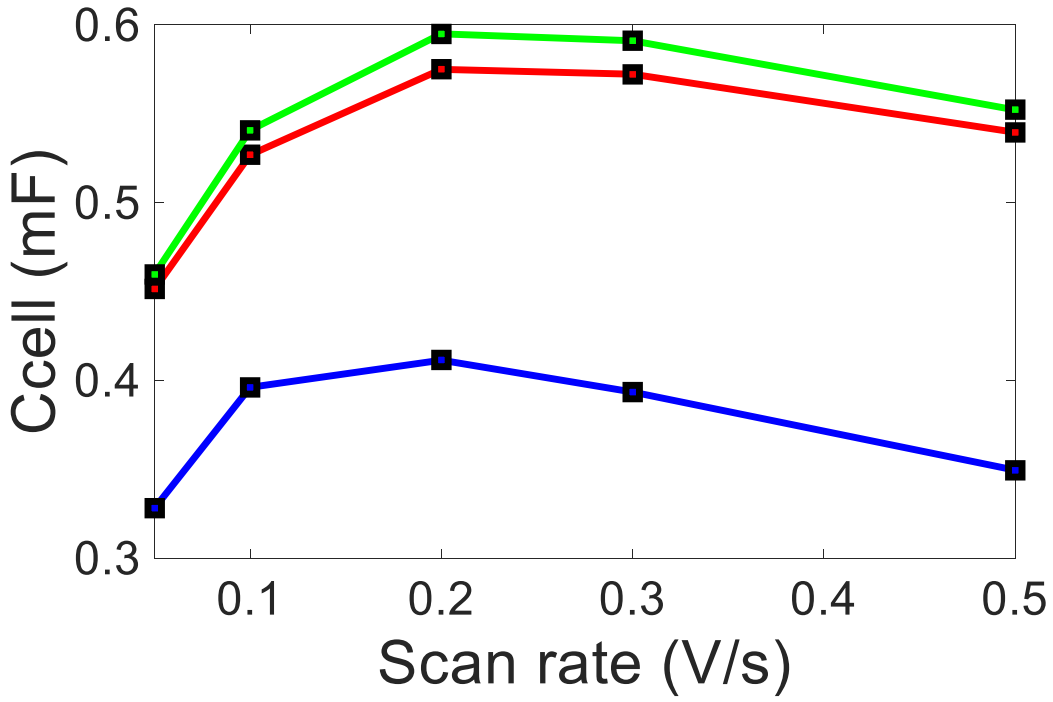

Figure 5.15 Capacitance of cell vs scan rate for different orientation of structured layer near the working electrode, n-layer facing towards working electrode (green), p-layer facing towards working electrode (red) and bare separator (blue).

5.4 Measurement of Capacitance of Gate Electrode

A gate, electrode consisted of p-n structured film is used as a separator in the cell with 1 M sodium chloride electrolyte solution. To assess the capacitance of the the gate itself, 3-electrode set up is employed: the working electrode is the p-side, platinum wire is the counter electrode and Ag/AgCl is used as a reference electrode. The goal here is to assess whether the order of the structured electrode with respect to the position of the reference and counter electrodes has an effect on the overall cell capacitance. The the experimental configuration is shown in Figure 5.16a where referenece and counter electrodes are close to n-type side of the gate. For the flip case, the reference and counter electrode are placed near the p-type side of the gate as shown in Figure 5.16b.

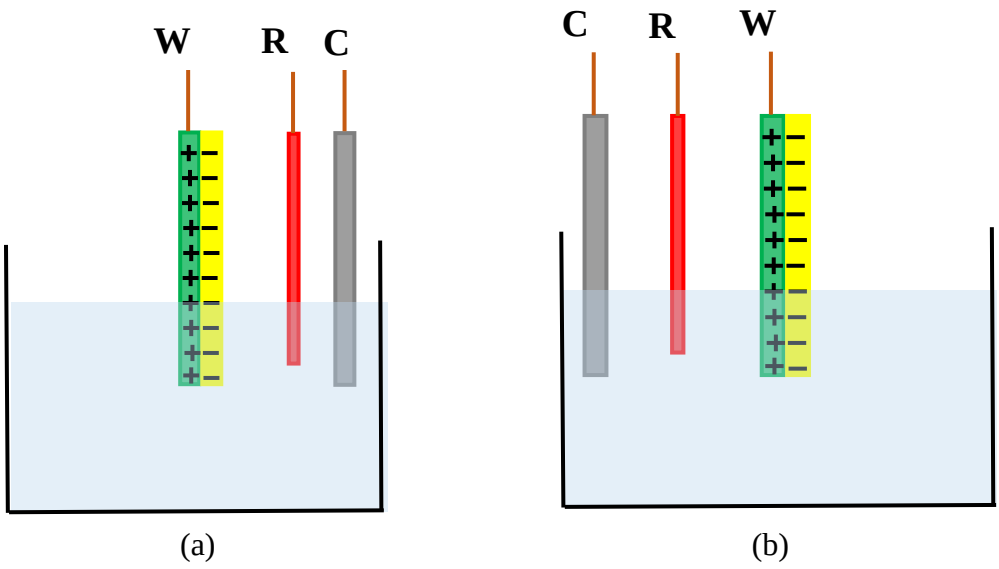

Figure 5.16 The experimental 3- electrode set-up used to measure capacitance of the gate electrode alone and the effect of working electrode position compared to reference electrode (red) and counter electrode (grey) position. W, R and C are the working, reference and counter electrodes, respectively.

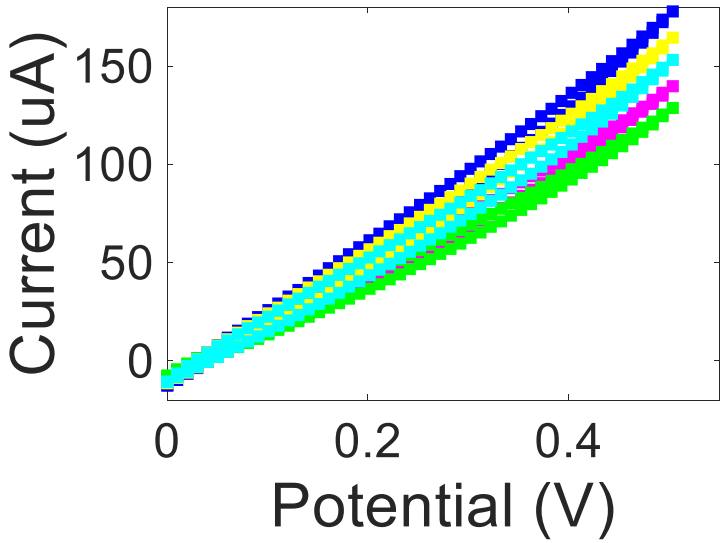

(a)

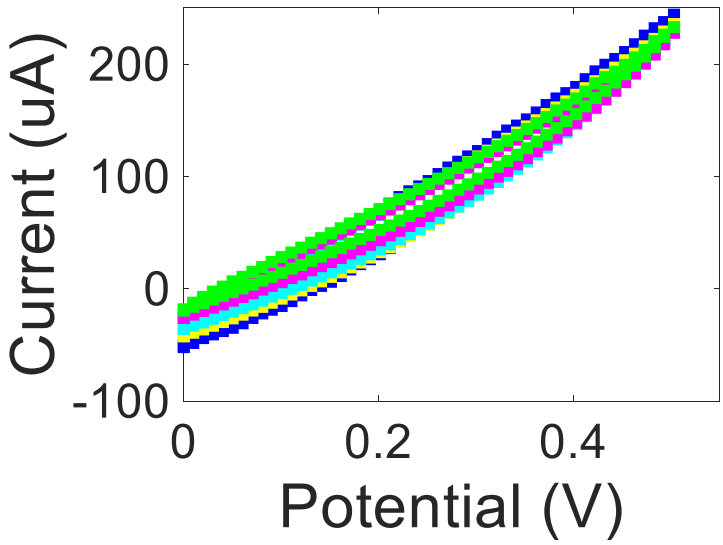

(b)

Figure 5.17 CV for p-n gate electrode in 1 M sodium chloride solution using 3-electode set up for various scan rates: 0.5 V/s (blue), 0.3 V/s (yellow), 0.2 V/s(light blue), 0.1 V/s(magenta), 0.05 V/s(green) when (a) the reference and auxiliary electrodes are placed near the n-type side and (b) reference and auxiliary electrodes are placed near the p-type side.

The tests for a gate without bias have been carried out at various scan rates. CV curves shown in Figure 5.17. Further openings in the curves is exhibited for lower scan rate 0.05 V/s than for the higher scan rate of 0.5V/s for either p-n order (with respect to the

counter electrode). In order to be consistent with the two electrode set up, the same potential range from 0 to +0.5 V is chosen.

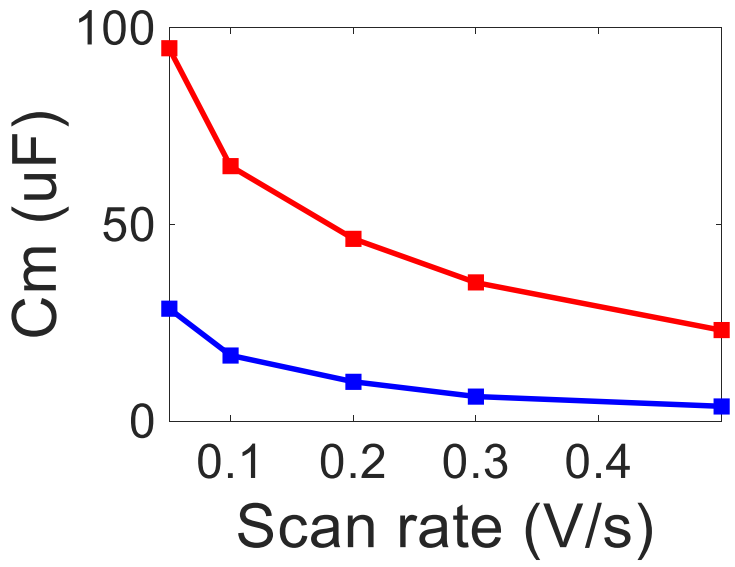

Figure 5.18 Capacitance of gate vs Scan rate. blue curve: p serves as working electrode; reference and counter electrodes are placed near the n side. Red curve: p-layer serves as the working electrode; reference and counter electrodes are placed near the p-side.

As mentioned before, the order of the p-n junction with respect to the counter electrode varied. In one case, the p served as a working electrode while the reference and counter electrodes were placed at the n side. This case tends to have lower capacitance than the case where the reference and auxiliary electrodes are facing the p-side, as shown in Figure 5.18. This experiment indicates that the position of reference and counter electrode along with the ordering of structured gate play a role in the capacitance increase. The maximum capacitance is obtained at 0.05 V/s and is 0.1 mF.

5.5 Ionic Liquids Cells

Ionic liquid was used as an electrolyte in a cell with copper electrodes. The configuration of the gate is shown in Figure 5.19. For both working and counter electrode, we used bare copper foil cut into two 5 cm × 3 cm strips. In order to ensure a compact cell, we pressed electrodes with glass slides as shown in Figure 5.19. Ionic liquid (1-n-Butyl-3-methyl-imidazolium hexafluro-phosphate) is drop casted onto the structured separator membrane. Two pieces of thin lens clothes (Bausch & Lomb)of 0.1 mm thickness between separator membrane and electrode were placed as well to isolate any contact between electrode and separator. After assembly, the sample was resting overnight.

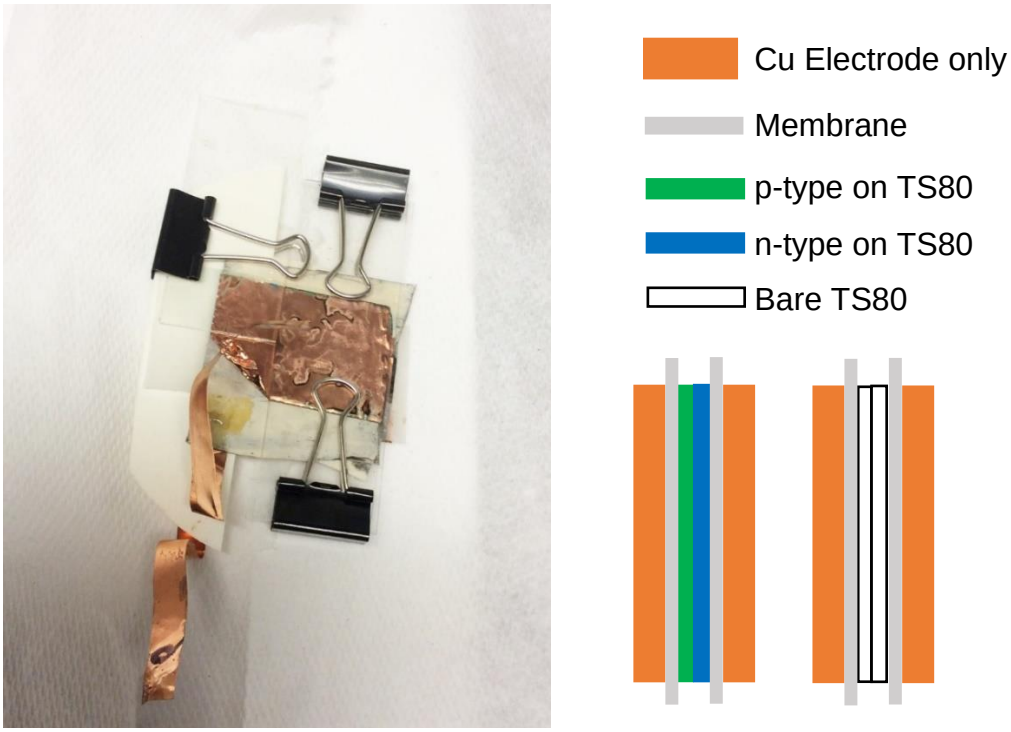

Figure 5.19 Freshly prepared sample put together with 2-electrode cell using bare TS80 and p-n electrode and ionic liquid electrolyte.

The bare separator consists of only TS80 membrane, soaked with ionic liquid. Cyclic voltammetry is performed with a 2-electrode setup from 0 to 0.5V at various scan rates. The CV curves for bare and structured gates are shown in Figure 5.20 and Figure 5.21. The opening of the curve is indicative of their capacitive nature; no reaction is observed in any of the CV curves (noted as absence of reduction peaks). Copper electrodes are not porous

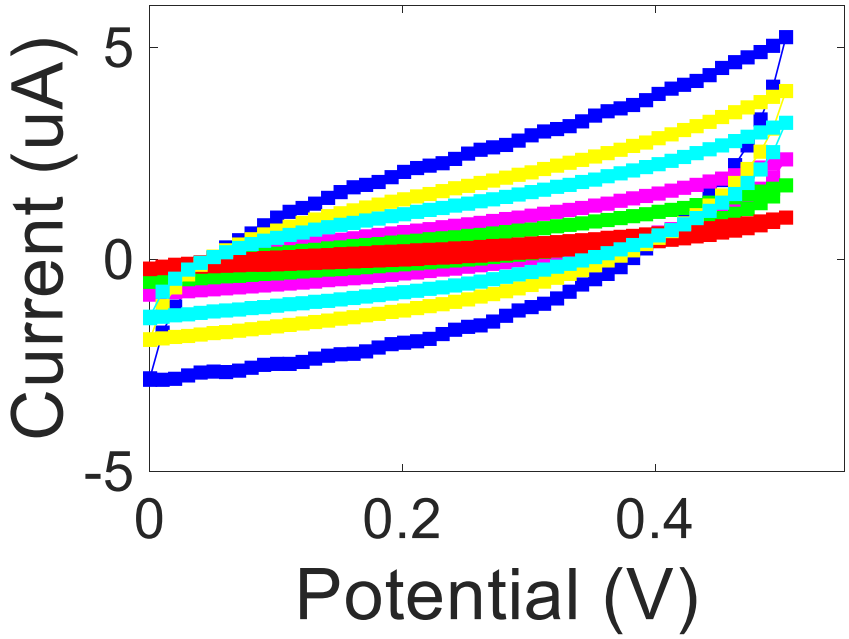

Figure 5.20 Cyclic voltammetry of cell with bare separator (TS80) soaked with ionic liquid at various scan rates, 0.5 V/s (Blue), 0.3 V/s (yellow), 0.2 V/s (light blue), 0.1 V/s (magenta), 0.05 V/s (green), 0.01 V/s (red).

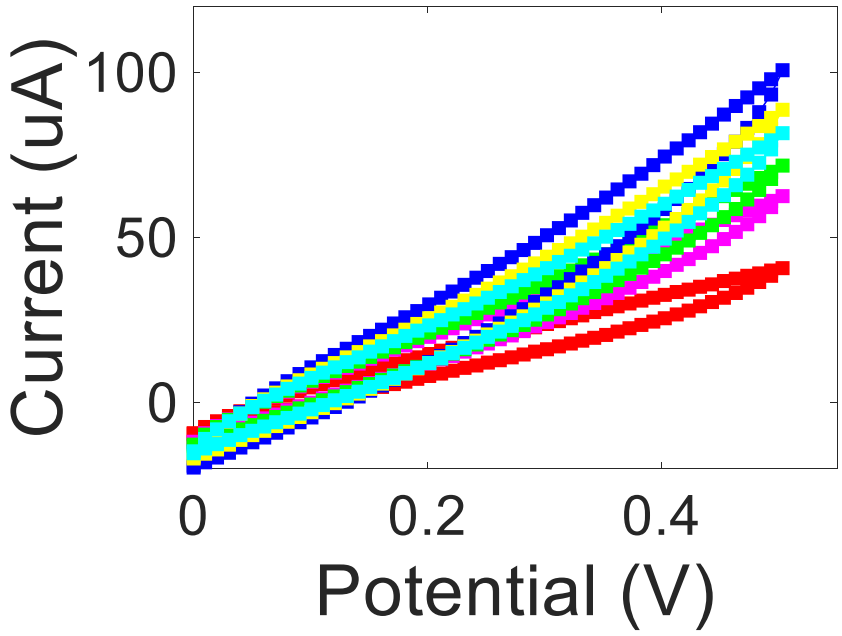

Figure 5.21 Cyclic voltammetry of cell with p-n gate soaked in ionic liquid at various scan rates, 0.5 V/s (Blue), 0.3 V/s (yellow), 0.2 V/s (light blue), 0.1 V/s (magenta), 0.05 V/s (green), 0.01 V/s (red).

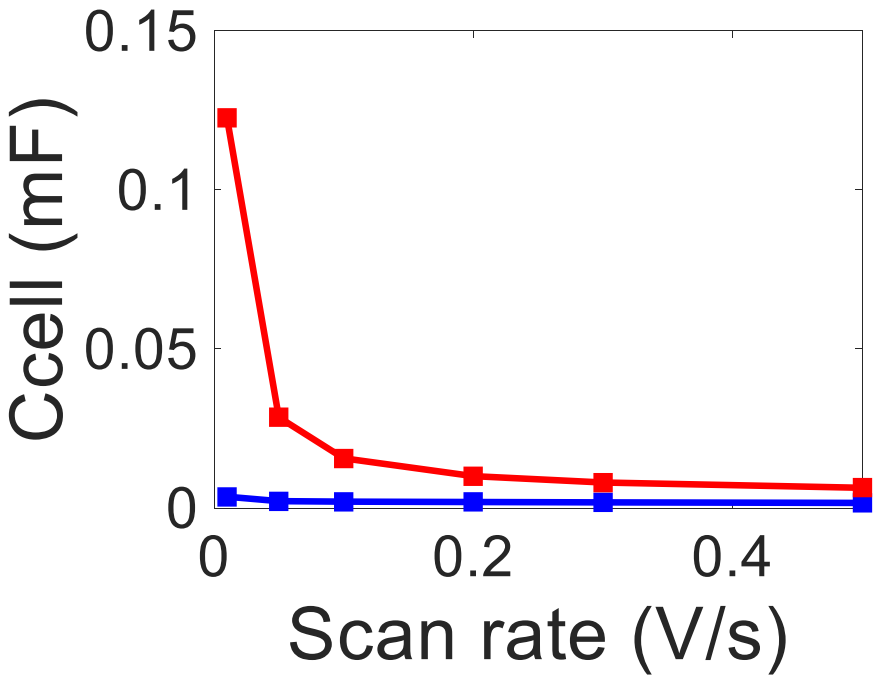

Figure 5.22 Capacitance of cell vs Scan rate for bare (blue) and p-n structured gates (red) at various scan rates: 0.5 V/s, 0.3 V/s, 0.2 V/s, 0.1 V/s, 0.05 V/s, 0.01 V/s.

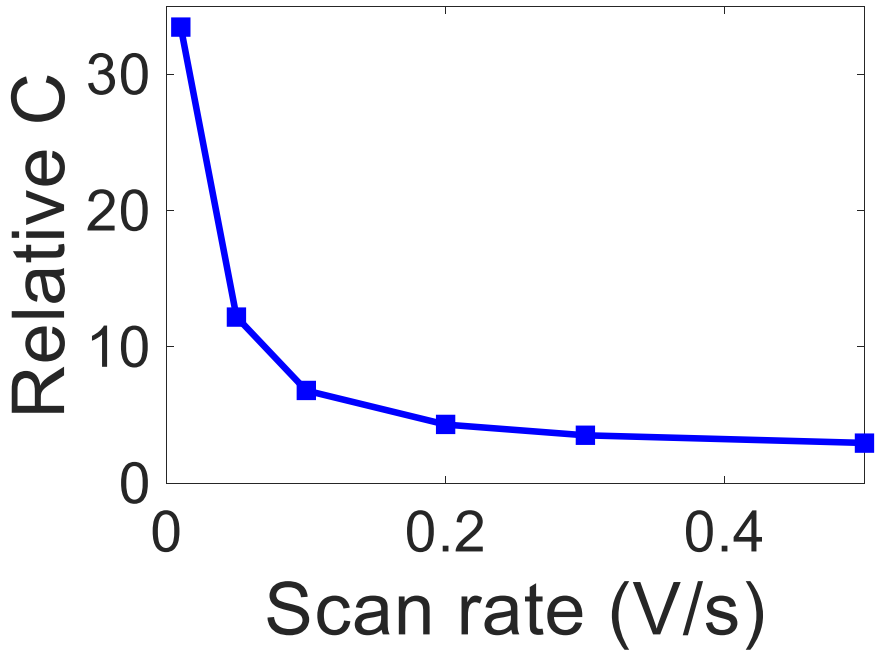

Figure 5.23 Relative capacitance of a cell with p-n gate in ionic liquid at various scan rates, 0.5 V/s (Blue), 0.3 V/s (yellow), 0.2 V/s (light blue), 0.1 V/s (magenta), 0.05 V/s (green), 0.01 V/s (red).

yet, the porosity of the gate increases the overall cell capacitance as assessed by Equation (5.1). The capacitance vs scan rate plot is shown in Figure 5.22 and exhibits a capacitance increase. The curve decreases with increased scan rate which is due to diffusion; high scan rates are impeded by the electrolyte viscosity. Relative capacitance, which is the capacitance of structured gate normalized by the capacitance of a bare separator is shown in Figure 5.23.

5.5.1 Cell Electrodes with Carbon Powder

Configuration of the sample is in Figure 5.19. Current collectors for the working and counter electrodes were made of copper foil, cut into two 5 cm × 3 cm strips. The stripes were coated with double sided carbon tape. The carbon taped was coated with carbon powder to increase its porosity. The loose powder was scraped off to ensure a uniform coverage. The weight of the powder was 2 mg. The cell was compacted with two pressed glass slides as shown in Figure 5.19. Ionic liquid (1-n-Butyl-3-methyl-imidazolium hexafluro-phosphate) soaked in a TS80 membrane as well as two pieces of thin lens clothes (Bausch & Lomb) between separator membrane and electrode. Figure 5.24 shows the supercapacitor cell assembly.

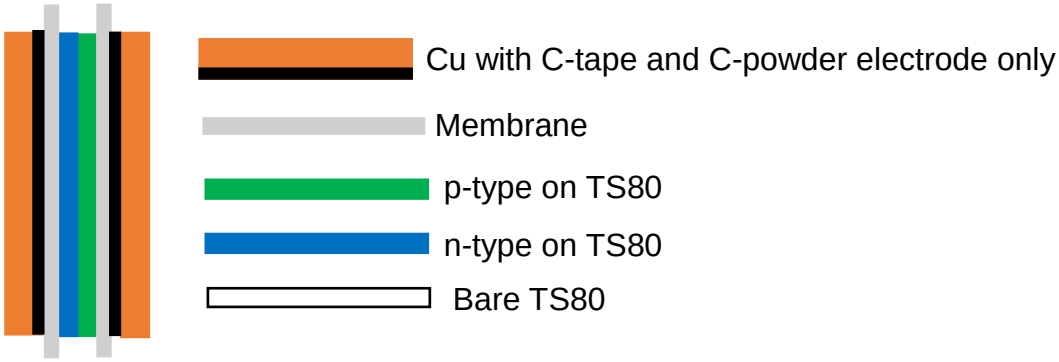

Figure 5.24 Supercapacitor cell assembly using structured separator and a copper electrode interfaced with carbon powder and two thin piece of lens clothes separates the electrode and separator.

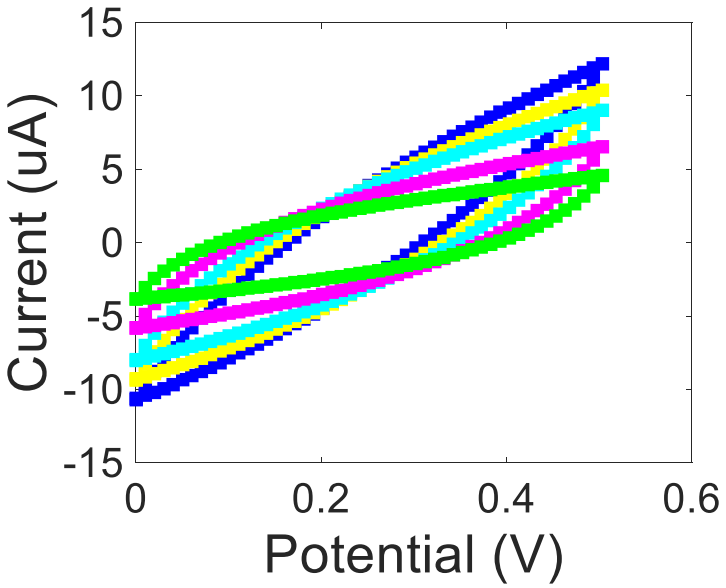

Figure 5.25 Cyclic voltammetry using two copper electrodes interfaced with carbon powder and p-n structured separator with ionic liquid at scan rates, 0.5 V/s, 0.3 V/s, 0.2 V/s, 0.1 V/s, 0.05 V/s.

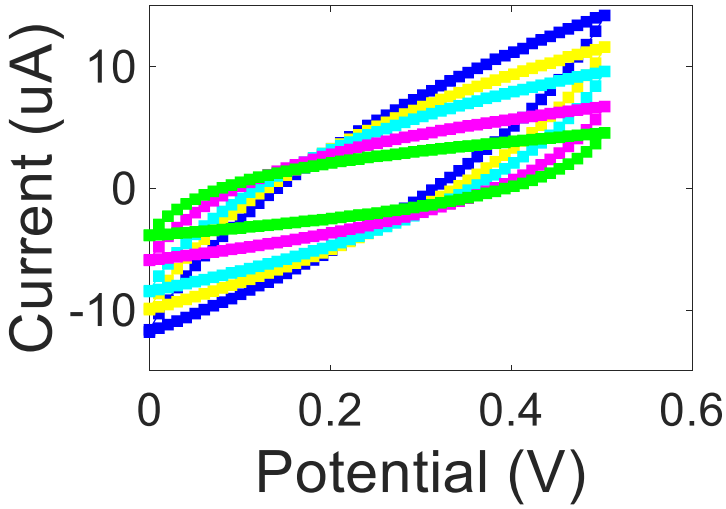

Figure 5.26 Cyclic voltammetry using two copper electrodes interfaced with carbon powder with p-n structured separator soaked in ionic liquid scan rates, 0.5 V/s, 0.3 V/s, 0.2 V/s, 0.1 V/s, 0.05 V/s.

Figure 5.24 shows the experimental set up using two copper electrodes interfaced with carbon powder. In this section, we interchanged the order of p-n layers with respect to auxiliary electrode . In Figure 5.25, the n side is near the auxiliary electrode; in Figure 5.26, the p side is near the auxiliary. Irrespective of the order of the layers, the overall cell capacitance has increased compared to a bare separator for any scan rate. In Figure 5.27, CV after interchaning layer layout along with bare membrane is shown for high scan rate (0.5V/s) and low (0.1V/s) for better visualization. It clearly indicates that irrespecting of any layer layout, the measured capacitance is increased compared to bare.

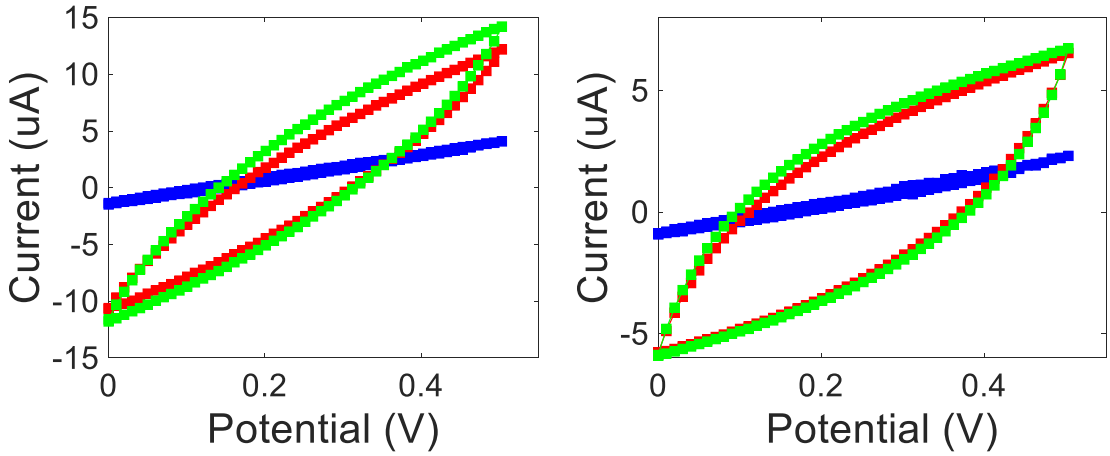

(a) (b)

Figure 5.27 CV of cell with two copper electrodes and a separator. Blue curve: bare separator; Red curve: p-n structured film where the n-side is facing the auxiliary electrode; Green curve where the p-side interface the auxiliary electrode. Ionic liquid was used as electrolyte at (a) 0.5 V/s and (b) 0.1 V/s scan rates.

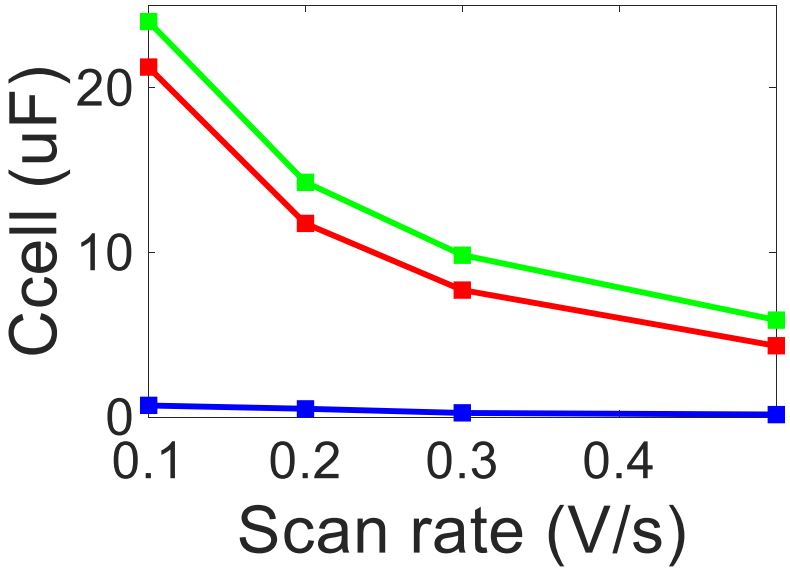

Figure 5.28 Capacitance of cell with two copper electrodes and a separator. Blue curve: bare separator; Red curve: p-n structured film where the n-side is facing the auxiliary electrode; Green curve where the p-side interface the auxiliary electrode. Ionic liquid was used as electrolyte at various scan rates, 0.5 V/s, 0.3 V/s, 0.2 V/s, 0.1 V/s.

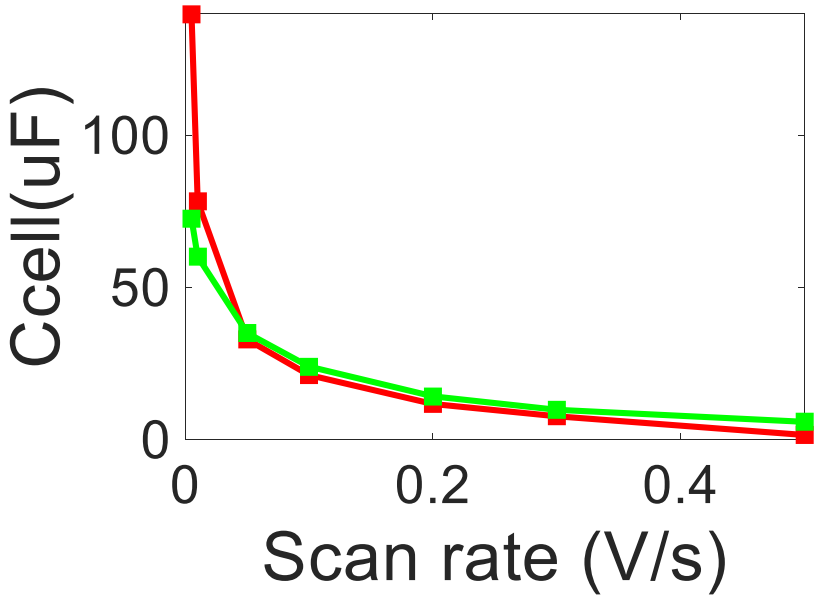

Figure 5.29 Capacitance of cell when the copper electrodes are covered with carbon powder. Structured separator case: Red: the n-side is facing the auxiliary electrode; Green: the p-side is facing the auxiliary electrode. The electrolyte is an ionic liquid and the experiment was performed at various scan rates, 0.5 V/s, 0.3 V/s, 0.2 V/s, 0.1 V/s, 0.05 V/s, 0.01 V/s, 0.005 V/s.

The stability of the cell is confirmed using cyclic voltammetry from 0 to +0.5 V for as many as 100 cycles at 10 mV/s scan rate for the configuration shown in Figure 5.30. Similar stability test is performed for the other configuration where n-side is facing the auxiliary electrode as shown in Figure 5.32. There was no reaction observed for either cases demonstrating that ionic liquid and the carbon nanotubes possess good stability over that many cycles. We calculated the overall cell capacitance for 100 cycles for either cases. Figure 5.31 shows that after the 10^{th} cycle, the overall capacitance becomes stable and maintains its retentivity with small deviation. After 10^{th} and 100^{th} cycle the cell capacitance was 64.04 uF and 65.56 uF, respectively. The change of capacitance after 100^{th} cycle is very small (~2%). Similarly, Figure 5.33 shows that after 10^{th} cycle the overall cell becomes stable. The cell capacitance for 10^{th} and 100^{th} cycle is measured to be 65.77 uF

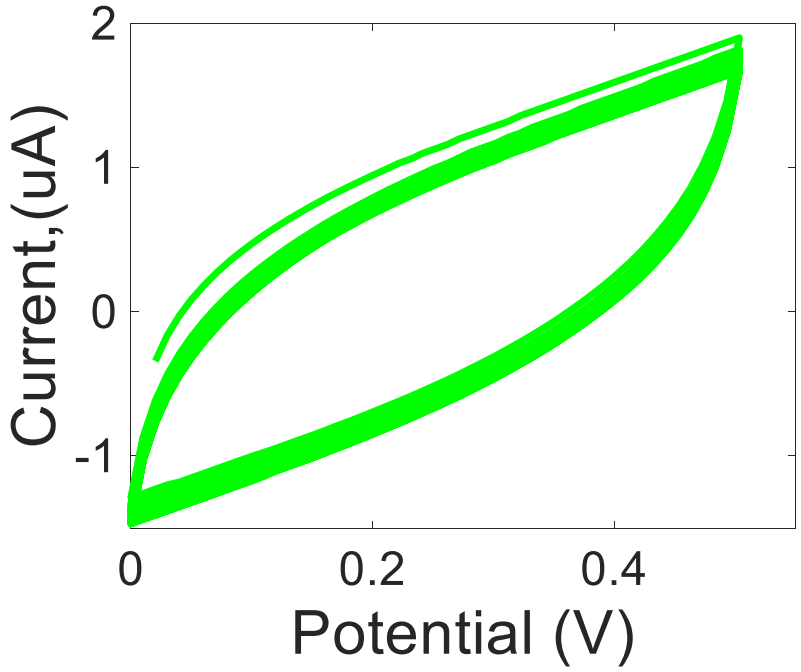

Figure 5.30 Cyclic voltammetry using copper electrodes interfaced with carbon powder a p-n structured gate immersed in ionic liquid. Experiments were made at a scan rate of 0.01V/s for 100 cycles.

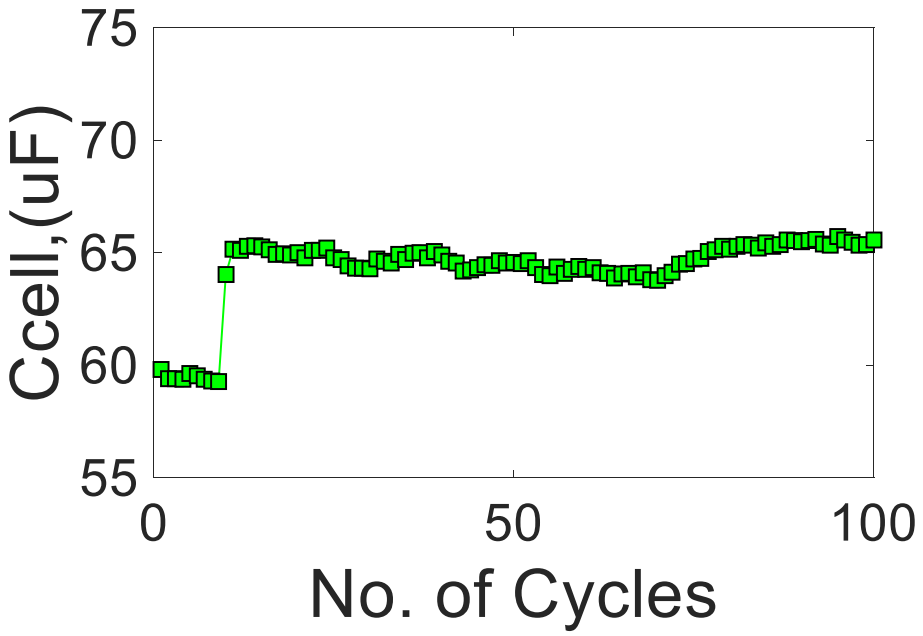

Figure 5.31 Stability measurements. Capacitance of cell vs number of cycles performed using cyclic voltammetry; the p-side was facing the auxiliary electrode.

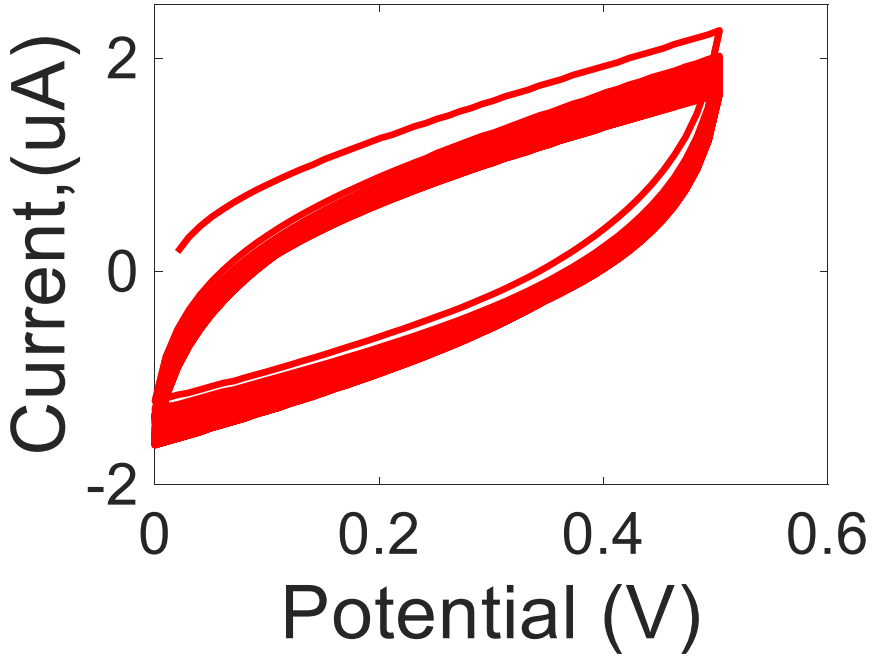

Figure 5.32 Capacitance of cell vs number of cycles performed in using cyclic voltammetry; the n-side was facing the auxiliary electrode. Ionic liquid electrolyte was used and the scan rate was 0.01V/s.

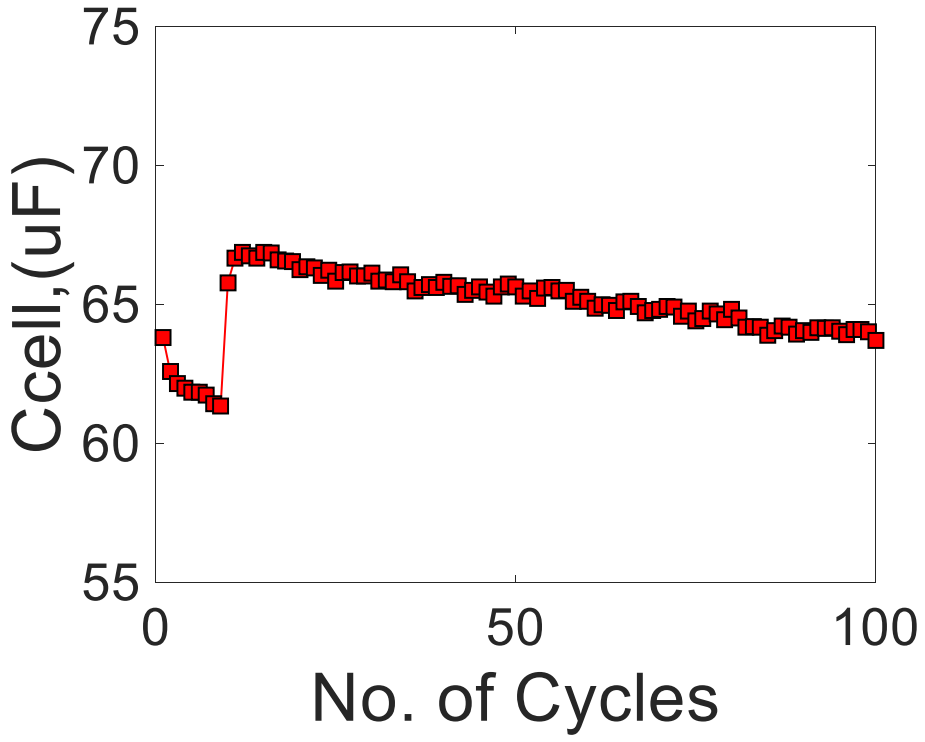

Figure 5.33 Stability measurements for copper electrodes that are interfaced with a carbon powder. The n-side was facing the auxiliary side.

and 63.69 uF. The deviation between the initial and final cycle is small (about 3%).

EIS measurement is performed from 50 kHz to 50 mHz for 10 mV perturbation signal for ionic liquid based electrolyte cell with and without structured separator layer. The position of structured separator layer has been interchanged and EIS measurement and analysis has been performed. The knee frequency is measured to be 19 Hz (red) and 14.42 Hz (green) when auxiliary electrode is near n- type layer and p-type layer, respectively. The equivalent series resistance for ionic liquid electrolyte based cells are quite high in the order of kΩ compared to the aqueous electrolyte based cells shown in Figure 5.34.

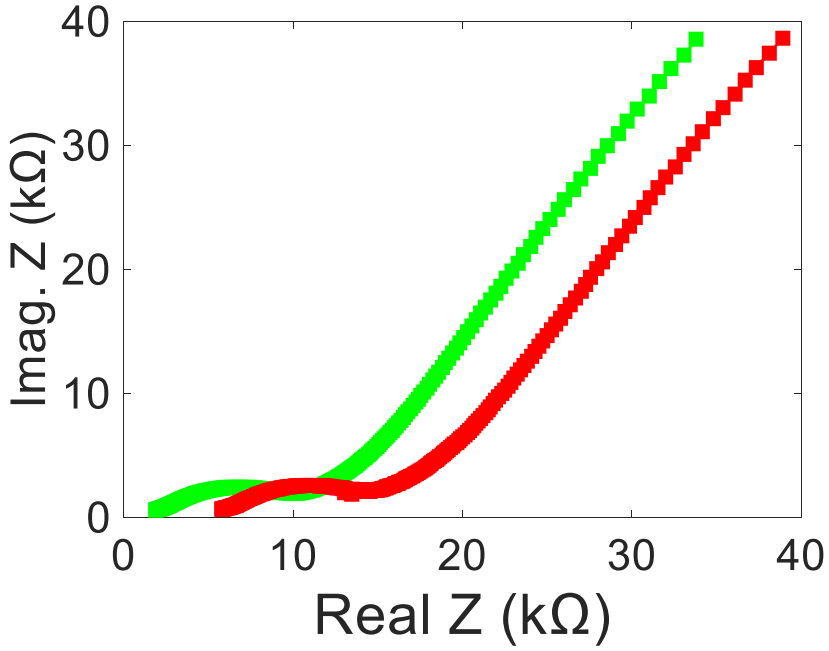

Figure 5.34 Nyquist plot of cell using carbon powder on carbon tape on copper as working and auxiliary electrode for both configuration (aux cu-np-work cu in red) and (work cu-np-aux cu in green) for p-n structured film as separator in ionic liquid electrolyte.

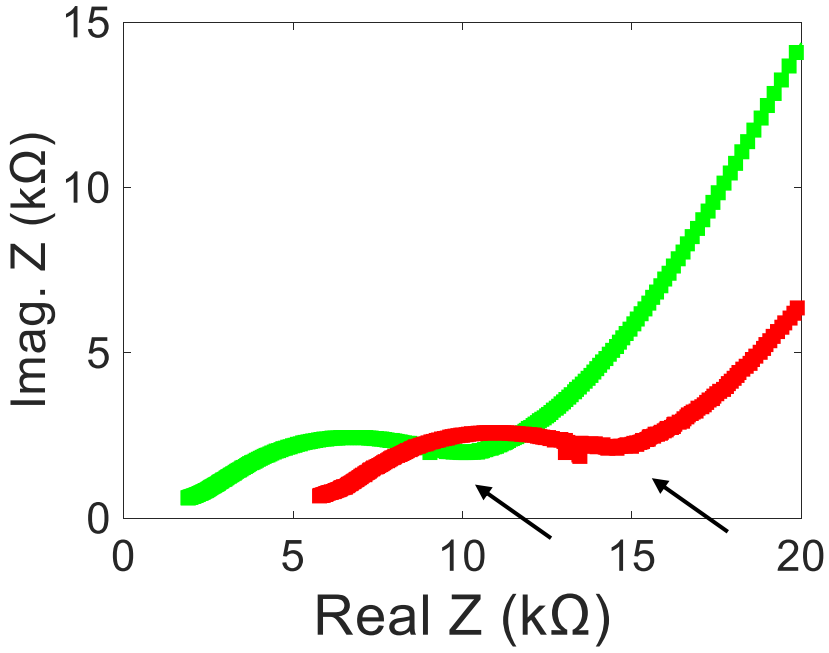

Figure 5.35 Nyquist plot magnified version of ionic liquid electrolyte based cell using p-n structured electrode.

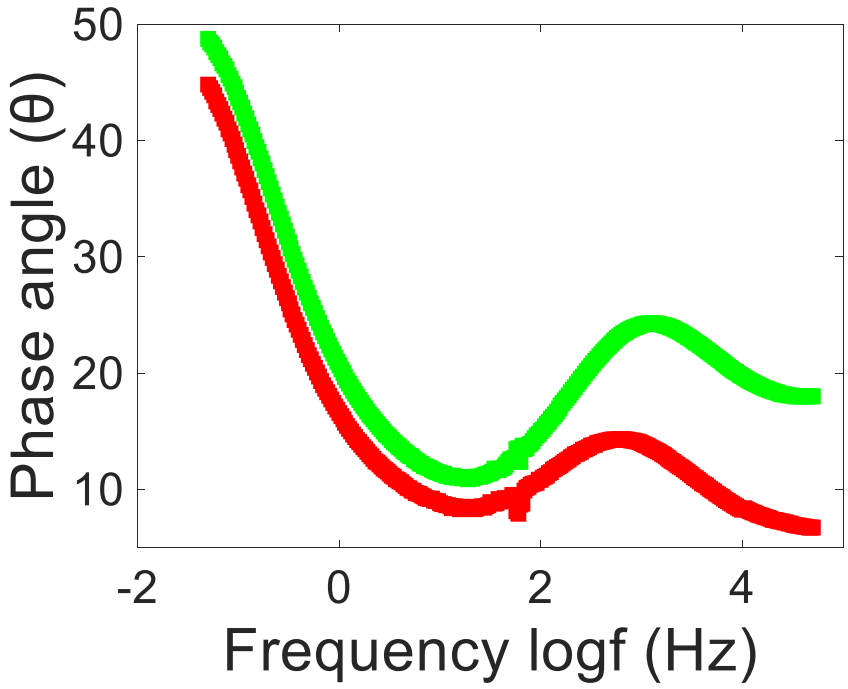

Figure 5.36 Bode plot of cell using carbon powder on carbon tape on copper as working and auxiliary electrode for both configuration (aux cu-np-work cu in red) and (work cu-np-aux cu in green) for p-n structured film as separator in ionic liquid electrolyte.

5.6 Multiple Structured Gate Electrode

Multiple gate electrodes were placed in mid-position between the anode and the cathode of the cell. The gates tested were: p-n junction, p-i-n junction and metallic, Au/Pd film. The study describes the overall effect of incorporating those gate in the cell.

5.6.1 Electrochemical Test

Cyclic voltammetry is conducted with a 3-electrode set-up. Scans were performed from -1 V to +1 V at scan rates of 10, 50, 100, and 500 mV/sec. Stability test was conducted at 0.01

V/s scan rate using p-n and p-i-n structured gate electrodes from -1 V to +1 V. All measurements were carried out at room temperature and using 1 M NaCl as an electrolyte.

5.6.2 Three Electrode Measurement

Comparison was made between a bare, p-n, p-i-n and Au/Pd structured gate at various scan rates without applying a bias to the gate. 3-electrode cyclic voltammetry (CV) was used. The potential range was -1 to +1 V. The potential range is chosen such that the cell remains stable throughout the experiment (namely, does not undergoes hydrolysis or any other chemical reaction). The CV area has increased for a structured gate compared to a bare gate. This is indicative of a higher cell capacitance for structured gate shown in Figure 5.37. The CV curve also exhibits no peak, which implies to no reaction in this voltage range.

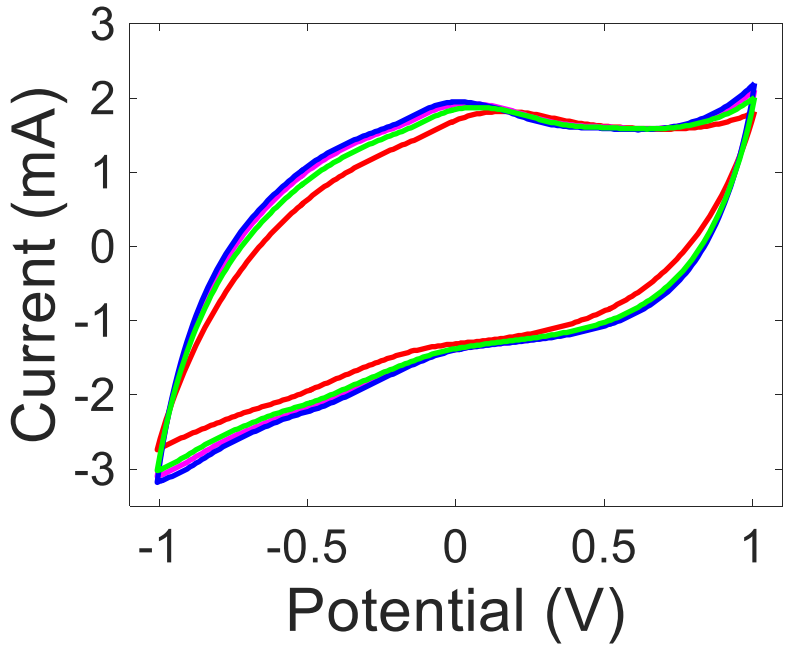

Figure 5.37 3-electrode cyclic voltammetry curve for bare separator (red), p-n gate electrode (blue), p-i-n (magenta) and green (metallic film) at 0.01 V/s scan rates.

Table 5.4 Cell Capacitance Measurement for Multiple Gate Electrode in Cell

Scan rate (V/s)	C_Bare (in F)	C_Au/Pd (in F)	C_p-n (in F)	C_p-i-n (in F)
0.5	0.0014	0.0033	0.0043	0.0038
0.1	0.0139	0.0258	0.0316	0.0296
0.05	0.0352	0.0548	0.0640	0.0611
0.01	0.1128	0.1265	0.1346	0.1315

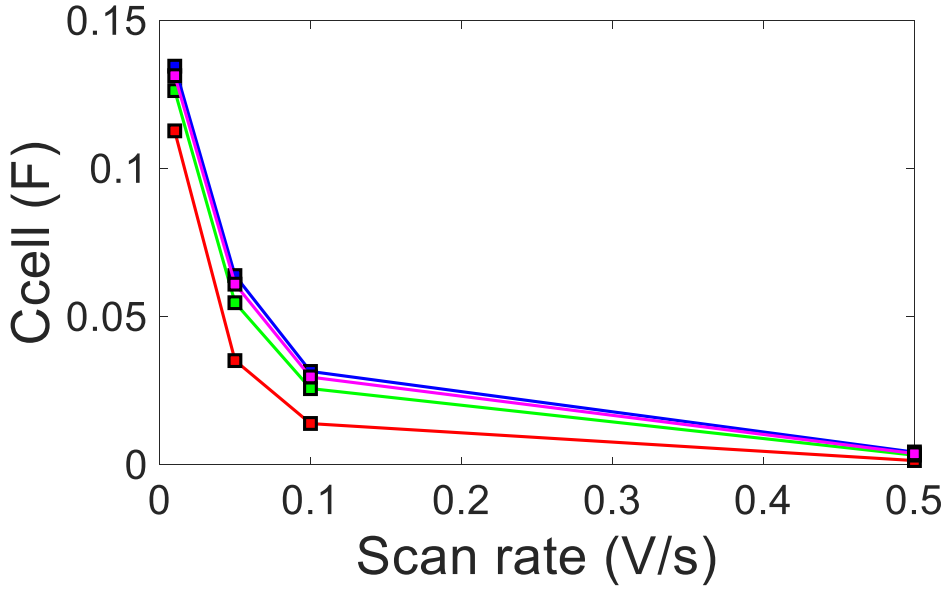

Figure 5.38 Cell capacitance vs scan rate from 3-electrode cyclic voltammetry curve for bare separator (red), p-n gate electrode (blue), p-i-n (magenta) and green (metallic film).

Table 5.4 compares the overall capacitance of a cell using various gate electrodes. Figure 5.38 shows the trend of an increasing cell's capacitance upon a decreasing scan rate. Incorporating a gate electrode improves the overall cell capacitance and the effect is more prominent for low scan rates. The Relative Cell's Capacitance (RCC) is the capacitance ratio between cells interfaced with a structured film and a cell interfaced with only a bare

membrane separators. Relative capacitance is larger for higher scan rates than for lower scan rates as shown in Figure 5.39.

Stability test using cyclic voltammetry has been performed at 0.01 V/s scan rate from -1 V to +1 V for 80 cycles using p-n and p-i-n structured gateas shown in Figure 5.40. There was no reaction observed for either cases demonstrating that the carbon nanotube based gate possess good stability over that many cycles shown in Figure 5.40. After 1st and 80th cycle the cell capacitance was 115 mF and 121 mF respectively for p-n gate electrode. For the p-i-n structured gate, the cell capacitance values after the 1st and 80th cycles were 98 mF and 100 mF, respectively, as shown in Figure 5.41.

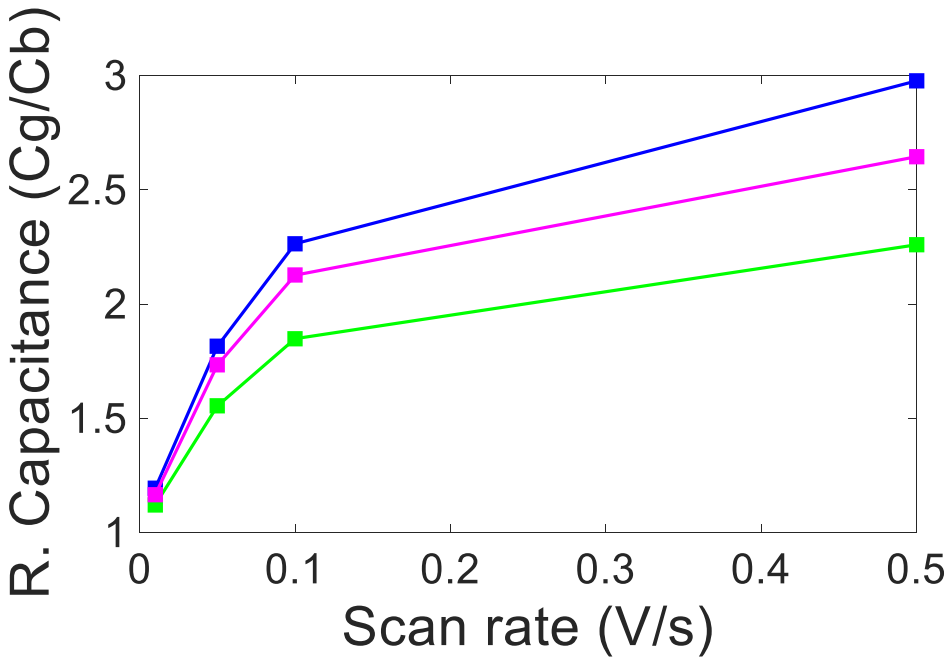

Figure 5.39 Relative cell capacitance vs scan rate for p-n gate electrode (blue), p-i-n (magenta) and green (metallic film).

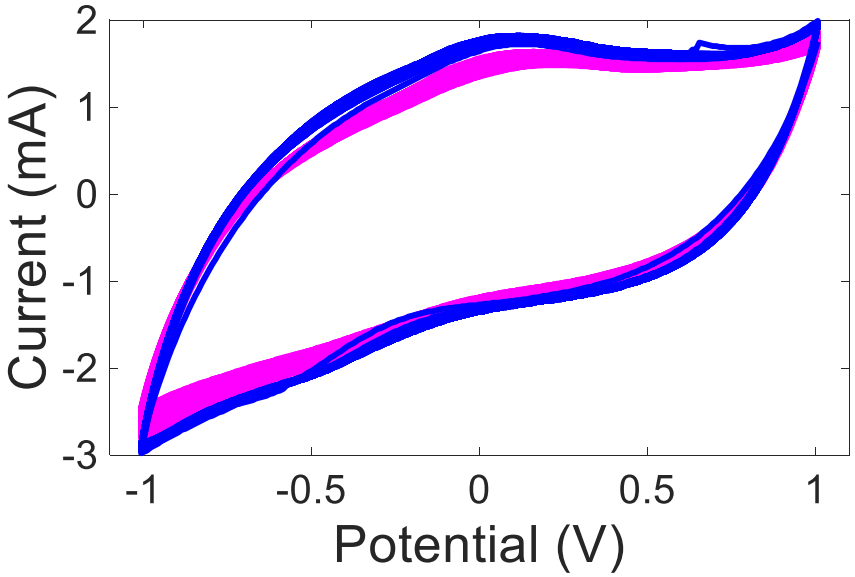

Figure 5.40 Stability test performed at 0.01 V/s scan rate for 80 cycles using p-n gate electrode (blue) and p-i-n (magenta).

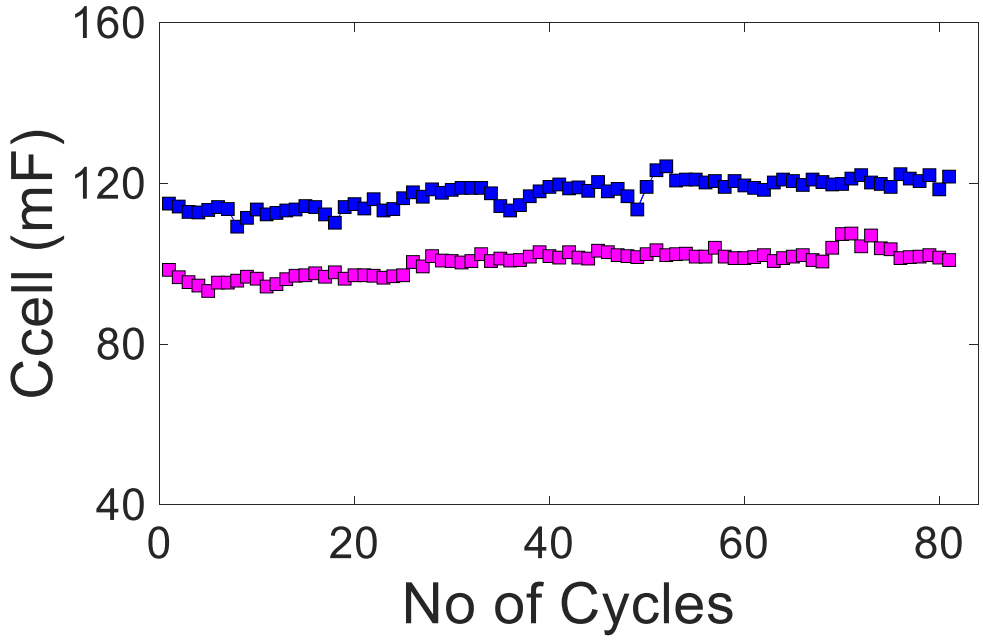

Figure 5.41 Cell capacitance measurement vs number of cycles performed at 0.01 V/s scan rate for 80 cycles using p-n gate electrode (blue) and p-i-n (magenta).

5.6.3 Two Electrode Measurement

2-electrode measurement was carried out using bare and p-n strcutured films using Cyclic voltammetry (CV) and Charge-discharge (CD). Chrono-potentiometry was performed for 2-electrode configuration from 0 to 0.8 V at 1 mA discharge current. The effect of the gate electrode incorporation on the overall cell's capacitance has been assessed. All measurements were carried out at room temperature and using 1 M NaCl as an electrolyte. 2-electrode measurements were performed from 0 V to +1 V at 10, 50, 100, and 500 mV/sec, various scan rates respectively using bare and p-n structured gate electrode. Figure 5.42 and 5.43 show the CV curve for bare and p-n film, respectively. Both curve exhibit quasi-rectangular curve. The inclusion of p-n structured increased the overall cell capacitance when compared to a bare separator (Figure 5.44).

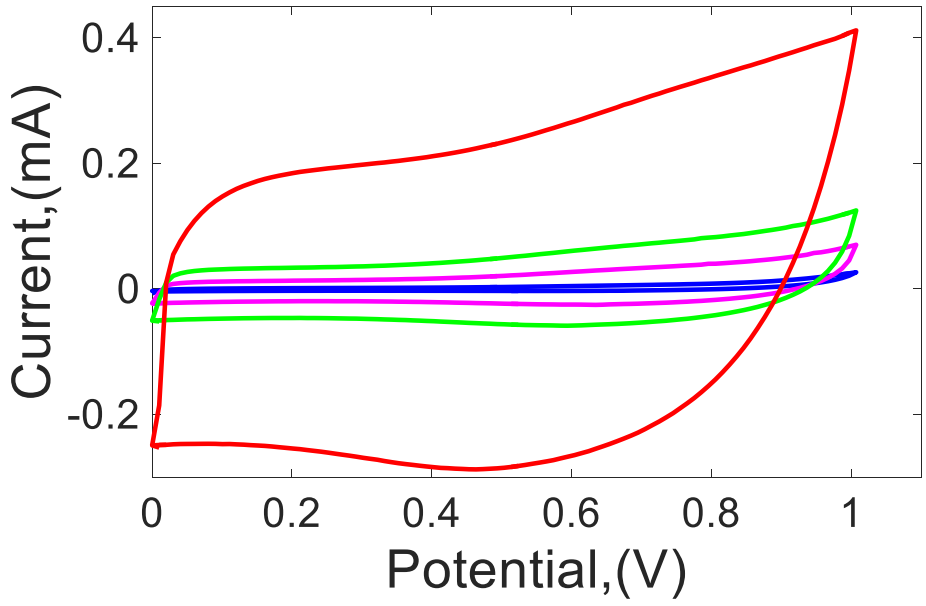

Figure 5.42 2-electrode cyclic voltammetry curves for a bare separator at various scan rates, 0.5 V/s (red), 0.1V/s (green), 0.05 V/s (magenta) and 0.01 V/s (blue).

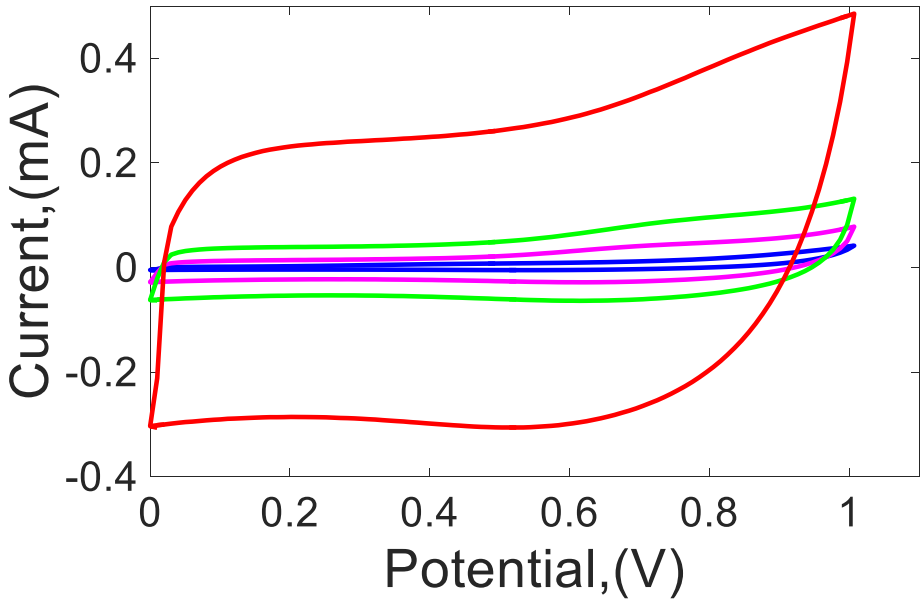

Figure 5.43 2-electrode cyclic voltammetry curves for p-n structured separator at various scan rates, 0.5 V/s (red), 0.1V/s (green), 0.05 V/s (magenta) and 0.01 V/s (blue).

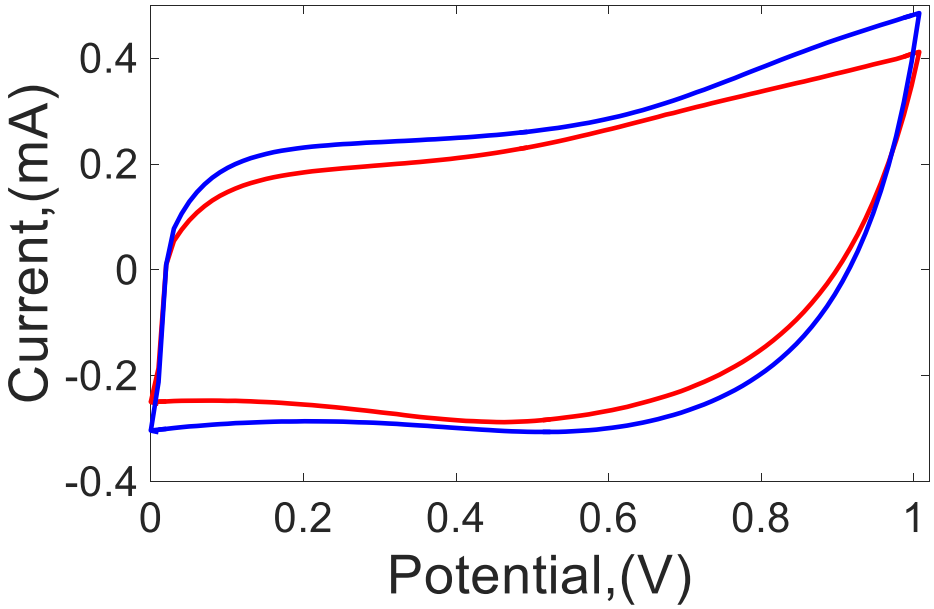

Figure 5.44 2-electrode cyclic voltammetry curve of the cell using bare (red) and structured film (blue) at 0.5 V/s scan rate.

Two-electrode chronopotentiometry for bare and p-n structured gate at 1 mA current discharge rates were performed without a bias to the gate. The curves are shown in Figure 5.45. The voltage range was set from 0 to +0.8 V. The triangular curve of chronopotentiometry indicates the capacitive behavior of the cell. All the chrono-potentiometry curves are well-defined and symmetric. Note an ohmic drop of ca 0.1 V at the end of the charge stage to the beginning of the discharge stage. In order to minimize the ohmic drop, a lower discharge current rate should be chosen. The measured cell capacitance for bare and structured p-n gate is 59.5 mF and 78 mF, respectively.

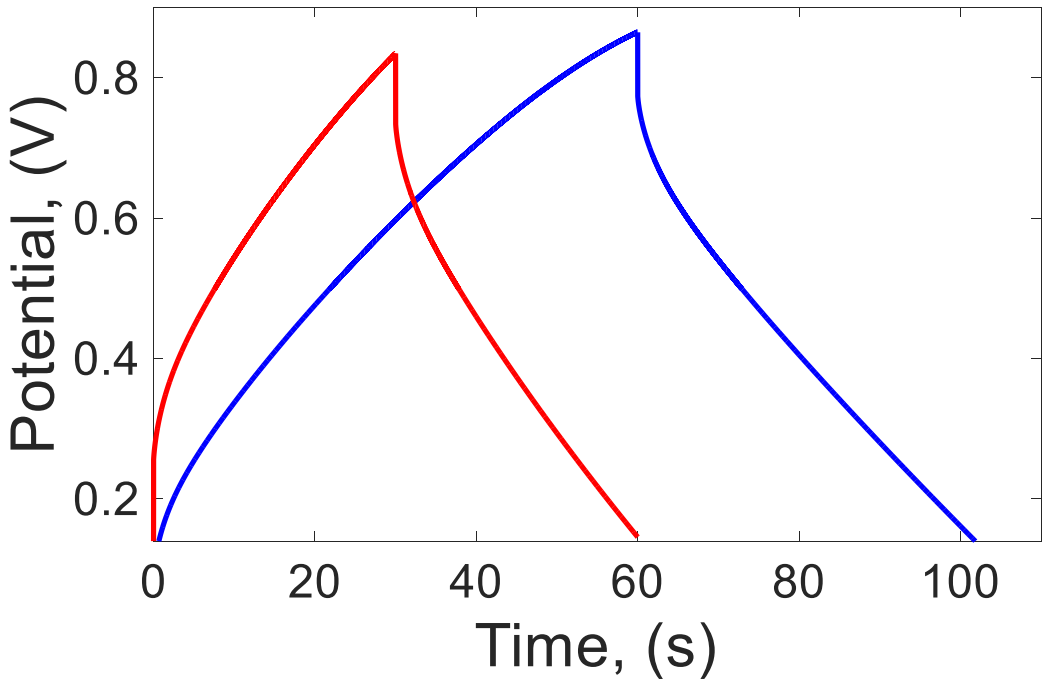

Figure 5.45 2-electrode chronopotentiometry curve of the cell using bare separator (red) and p-n structured film (blue).

CHAPTER 6

CONCLUSION

A new concept of incorporating active separator layer into a supercapacitor is introduced and its effect and contribution to the capacitance of the overall cell is analyzed for aqueous and ionic liquid electrolytes. The comparative study has also been performed about using a passive separator and active separator. Active separator layer creates a potential barrier in the form of electronic structures made of functionalized semiconducting films. In the first case study, diode-like p-n junctions used as an active separator were fabricated and inserted into a 2-electrode configuration with non-porous graphite rod as working and auxiliary electrode and aqueous sodium chloride as supporting electrolyte. Here it was demonstrated that active separator provides higher overall cell capacitance than that of passive separator irrespective of scan rate. Two electrochemical methods, both cyclic voltammetry (CV) and Chronopotentiometry validates the claim. The overall improvement of capacitance is calculated to be as low as 4% for highest scan rate and as high as 10% for lowest scan rate. It is also shown that due to the active separator layer discharge time is prolonged. In another study, if any voltage is applied to the active separator layer the capacitance of the supercapacitor increases additionally 10-15%. Electrochemical impedance spectroscopy (EIS) method reported that equivalent series resistance decreases due to the active separator layer insertion which eventually increases the power capacity of the supercapacitor cell. A complex model which fits the experimental data has also been proposed to describe the cell.

In another study, 3-electrode configuration is used to assess the capacitance of the

active separator layer made of p-n junction. It exhibits that the position of reference and counter electrode along with the ordering of structured gate play a role in the capacitance increase. Only cyclic voltammetry analysis was performed.

In the second case study, similar active layer were fabricated but the electrodes were changed to copper electrodes with ionic liquid electrolyte. The idea here was to use CV and EIS method to compare the cell capacitance increase with and without active separator layer in ionic liquid electrolyte. It was indeed shown that active separator layer improves the overall cell capacitance.

In the third case study, the electrodes were carbon taped copper electrode with carbon powder but the separator layer and electrolytes were kept same. In this study, the effect of the position of reference and counter electrode along with the ordering of structured gate was explored. Additionally for both cases stability test has been performed for as many as 100^{th} cycles. Not only did the ordering exhibits the difference of cell capacitance increment but it was also demonstrated that the cell becomes stable and maintains its retentivity with small deviation. Finally, it was shown that there was no reaction observed for either cases demonstrating that ionic liquid and the carbon nanotubes possess good stability over that many cycles.

CHAPTER 7

FUTURE WORK

Carbon nanotube electronic junctions as an active separator layer in aqueous and ionic liquid electrolyte based supercapacitor has been demonstrated. Even after contact protection, aqueous NaCl solution is corrosive for the copper contact of the active separator when exposed for long time. An alternative metal electrode prone to corrosion in sodium chloride with ohmic contact with CNT film is required for longer life of the cell. The mechanical adherence of the CNT films to the metal contact needs to be further improved: a more robust method ought to be developed. The porosity of separator is important to the cell capacitance improvement but there is no standard method or process is established to control it. In addition to the already established passive layer, active layer with the electronic structures could help in increasing the cell capacitance of supercapacitor.

REFERENCES

[1] V. V. N. Obreja, "On the performance of supercapacitors with electrodes based on carbon nanotubes and carbon activated material", *Physica E*, vol. 40, pp. 2596-2605, 2008.

[2] J. R. Miller and P. Simon, "Electrochemical capacitors for energy management", *Science*, vol. 321, no. 5889, pp. 651-652, 2008.

[3] P. Simon and Y. Gogotsi, "Materials for electrochemical capacitors", *Nature Materials*, vol. 7, no. 11, pp. 845-854, 2008.

[4] E. Frackowiak, S. Gautier, H. Gaucher, S. Bonnamy, and F. Béguin, "Electrochemical storage of lithium multiwalled carbon nanotubes", *Carbon*, vol. 37, pp. 61-70, 1999.

[5] A. Burke, "Ultracapacitors: why, how and where is the technology", *Journal of Power Sources*, vol. 91, pp. 37-50, 2000.

[6] K. Naoi and P. Simon, "New materials and new configurations for advanced electrochemical capacitors", *Electrochemical Society Interface*, vol. 17, no. 1, pp. 34-37, 2008.

[7] C. Largeot, C. Portet, J. Chmiola, P. L. Taberna, Y. Gogotsi, and P. Simon, "Relation between the ion size a and pore size for an electric double layer capacitor", *Journal of American Chemical Society*, vol. 130, no. 1, pp. 2730-2731, 2008.

[8] M. Winter, and R. J. Brodd, "What are batteries, fuel cells and supercapacitors", *Chemical Reviews*, vol. 104, no. 10, pp. 4245-4270, 2004.

[9] S. Mayer, J. Kaschmitter, R. Pekala, "Aquagel Electrode Separator for use in Batteries and Supercapacitors", US Patent 5042306, 28 May, 1995.

[10] J. Day, C. Wei, "Ultra-capacitor Separator", US Patent 6084767, 4 July, 2000.

[11] J. Yang, H. Wang, and C. Yang, "Modification and characterization of semi-crystalline poly(vinyl alcohol) with interpenetrating poly(acrylic acid) by UV radiation method for alkaline solid polymer electrolytes membrane", *Journal of Membrane Science*, vol. 322, no. 1, pp. 74-80, 2008.

[12] Y. Yin, O. Yamada, Y. Suto, T. Mishima, K. Tanaka, H. Kita, and K. Okamoto, "Synthesis and characterization of proton-conducting copolyimides bearing pendant sulfonic acid groups", *Journal of Polymer Science. Part A: Polymer Chemistry*, vol. 43, pp. 1545-1553, 2005.

[13] J. A. Elliott, and S. J. Paddison, "Modelling of morphology and proton transport in PFSA membranes", *Physical Chemistry Chemical Physics*, vol. 9, pp. 2602-2618, 2007.

[14] B. G. Choi, J. Hong, W. Hong, P. Hammond, H. Park, "Facilitated ion transport in all-solid-state flexible supercapacitors", *American Chemical Society Nano*, vol. 5, no. 9, pp. 7205-7213, 2011.

[15] J. Zhou, J. Cai, S. Cai, X. Zhou, A. Mansour, "Development of all-solid-state mediator-enhanced supercapacitors with polyvinylidene fluoride/lithium trifluoromethanesulfonate separators", *Journal of Power Sources*, vol. 196, no. 23, pp. 10479-10483, 2011.

[16] P. Staiti, F. Lufrano, "Investigation of polymer electrolyte hybrid supercapacitor based on manganese oxide carbon electrodes", *Electrochimica. Acta*, vol. 55, no. 25, pp. 2436-7442, 2010.

[17] E. Frackowiak and F. Beguin, "Carbon materials for the electrochemical storage of Energy in capacitors," *Carbon*, vol. 39, no. 6, pp. 937-950, 2001.

[18] H. I. Becker, "Low voltage eletrolytic capacitors", US Patent 2800616, 23 July, 1957.

[19] R. A. Rightmire, "Electrical energy storage apparaturs", US Patent 3288641A, 29 November, 1966.

[20] D. L. Boos, "Electrolytic capacitor having carbon paste electrodes", US Patent 3536963, 27 October, 1970.

[21] B. E. Conway, "Transition from 'supercapacitor' to 'battery' electrochemical capacitor applications", *Journal of Electrochemical Society*, vol. 138, no. 6, pp. 1539-1548, 1991.

[22] S. Trasatti, and G. Buzzanca, "Ruthenium dioxide: A new interesting electrode material. Solid state structure and electrochemical behavior", *Journal of Electroanalytical Chemistry*", vol. 29, no. 2, pp. A1-A5, 1971.

[23] B. E. Conway, H. Angerstein-Kozlowska, "Electrochemical study of multiple state adsorption in monolayers", *Account of Chemical Research*, vol. 14, no. 2, pp. 49-56, 1981.

[24] S. Hadži-Jordanov, H. Angerstein-Kozlowska, and B. E. Conway, "Surface oxidation and H deposition at ruthenium electrodes: Resolution of component processes in potential sweep experiments", *Journal of Electroanalytical Chemistry*, vol. 60, no. 3, pp. 359-362, 1975.

[25] B. E. Conway. *Electrochemical supercapacitors: Scientific Fundamentals and Technological Applications*, Newyork, NY: Plenum Press, 1999.

[26] S. Sarangapani, B.V. Tilak, and C. P. Chen, "Review-Materials for Electrochemical Capacitors", *Journal of Electrochemical Society*, vol. 143, no. 11, pp. 3791-3799, 1996.

[27] T. C. Murphy, R. B. Wright, R. A. Sutula, in: F. M. Delnick, D. Ingersoll, X. Andrieu, K. Naoi (Eds.), "US Department of Energy electrochemical capacitor Development and testing activities", *Electrochemical Capacitors II Proceedings, The Electrochemical Society*, vols. 96–25, pp. 258-267, 1997.

[28] R. Kotz, and M. Carlen, "Principles and applications of electrochemical capacitors", *Electrochimica Acta,* vol. 45, no. 15-16, pp. 2483-2498, 2000.

[29] H. V. Helmholtz, "Ueber einige Gesetze der Vertheilung elektrischer Ströme in körperlichen Leitern mit An-wendung auf die thierisch-elektrischen Versuche," *Annalen der Physik*, vol. 89, no. 6, pp. 211-233, 1853.

[30] M. Gouy, "Sur la constitution de la charge électrique à la surface d'un électrolyte", *Journal of Theoretical and Applied Physics*, vol. 149, pp. 457-468, 1910.

[31] D. L. Chapman, "A contribution to the theory of electrocapillarity", *The London Edinburgh and Dublin Philosophical Magazine and Journal of Science*, vol. 25, pp. 475-481, 1913.

[32] H. O. Stern, "Zur theorie der elektrolytischen doppelschicht", *Zeitschrift für Elektrochemie Und Angewandte Physikalische Chemie*, vol. 30, pp. 508-516. 1924.

[33] L. L. Zhang and X. S. Zhao, "Carbon-based materials as supercapacitor electrodes," *Chemical Society Reviews*, vol. 38, no. 9, pp. 2520-2531, 2009.

[34] E. Frackowiak, "Carbon materials for supercapacitor application", *Journal of Physical Chemistry Chemical Physics*, vol. 9, no. 15, pp.1774-1785, 2007.

[35] E. Raymundo-Pinero, K. Kierzek, J. Machnikowski and F. Beguin, "Relationship between the nanoporous texture of activated carbons and their capacitance properties in different electrolytes," *Carbon*, vol. 44, no. 12, pp. 2498-2507, 2006.

[36] M. Toupin, D. Belanger, I. R. Hill, D. Quinn, "Performance of experimental carbon blacks in aqueous supercapacitors", *Journal of Power Sources*, vol. 140, no. 1, pp. 203-210, 2005.

[37] E. Frackowiak, "Supercapacitors based on carbon materials and ionic liquids", *Journal of Brazilian Chemical Society*, vol. 17, no. 6, pp. 1074-1082, 2006.

[38] M. Galiński, A. Lewandowski, I. Stepniak, "Ionic liquids as electrolytes", *Electrochimica Acta*. vol. 51, no. 26, pp. 5567-5580, 2006.

[39] A. Lewandowski, M. Galiński, "Carbon-ionic liquid double-layer capacitors", *Journal of Physics and Chemistry of Solids*, vol.65, no. 2-3, pp. 281-286, 2004.

[40] S. Arzhantsev, H. Jin, G. A. Baker, M. Maroncelli, "Measurements of the complete solvation response in ionic liquids", *Journal of Physical Chemistry B.*, vol. 111, no. 18, pp. 4978-4989, 2007.

[41] J. Huang, B. G. Sumpter, V. Meunier, "A Universal Model for nanoporous carbon supercapacitors applicable to diverse pore regimes, carbon materials, and electrolytes", *Chemistry - European Journal*, vol. 14, no. 22, pp. 6614-6626, 2008.

[42] S. S. Sekhon, "Conductivity behaviour of polymer gel electrolytes: Role of polymer", *Bulletin of Material Science*, vol. 26, no. 3, pp. 321–328, 2003.

[43] P. Arora, Z. Zhang,"Battery separators", *Chemical reviews*, vol. 104, pp. 4419-4462, 2004.

[44] S. S. Zhang, "A review on the separators of liquid electrolyte Li-Ion batteries", *Journal of Power Sources*, vol. 164, pp. 351-364, 2007.

[45] M. Inagaki, H. Konno, O. Tanaike, "Carbon materials for electrochemical capacitors", *Journal of Power Sources*, vol. 195, pp. 7880-7903, 2010.

[46] D. Qu, H. Shi, "Studies of activated carbons used in double layer capacitors", *Journal of Power Sources*, vol. 74, pp. 99-107, 1998.

[47] H. Yu, Q. Tang, J. Wu, Y. Lin, L. Fan, M. Huang, J. Lin, Y. Li, F. Yu, "Using eggshell membrane as a separator in supercapacitor", *Journal of Power Sources*, vol. 206, pp. 463-468, 2012

[48] Y. M. Shulga, S. A. Baskakov, Y. V. Baskakova, Y. M. Volfkovich, N.Y. Shulga, E. A. Skryleva, Y. N. Parkhomenko, K. G. Belay, G. L. Gutsev, A. Y. Rychagov, V. E. Sosenkin, I. D. Kovalev, "Supercapacitors with graphene oxide separators and reduced graphite oxide electrodes", *Journal of Power Sources*, vol. 279, pp. 722-730, 2015.

[49] D. Karabelli, J. C. Leprêtre, F. Alloin, J. Y. Sanchez, "Poly (vinylidene fluoride) based macroporous separators for supercapacitors", *Electrochimica Acta*, vol. 57, pp. 98-103, 2011.

[50] J. Tabuchi, "Large capacitance electric double layer capacitor using activated carbon-carbon composite", *IEEE Transanctions on Components, Hybrids and Manufacturing Technology*, vol. 16, no. 4 , p. 431, 1993.

[51] M. Nakamura, M. Nakanishi, K. Yamamoto, "Influence of physical properties of activated carbons on characteristics of electric double-layer capacitors", *Journal of Power Sources*, vol. 60, no. 2, pp. 225-231, 1996.

[52] M. M. Inagaki in *Carbons for Electrochemical Energy Storage and Conversion Systems* (eds F. Beguin and E.´ Frackowiak), Boca Raton, FL: Taylor & Francis Group, pp. 37–76, 2010.

[53] A. Yoshida, S. Nonaka, I. Aoki, A. Nishino "Electric double-layer capacitors with sheet-type polarizable electrodes and application of the capacitors", *Journal of Power sources*, vol. 60, no. 2, pp. 213-218, 1996.

[54] M. Endo, Y. J. Kim, T. Maeda, K. Koshiba, K. Katayam, M. S. Dresselhaus, "Morphological effect on the electrochemical behavior of electric double-layer capacitor", *Journal of Material Research*, vol. 16, no. 12, pp. 3402-3410, 2001.

[55] M. Endo, T. Maeda, T. Takeda, Y. J. Kim, K. Koshiba, H. Hara, M. S. Dresselhaus, "Capacitance and pore-size distribution in aqueous and nonaqueous electrolytes using various activated carbon electrodes", *Journal of electrochemical Society*, vol. 148, no. 8, pp. A910-A914, 2001

[56] S. I. Pyun, C. H. Kim, S. W. Kim, J. H. Kim, "Effect of pore size distribution of activated carbon electrodes on electric double layer capacitor performance", *Journal of New Materials for Electrochemical System*, vol. 5, no. 4, pp. 289-295, 2002.

[57] C. Niu, E. K. Sichel, R. Hoch, D. Moy, H. Tennent, "High power electrochemical capacitors based on carbon nanotube electrodes", *Applied Physics Letter*, vol. 70, no. 11, 1480-1482, 1997.

[58] R. Z. Ma, J. Liang, B. Q. Wei, B. Zhang, C. L. Xu, D. H. Wu, "Study of electrochemical capacitors utilizing carbon nanotube electrodes", *Journal of Power Sources,* vol. 84, pp. 126-129, 1999.

[59] E. Frackowiak, K. Jurewicz, S. Delpeux, F. Beguin, "Nanotubulars materials for supercapacitors", *Journal of Power Sources*, vol. 97-98, pp. 822-825, 2001.

[60] J. N. Barisci, G. G. Wallace, R. H. Baughman, "Electrochemical quartz crystal microbalance studies of single-wall carbon nanotubes in aqueous and non-aqueous solutions", *Electrochimica Acta,* vol. 46, pp. 509-517, 2000.

[61] J. N. Barisci, G. G. Wallace, R. H. Baughman, "Electrochemical characterization of single walled carbon nanotubes electrodes", *Journal of Electrochemical Society*, vol. 147, no. 12, pp. 4580-4583, 2000.

[62] J. N. Barisci, G. G. Wallace, D. Chattopadhyay, F. Papadimitrakopoulos, R. H. Baughman, "Electrochemical properties of single walled carbon nanotubes electrodes", *Journal of Electrochemical Society*, vol. 150, no. 9, pp. E409-E415, 2003.

[63] S. Shiraishi, H. Kurihara, K. Okabe, D. Hulicova, A. Oya., "Electric double layer capacitance of highly pure single-walled carbon nanotubes (HiPco™Buckytubes™) in propylene carbonate electrolytes", *Electrochemistry Communications*, vol. 4, pp. 593-598, 2002.

[64] C. Y. Liu, A. J. Bard, F. Wudl, I. Weitz, J. R. Heath, "Electrochemical characterization of films of single-walled carbon nanotubes and their possible application in supercapacitors" *Electrochemical and Solid-State Letters*, vol. 2, no. 11, pp. 577-578, 1999.

[65] J. N. Barisci, G. G. Wallace, D. R. MacFarlane, R. H. Baughman, "Investigations of ionic liquid as electrolytes for carbon nanotube electrodes", *Electrochemistry communications*, vol. 6, pp. 22-27, 2004.

[66] H. J. Xe, B. Gelinas, D. Rochefort, "Redox active electrolyte supercapacitors using electroactive ionic liquid", *Electrochemistry Communications*, vol. 66, pp. 42-45, 2016.

[67] Y. Z. Su, Y. -P. Niu, Y. -Z. Xiao, M. Xiao, Z. -X. Liang, K. -C. Gong. *Journal of Polymer Science, Part A: Polymer Chemistry*, vol. 42, no.10, pp. 2329-2339, 2004.

[68] A. Rudge, J. Davey, I. Raistrick, S. Gottesfeld, J. P. Ferraris, "Conducting polymers as active materials in electrochemical capacitors", *Journal of power sources*, vol. 47, pp. 89-107, 1994.

[69] K. Zhang, L. L. Zhang, X. S. Zhao, J. Wu, "Graphene–polyaniline nanofiber composites as supercapacitor electrodes", *Chemistry of Materials,* vol. 22, pp. 1392–1401, 2010.

[70] E. Frackowiak, V. Khomenko, K. Jurewicz, K. Lota, F. Béguin "Supercapacitors based on conducting polymer–nanotube composites", *Journal of Power Sources*, vol. 153, pp. 413–418, 2006.

[71] J. Yan, T. Wei, Z. Fan, W. Qian, M. Zhang, X. Shen, and F. Wei,"Preparation of graphene nanosheet/carbon nanotube/polyaniline composite as electrode material for supercapacitors", *Journal of Power Sources*, vol. 195, no. 9, pp. 3041–3045, 2010.

[72] L. L. Zhang, T. Wei, W. Wang, X. S. Zhao, "Manganese oxide–carbon composite as supercapacitor electrode material", *Microporous and Mesoporous Materials*, vol. 123, no. 1-3, pp. 260–267, 2009.

[73] J. P. Zheng, P. J. Cygan, and T. R. Jow, "Hydrous ruthenium oxide as an electrode material for electrochemical capacitors", *Journal of the Electrochemical Society*, vol. 142, no. 8, pp. 2699–2703, 1995.

[74] M. Jayalakshmi, M. M. Rao, N. Venugopal, and K. B. Kim,"Hydrothermal synthesis of SnO_2–V_2O_5 mixed oxide and electrochemical screening of carbon nanotubes (CNTs), V_2O_5, V_2O_5 CNTs, and SnO_2-V_2O_5-CNT electrodes for supercapacitor applications", *Journal of Power Sources*, vol. 166, no. 2, pp. 578–583, 2007.

[75] T. Cottineau, M. Toupin, T. Delahaye, T. Brousse, D. Bélanger, "Nanostructured transition metal oxides for aqueous hybrid electrochemical supercapacitors", *Applied Physics A*, vol. 82, pp. 599–606, 2005.

[76] M. D. Stoller, S. J. Park, Y. W. Zhu, J. H. An and R. S. Ruoff, "Graphene-Based Ultracapacitors," *Nano Letters*, vol. 8, no. 10, pp. 3498-3502, 2008.

[77] H. C. Wu, Y. P. Lin, E. Lee, W. T. Lin, J. K. Hu, H. C. Chen, and N. L. Wu, "High performance carbon based supercapacitors using Al current collector with conformal carbon coating", *Materials Chemistry and Physics*, vol. 117, pp. 294-300, 2009.

[78] K. Ku, B. Kim, H. Chung, and W. Kim, "Characterization of graphene based supercapacitors fabricated on Al foils using Au or Pd thin films as interlayers", *Synthetic Metals*, vol. 160, pp. 2613-2617, 2010.

[79] M. J. O'Connell, P. Boul, L. M. Ericson, C. Huffman, Y. Wang, E. Haroz, C. Kuper, J. Tour, K. D. Ausman, and R. E. Smalley, "Reversible water solubilization of single-walled carbon nanotubes by polymer wrapping", *Chemical Physics letters*, vol. 342, pp. 265-271, 2001.

[80] M. Shim, A. Javey, N. W. S. Kam, and H. Dai, "Non-covalent sidewall functionalization of single-walled carbon nanotubes for protein immobilization", *Journal of American Chemical Society*, vol. 123, article 11512, 2001.

[81] W. Zhou, and Z. L. Wang. *Scanning Microscopy for Nanotechnology: Techniques and Applications*, Berlin, Germany: Springer, 1–32, 2006.

[82] O. C. Wells. *Scanning Electron Microscopy*, New York, NY: McGraw Hill, 1–13, 1974.

[83] http://serc.carleton.edu/research_education/geochemsheets/techniques/SEM.html, Accessed 15 October, 2018

[84] E. Frackowiak, "Carbon materials of supercapacitor application", Journal of *Physical Chemistry-Chemical Physics*, vol. 9, pp. 1714–1785, 2007.

[85] V. Khomenko, E. Frackowiak, and F. Beguin, "Determination of the specific capacitance of conducting polymer/nanotubes composite electrodes using different cell configurations", *Electrochimica Acta*, vol. 50, pp. 2499-2506, 2005.

[86] L. B. Hu, J. W. Choi, Y. Yang, S. Jeong, F. La Mantia, L. F. Cui and Y. Cui, "Highly conductive paper for energy storage devices", *Proceedings National Academy Science, USA*, vol. 106, pp. 21490-21494, 2009.

[87] G. A. Mabbott, G. A., "An introduction to Cyclic Voltammetry", *Journal of Chemical Education*, vol. 60, no. 9, pp. 697-702, 1983.

[88] K. Izutsu, "Electrochemistry in non-aqueous solutions", Wiley-VCH: Weinheim, Germany, 2003.

[89] P. T. Kissinger, W. R. Heineman, "Cyclic Voltammetry", *Journal of Chemical Education*, vol. 60, pp. 702-706, 1983.

[90] A. J. Bard, L. R. Faulkner, Electrochemical methods: fundamentals and applications, 2nd edition, John Wiley & Sons, Hoboken, NJ, 2001: xviii, 718 p.

[91] J. M. Savéant, Elements of Molecular and Biomolecular Electrochemistry; John Wiley & Sons: Hoboken, NJ, 2006

[92] K. B. Oldham, N. P. C. Stevens, "Uncompensated Resistance. 2. The effect of reference electrode nonideality", *Analytical Chemistry*, vol. 72, no. 17, pp. 3981-3988, 2000.

[93] J. C. Mylaand, K. B. Oldham, "Uncompensated Resistance. 1. The effect of cell geometry", *Analytical Chemistry*, vol. 72, no. 17, pp. 3972-3980, 2000.